UNIVERSIDAD POLITÉCNICA DE VALENCIA
Departamento de Ingeniería Hidráulica y Medio Ambiente

INVERSE MODELLING OF TWO-PHASE FLOW: CALIBRATION OF RELATIVE PERMEABILITY CURVES

TESIS DOCTORAL

By
Carolina Guardiola-Albert

Adviser:
Jaime Gómez-Hernández

Abstract

Stochastic mathematical modeling of multi-phase flow in heterogeneous porous media is of great interest in petroleum engineering and subsurface hydrology. Reservoir simulation models are essential for the management of petroleum production or remediation water resources. The stochastic framework gives the possibility to characterize the natural spatial variability of the flow parameters. Within this stochastic framework, multiphase flow simulations are used in order to evaluate different recovery or clean up processes, to make decisions regarding the placement of the wells, and to specify various operating procedures associated with injection and production wells.

It is common knowledge that inverse modeling theory provides a methodology to integrate both static and dynamic data in reservoir characterization. The inversion method can make the model geologically consistent at the same time that it reproduces parameter measurements and dynamic responses of the reservoir. Production data integration in reservoir modeling is performed through an inverse technique because dynamic data are non linearly related with reservoir heterogeneous properties through multiphase flow equations. In fact, the inverse modeling tool is a key factor in drawing up the field development plan, and for managing the available reserves over time. The advances in computational algorithms and hardware are continuously improving every day. New inverse numerical techniques take advantage of these progresses. However, still remains a practical tool for reservoir characterization which takes into account all the complex processes and parameters that are important for multiphase flow.

Absolute permeability is one of the parameters that are typically estimated with inverse flow simulators. The inversion techniques that estimate the spatial distribution of absolute permeability are commonly apply to multi and single phase flow problems. During last decades this issue has been submitted to intensive research. However, when studying multiphase flow there is another important property that complements absolute permeability. This parameter is relative permeability, which controls the rate of displacement of the different phases present in the reservoir. Altough relative permeabilities are so important to characterize the movement of two immiscible fluids, like oil and water or non aqueous contaminants and water, there are not studies nor

techniques to estimate the spatial distribution of relative permeabilities as it is done with absolute permeability. Normally these functions are assumed to be equal to measured values from laboratory experiments performed on core samples. Or, if there are not core samples available, they are taken from studies with similar geology and flow configuration.

In any case, if the output value from the core experiment is assigned to represent the relative permeability value of the whole reservoir, or if the relative permeability is taken from another reservoir study, the model of the multiphase flow simulator is subjected to an important source of error. This dissertation proposses to characterize relative permeabilities assuming that they have a spatial distribution, and estimate this spatial variability as it is usually done with absolute permeability distributions. The objective of the research work presented here is to develop a new inverse technique to estimate both absolute and relative permeabilities spatial distributions from static parameter measurements and production data, such as pressures and saturations. This technique has to deal with the non linearities present in the multiphase flow equations. As relative permeabilities are dependent on one of the state variables (saturations) the optimization problem is highly non linear, increasing the difficulty of the problem that has to be solved.

The governing equations for immiscible two-phase flow are formulated in terms of water saturation and fluid pressure. The proposed formulation simplifies the equation by disregarding gravity and capillary pressure terms, and using finite differences numerical approach. Calibration of the flow model to non linear data is formulated as an optimization problem, which tries to minimize some objective function. This objective function measures the differences between the historical production data (water breakthrough and pressure changes) and the corresponding simulated values. The inverse method presented here follows the technique developed in the Sequential Self-Calibrated method. A computer code, written in C, couples the forward two-phase flow simulator TOUGH with the iterative inverse method. The optimization algorithm is based on gradient methods, and the concept of master points is borrowed from the Sequential Self-Calibrated method to reduce the number of parameters subjected to calibration. After calibration, the result is one equally likely reservoir realization honoring historical pressure and saturation data.

Calibration parameters were chosen from the relative permeability expressions in function of saturation. These parameters are: the two end-points of oil and water relative permeability functions and the two residual saturations. These four values control the shape of the relative permeability curves. The method is tested with different synthetic examples in one and two dimensions. All simulations shown in this dissertation

assume that porosity is known. The goal of these examples is to test the applicability of the method and to study the influence of relative permeability parameters in the dynamic behavior of the reservoir. In the implementation different injection/production configurations have been assumed and different kind of heterogeneities for the relative permeability function have been proposed.

Results given by several examples of inversion simulations have shown that the method works. Once the calibration is performed, the result is just one of the possible representations of the medium. Using multiple equiprobable realizations it is possible to develop a study of uncertainty of the reservoir model, and then to translate it into uncertainty of reservoir performance predictions for reservoir management. This way to carry out an uncertainty analysis is normally known as Monte Carlo simulation. The objective is to analyze the influence of relative permeability parameters on the model, as well as on the predictions of the reservoir performance. It has been found out that uncertainties related with oil and water end-points of the relative permeability curves are higher than the uncertainties related with residual saturations. In general, it looks like uncertainties related with the four relative permeability parameters in study are important. Breakthrough saturation predictions appear to have small uncertainty when they are forecasted with the inversion technique developed, and to be better predicted in the first states of the exploitation. The most important conclusion of the dissertation is the high influence of relative permeability heterogeneities in the values of the saturation shock front. Hence, the importance of research studies about how to estimate the spatial distribution of relative permeability parameters and absolute permeability, in order to improve predictions of the water displacement in two-phase immiscible flow problems.

Resumen

Los modelos matemáticos estocásticos para la simulación de flujo multifase en medios porosos heterogéneos tienen un gran interés en ingeniería del petróleo e hidrología subterránea. Los modelos de simulación de yacimientos son esenciales en la gestión de producción petrolífera o en la recuperación de acuíferos contaminados. El entorno estocástico da la posibilidad de caracterizar la variabilidad espacial intrínseca de los parámetros de flujo. Dentro de este marco estocástico, la simulación de flujo multifase se usa para poder evaluar los diferentes procesos de recuperación o limpieza, y así tomar decisiones con respecto al emplazamiento de los pozos o a los procedimientos asociados a los bombeos o las inyecciones.

La teoría de modelización inversa da la posibilidad de integrar variables estáticas y dinámicas en la caracterización del yacimiento. El método inverso puede hacer que el modelo sea geológicamente consistente al mismo tiempo que reproduce las medidas de los parámetros y las repuestas dinámicas del medio. La integración de los datos de producción en la modelización del yacimiento se realiza a través de las técnicas de modelización inversa porque los datos dinámicos están relacionados de forma no lineal con las propiedades heterogéneas del yacimiento por las ecuaciones de flujo multifase. De hecho, la modelización inversa es un factor clave a la hora de planificar el plan de desarrollo de un campo petrolífero, o para la gestión de las posibles reservas a explotar. Los avances en algorimos de computación y hardware mejoran día a día. Los métodos más modernos hacen uso de estos avances para mejorar la rapidez en la simulación de flujo. Sin embargo, todavía no existe una herramienta que sea práctica y que además tenga en cuenta todos los procesos y parámetros que son importantes en el flujo multifase.

La permeabilidad absoluta es uno de los parámetros que que son típicamente estimados por medio de simulaciones inversa de flujo. Las técnicas de simulación inversas que estiman la distribución espacial de la permeabilidad absoluta se utilizan normalmente tanto en problemas de flujo de multifase como para flujo de una sola fase. En las últimas décadas este tema ha sido sujeto de intensas investigaciones. En cambio, cuando se estudia flujo multifase hay que tener en cuenta otra propiedad que com-

plemente la permeabilidad absoluta, y que es muy importante. Este parámetro es la permeabilidad relativa, que controla la tasa de desplazamiento de las diferentes fases presentes en el yacimiento. A pesar de que la permeabilidad relativa es muy importante para caracterizar el movimiento de dos fluidos inmiscibles, como por ejemplo el agua y el petróleo o el agua y un contaminante no acuoso, no existen estudios o técnicas que estimen la distribución espacial de las permeabilidades relativas como se hace habitualmente con la permeabilidad absoluta. Normalmente, estas funciones se suponen conocidas, cuyo valor se toma de medidas en laboratorio tomadas en testigos. En el caso de que no hayan testigos, las permeabilidad relativas se asignan por similitud con otros yacimientos de geología y condiciones de flujo similares.

En cualquier caso, si se asume que el valor obtenido en el laboratorio representa el valor de la permeabilidad relativa en todo el yacimiento, o incluso si se toma de otro yacimiento similar al de estudio, el modelo del flujo multifase experimentará importantes errores. Esta tesis doctoral propone caracterizar las permeabilidades relativas asumiendo que tienen variabilidad espacial, y estimar esta variabilidad espacial como se hace normalmente con las distribuciones de permeabilidad absoluta. El objetivo del trabajo de investigación que se presenta a continuación es desarrollar una nueva técnica de simulación inversa que estime la distribución espacial de las permeabilidades absoluta y relativa a partir de las medidas de parámetros estáticos y los datos de producción, como las presiones y las saturaciones. Esta técnica tiene que tener en cuenta las no linearidades que existen en las ecuaiones de flujo multifase. Al ser la permeabilidades relativas dependientes de una de las variables de estado (la saturación) el problema de optimización el altamente no lineal, incrementando las dificultades del problema a resolver.

Las ecuaiones que gobiernan el flujo inmiscible bifase están formuladas en términos de las saturaciones y las presiones. Además, las ecuaciones se simplifican desestimando las fuerzas gravitatorias y capilares, y usando aproximación numérica por diferencias finitas. La calibración del modelo de flujo a los datos no lineales se expresa como un problema de optimización, que minimiza una función objetivo. Esta función objetivo mide las diferencias entre los datos históricos de producción y los valores simulados correspondientes. El método inverso que se presenta en esta tesis sigue la técnica desarrollada por el método autocalibrante. Se ha escrito un código, en lenguaje C, que acopla el modelo de flujo directo TOUGH con el método inverso iterativo. El algoritmo de optimización se basa en el método de los gradientes, y el concepto de puntos maestros se toma prestado del método autocalibrante para reducir el número de parámetros que se van a calibrar. Después de realizar una calibración se obtiene una realización, que una más del conjunto de realizaciones posibles que reproducen los

datos de saturación y presión.

Los parámetros elegidos para la calibración se toman de las expresiones de las permeabilidades relativas en función de la saturación. Estos parámetros son: los dos puntos finales de las curvas de permeabilidad relativa del agua y del petróleo y las saturaciones residuales. Estos cuatro parámetros controlan el tamaño y la forma de las curvas de permeabilidad relativa. Se ha probado el método con varios ejemplos sintéticos en una y dos dimensiones. En todas las simulaciones mostradas en esta tesis la porosidad es conocida. El objetivo de estos ejemplos es mostrar que el método es aplicable y estudiar la influencia de la distribución espacial de los parámetros de la permeabilidad relativa. Se han probado distintas configuraciones de inyección/producción y diferentes tipos de heterogeneidad para las curvas de permeabilidad relativa.

Los resultados dados en distintos ejemplos de simulaciones inversas han demostrado que el método funciona. Una vez que la calibración se ha realizado, el resultado es una posible representación del yacimiento. Usando múltiples realizaciones equiprobables es posible desarrollar un estudio de incertidumbre del modelo del yacimiento, para trasladarlo a incertidumbres en las predicciones de gestión del mismo. Esta forma de realizar un estudio de incertidumbre es lo que comúnmente se conoce como simulación de Monte Carlo. El objetivo es analizar la influencia de los parámetros de permeabilidad relativa en el modelo, así como en las predicciones del funcionamiento del yacimiento. Los resultados encontrados en este trabajo de investigación muestran que las incertidumbres relacionadas con los puntos finales de las curvas de permeabilidad relativa son mayores que las incertidumbres relacionadas con las saturaciones residuales. En general parece que las incertidumbres para los cuatro parámetros que se calibran son bastante importantes. Las predicciones de los datos de saturación tienen menor incertidumbre cuando se predicen con la técnica aquí desarrollada, y se obtienen mejores resultados para los primeros tiempos de explotación del yacimiento. La conclusión más importante que aporta este trabajo es la gran influencia que tienen las heterogeneidades de las curvas de permeabilidad relativa en los valores de saturación. Es por ello que es muy importante que los estudios sobre como estimar la distribución espacial de la permeabilidad absoluta y relativa continúen y sobretodo que se consigan algoritmos más rápidos para hacer estudios de mayores dimensiones más reales.

Resum

Agradecimientos

Esta tesis ha sido posible gracias a la ayuda y apoyo de muchas personas que me han acompañado durante estos años. En primer lugar quiero agradecer a mi director de tesis, Jaime Gómez-Hernández, por darme la oportunidad de hacer este trabajo de investigación. Sin sus ideas, propuestas y supervisión este trabajo simplemente no existiría. Quiero agradecerle también los consejos que me ha dado, los 'entrenamientos' en las exposiciones, y todas las oportunidades que me ha ofrecido.

La fundación Repsol-YPF y la Empresa Nacional de Residuos Radioactivos S.A. (ENRESA) a través de la Universidad Politécnica de Valencia han financiado estos años de investigación.

Mis compañeros de departamento me han ayudado en los problemas del día a día y además han hecho que mi experiencia en Valencia sea inolvidable. En especial me gustaría agradecer a Eduardo Cassiraga por sus animos para que realizase la tesis en la UPV, su ayuda y su amistad durante estos años. A Rafael Aliaga, compañero de luchas con linux y demás problemas informáticos, siempre dispuesto a ayudarme y animarme. A Harrie Hendricks-F., por su legado de INVERTO. A Andrés Sahuquillo, Edu, Rafa, Harrie, Claudia, Lourdes, Carmen, Carlos, Hector, y JianLin por todas las horas de convivencia y por hacer más agradables los momentos de trabajo. Por supuesto me siento agradecida a todos los 'materos', por la compañía en los descansos y por las risas, las comidas en derecho y las tertulias en Dos Hermanos. A Andrés, Julián y Andrea por su amistad y su apoyo. A Guey, por la gran amiga que he ganado.

Fuera del departamento no me puedo olvidar de Jose, Manuela, Victor, Ivan y los demás del grupo, por cuidarme tanto y hacer que no me sintiera una extraña en esta ciudad, por los momentos en el Roca. A todos mis amigos de Madrid, por el apoyo en la distancia. Habría mucha más gente que mencionar, que están o han estado cerca de mí. Las limitaciones de espacio no me permiten escribir sus nombres, aunque ello no significa que hayan sido menos importantes en estos años. Le agradezco enormemente a mis padres su apoyo y su confianza en mí. A mi padre su asesoramiento constante en programación en C y FORTRAN, y en los problemas con linux.

Finalmente quiero dedicar esta tesis a Carlos, por su amor y su espera.

Contents

List of Figures

List of Tables

Nomenclature

ϕ	Porosity of the medium (no dimensions)
w	Subscript water phase qualifier
o	Subscript for oil phase qualifier
l	Phase qualifier
S_w	Water saturation
S_o	Oil saturation
S_l	Saturation of fluid l
t	Time variable $[T]$
$\mathbf{u}_l$	Darcy's velocity of the phase l $[L/T]$
ρ_l	Phase density $[M/L^3]$
q_l	Injection/production rate per unit volume $[T^{-1}]$
$\mathbf{k}$	Absolute permeability tensor $[L^2]$
k_{rw}	Water relative permeability (no dimensions)
k_{ro}	Oil relative permeability (no dimensions)
μ_l	Viscosity of the phase l $[M/LT]$
p_w	Water pressure $[M/LT^2]$
p_o	Oil pressure $[M/LT^2]$
∇p_l	Pressure gradient $[M/L^2T^2]$
P_c	Capillary pressure $[M/LT^2]$
β_l	l-fluid compressibility $[LT^2/M]$
β_m	Matrix compressibility $[LT^2/M]$
ϕ^0	Porosity at the reference pressure
C_l	l-fluid capacity coefficient
f_w	Fractional flow
$\mathbf{u}_T$	Total flux $[L/T]$
P	Total (or global) fluid pressure $[M/LT^2]$
J	Objective function
N_s	Number of saturation measured points
N_p	Number of pressure measured points

T_s	Number of times with saturation data
T_p	Number of times with pressure data
SIM	Index which refers to simulated values
$MEAS$	Index which referes to measured values
$w_{s,i}$	Weighthing term for the saturation part of the objective function
$w_{p,i}$	Weighting term for the pressure part of the objective function
k^0_{rw}	End-point of water relative permeability
k^0_{ro}	End-point of oil relative permeability
S_{rw}	Water residual saturation
S_{ro}	Oil residual saturation
n_w	Shape exponent for water relative permeability
n_o	Shape exponent for oil relative permeability
$\mathbf{k_{efec}}$	Effective permeability tensor $[L^2]$
Δx	Grid spacing between two sucessive nodes in direction x $[L]$
Δy	Grid spacing between two sucessive nodes in direction y $[L]$
Δt	Increment between two time steps $[T]$
A	Transversal area $[L^2]$
N	Number of nodes which are used to discretize the work domain
V_i	Cell volume multiplied by porosity
Γ	Closed surface
$\mathbf{n}$	Inward normal vector
M_l	Mass accumulation term for fluid l
$\mathbf{F}_l$	Mass flux term
V	Arbitrary subdomain
R	Residual
ξ	Unknown primary variable
ε	Tolerance
$f'_{w,i}$	Fractional flow derivative with respect water saturation S_w
x_D	Adimensional spatial coordinate
t_D	Adimensional time
N_m	Total number of master points
α	Step size along the gradient direction
Δk^0_{rw}	Perturbation
$D_{i,m}$	Distance between point i and point m
$e_{i,m}$	Interpolation weight
$\{g\}$	Gradient of the objective function

Chapter 1

Introduction

1.1 Motivation and scope

The mathematical modeling and simulation of fluid flow in underground reservoirs is an indispensable tool for planning aspects associated with production petroleum and remediation of water resources. Flow simulation is used in order to evaluate different recovery (or remediation) processes, to make decisions regarding the placement of the wells, and to specify various operating procedures associated with injection and production wells.

The objective of reservoir evaluation is to decide on a reservoir management strategy. The reservoir engineer needs not only to match the past, but also has to forecast the dynamic behavior of a reservoir over its total production period in order to optimize hydrocarbon production. Predictions of production, and the corresponding uncertainties, are commonly performed with simulation models and inverse modeling.

Current geostatistical methods for reservoir characterization can be effectively used to integrate a variety of static data such as cores, logs, seismic, etc. Nevertheless, they are not well suited to directly integrate dynamic data, that are for example transient pressure response, or water breakthrough measurements. Realizations generated just based on static data tend to overestimate uncertainty in performance predictions. Therefore, to better estimate uncertainty in the predictions, the incorporation of dynamic data becomes primarily important. Besides, in general there are much more measurements of dynamic variables, which provide information about the direct response of the reservoir to recovery processes.

It is now common knowledge that inverse problem theory provides a methodology to integrate both static and dynamic data in reservoir characterization. In fact, the

inverse modeling tool is a key factor in drawing up the field development plan, and for managing the available reserver over time. There has been a continual progress in both computational algorithms and hardware, however, numerical simulation and inverse modeling of multiphase flow through porous media remains a challenging task. Improvements are still needed in order to make the approach fast, so it can be partially automated to complete history matches and forecasts of stochastic models as they are updated with the drilling of additional wells. The fact that inverse modeling yields nonunique reservoir description and the widespread recognition that reservoir heterogeneities largely control the performance of reservoirs, has served to motivate intense interest in reservoir characterization.

In parallel to the reservoir interest, soil and groundwater contamination by nonaqueous phase liquids (NAPL), such as contaminants from oil and gasoline leakage or other organic chemicals, has received increasing attention in recent years. The techniques used in petroleum engineering have given a base for the analysis of immiscible contaminant migration, and have been adapted to conditions typical in groundwater contamination. The NAPL related environmental concern, has motivated research activities in developing and applying multiphase flow and transport models for assessing NAPL contamination and the associated clean up operations. As a result, many numerical models and computational algorithms have been developed and improved for solving multiphase fluid flow.

Multiphase flow inverse modeling, so far, has mainly focused on estimating spatial distribution of absolute permeability. Among the various properties important for simulating reservoir behavior, the relative permeability functions may be by far the most poorly determined by present methods. Typically relative permeabilities are assumed to be known homogeneous functions within the reservoir domain, while generally they are obtained from core analysis. However, only few small core samples are taken within the reservoir, and therefore, they can hardly represent the entire reservoir. When cores are not available, the relative permeability functions might have to be obtained by analogy with other similar reservoirs.

Thus, during reservoir characterization, the assumption that the relative permeabilities are known homogeneous functions can be a major source of weakness. This lack of an addequate technique to estimate the spatial distribution of relative permeability in reservoir characterization has motivated the subject of this dissertation. What is proposed here is to develop a new technique to estimate both absolute and relative permeabilities spatial distributions from production data, such as pressures and saturations. The estimation of relative permeability simultaneously with absolute permeability is a strongly nonlinear problem, which dramatically increases the simulation

difficulties.

1.2 The importance of stochastic inverse modeling

Eventhough there are analytical solutions for single phase flow (e.g., De Marsilly, 1986; Bear, 1979) and multiphase flow (e.g., Buckley y Leverett, 1942; Morel and Seytoux, 1973), the solutions are obtained under very restrictive assumptions for the reservoir properties and geometry. Alternatively, there are methods that are hybrids of numerical and analytical solutions, for both one phase (e.g., Bakr et al., 1978; Gutjahr et al., 1978; Gelhar, 1986) and multiphase flow (e.g., Douglas, 1983; Dahle et al., 1990; Langlo and Espedal, 1994). These semi-analytical solutions can handle the spatial variability of hydraulic parameters as permeability, however they only can be applied under certain suppositions (in groundwater flow, small hydraulic conductivity variance or simple aquifer geometries and boundary conditions). The lack of an analytical solution, applicable to the real cases, brought on numerical solutions for groundwater flow and mass transport equations (e.g., De Marsily, 1986; Kinzelbach, 1986; Zhen and Bennet, 1995), and similarly with the multiphase flow equations (Aziz and Settari, 1979).

Predicting multiphase flow and mass transport processes in the subsurface by means of numerical simulation involves a number of steps, represented in Figure 1.1 (Sun, 1994; Deutsch, 2002):

I Developing a conceptual model of the natural system.

II Assigning values to the input parameters through the available static data.

III Running the model in order to predict the system state.

IV Interpreting the results and assessing the uncertainty of the predictions.

The first step is the most difficult and also most important task, because the conceptual model provides the basis for all the subsequent steps. The errors in the conceptual model usually have the largest impact on model predictions.

The second step, assigning parameter values, can be tedious because some of these properties display a large spatial heterogeneity, with possible variations of several orders of magnitude within a short distance. Moreover, while the equations for modeling many different displacement processes are fairly well established, the specification of the appropriate porous media properties to input into the flow simulator is an enormous problem. The characterization of the parameter spatial variability in a deterministic

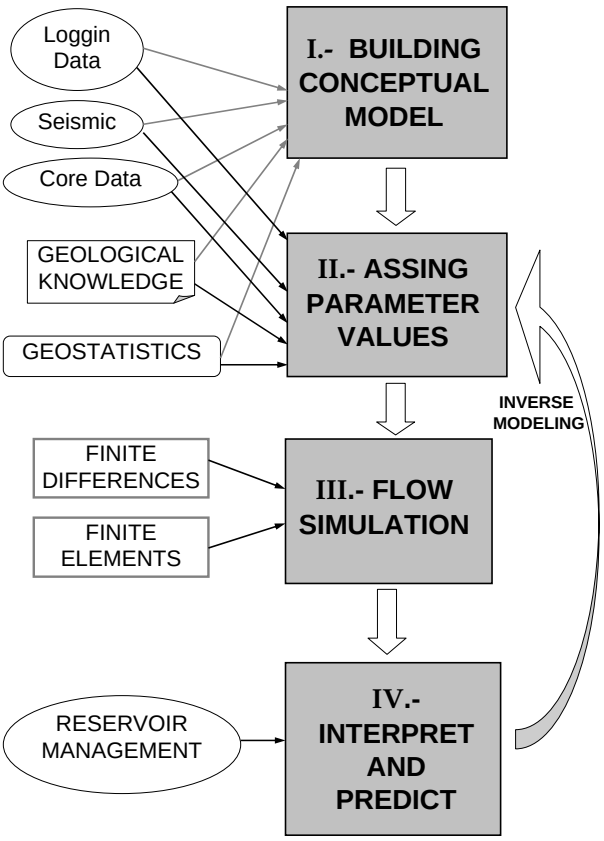

Figure 1.1: Here are schemed the different steps that should be followed when performing numerical model for flow simulation.

way is difficult, if not impossible. This fact was first pointed out by Matheron (1973) and Freeze (1975): *there is some structure in the natural spatial variability that can be characterized only in a statistical way*, and nowadays it is commonly accepted (Smith, 1981; Hoeksema and Kitanidis, 1985a; Sudicky, 1986). A stochastic framework has been addopted in order to give this statistical nature to the spatial distribution of parameters, resulting in more realistic models.

Another important task in the numerical modeling is the integration of static and dynamic data, particularly it is very effective in identifying preferential flow paths or barriers to flow that can adversely impact sweep efficiency. This integration of different data, here called inverse modeling, it is also termed with different names as parameter estimation, history matching and model calibration. All of them describe essentially the same technique with a slightly different objective in mind. During the last two decades a considerable number of inverse methods, for groundwater flow and transport modeling, have been developed towards the generation of hydraulic realizations conditioned on

different kinds of field data (e.g., Hoeksema and Kitanidis, 1984; Carrera and Neuman, 1986a; Rubin and Dagan, 1992; Sahuquillo et al., 1992; RamaRao et al., 1995; Oliver et al., 1996; Yeh et al., 1996; Wen, 1996; Gómez-Hernández et al., 1997; Oliver et al., 1997; Abbaspour et al., 1997; Hendricks-Franssen, 2001; Jang and Choe, 2002). Among them, the Sequential Self-Calibrated (SSC) method is computationally efficient and flexible for the fast generation of permeability realizations conditioning on both permeability and pressure data (Sahuquillo et al.,1992; Gómez-Hernández et al. 1997; Hendricks-Franssen, 2001).

There is also an enormous number of papers published about multiphase flow inverse modeling with historical data (Guérillot and Roggero ,1995; Roggero and Guérillot, 1996; Batycky et al., 1996a; 1996b; Batycky, 1997; Ates and Kelkar, 1998; Roggero and Hu, 1998; Vasco et al., 1999; Wu et al., 1999; Wang and Kovscek, 2000; Hu, 2000a; Hu, 2000b; Romero et al., 2000; Wen et al., 2002;). Wen et al. (1997) and Oliver et al. (2001) provide a thorough review of the most important inverse techniques.

In general, the aim is not only to search a single best estimate of the parameter spatial distribution, which matches the historical data. The best estimate is usually oversmoothed compared to the spatial variability observed in the reality. Modern inverse approaches have shown a great ability to construct multiple realizations of reservoir properties, having the same spatial variability as observed from field data, at the same time that honoring historical data. These techniques are generally within a stochastic framework and are used to find a measure of the uncertainty in the parameter estimates and, more importantly, in the response values of the models in which these parameters are used.

The propose of this dissertation is to develop a technique to incorporate dynamical data to better define both spatial distribution of absolute and relative permeabilities. The inverse philosophy followed is the same as the one of the Sequential Self-Calibrated method. This method is adapted for two-phase flow. The extensions of the Sequential Self-Calibrated method are: (i) to consider two immiscible fluids, (ii) to incorporate the information about the differential variation in water breakthrough and pressure response, (iii) to characterize the spatial variability of the relative permeability curves.

1.3 Why calibration of relative permeability curves?

Simulation of multiphase flow in porous media requires knowledge of relative permeability. The relative permeability is a macroscopic property that is defined through extensions of Darcy's law to multiphase flow. The relative permeabilities are satura-

tion dependent functions describing the fluid flow when several phases are present and flowing in a porous media. Accurate estimates of these functions are of great importance for proper exploitation of the petroleum resources. These functions are, however, inaccessible to direct measurement, and are typically determined through interpretation of flow data collected from laboratory displacement experiments in which one fluid is injected into a core sample that is saturated with another fluid or fluids. The interpretation of displacement data, at the core scale, is usually based on the application of semi-analytical approaches (Mitlin et al., 1999), or inverse modeling (Grimstad et al., 1997; Valestrand et al., 2002)

After estimating a relative permeability curve from the core sample, it is usually assumed that it represents the entire reservoir, being this assumption a major source of error. To the best of our knowledge, there exist few studies trying to estimate relative permeability curves at reservoir scale (e.g., Kulkarni and Datta-Gupta, 1999; Ates and Kelkar, 2000; Bennett and Graf, 2002), but none of them treats the heterogeneity of the relative permeabilities. Relative permeability is often assumed to control the part of the history match that corresponds to the saturation match, consequently not only absolute permeabilities should be adjusted in the inversion, but also relative permeabilities. This dissertation explores the development and application of an inverse modeling technique for the simultaneous calibration of absolute and relative permeabilities, considering their heterogeneous nature. Reservoir production data, such as well pressures and water saturations are used in the calibration.

1.4 Objectives and dissertation outline

The purpose of this dissertation is to develop and new two-phase flow inverse technique and to address practical issues related with the heterogeneity of relative permeability curves. To resume, the main objectives of this dissertation are:

- To perform a literature research on the methods for multiphase flow inverse modeling, looking for existing techniques which calibrate relative permeability functions to static and dynamic data. The research has to be focused on the estimation of relative permeabilities at reservoir scale.
- To develop a new two-phase flow inverse technique following the ideas of the SSC method, in what refers to perturbation on master points, static and dynamic data integration and generation of multiple realizations.
- To program a computer code that enables the automatic calibration of absolute and permeability parameters against static and dynamic measurements.

- To apply the developed technique to 1D and 2D cases in order to test its feasibility.
- To study the uncertainties related with relative permeability parameters.
- To study the influence of these parameters on the prediction of the reservoir performance, how important these parameters are to obtain a good model predictor.

This dissertation is organized as follows. Chapter 2 presents a literature review on relevant studies on stochastic simulation and inverse modeling of groundwater flow, mass transport and multiphase flow, conditioning on field data, with emphasis in the relative permeability calibrations. Chapter 3 recalls the general procedure of numerical solution of multiphase flow and presents the numerical difficulties that have to be taken into account. Chapter 4 is dedicated to the inverse technique for the generation of permeability realizations conditioned on both pressure and saturation data. The SSC method adaptation to two-phase flow is presented. Practical considerations related to the implementation of this technique are discussed. In chapter 5 different applications in 2D are tested. The consideration of additional data as seismic information is also analyzed in this chapter. In chapter 6 the worth of taking into account the heterogeneity of relative permeability curves is investigated, as well as the improvements get when conditioning on pressure and saturation data. Several uncertainty studies are described. This is done through a series of Monte Carlo analyses. Finally, chapter 7 summarizes the discussion and conclusions of this dissertation, recalls the limitations of the method proposed, and provides some guidelines for the future research directions.

Chapter 2

Literature Review

This chapter presents a literature review of the numerical modeling for groundwater and multiphase flow, inverse modeling and production data integration. It was pointed out before that calibration of relative permeability curves at reservoir scale still needs further research. Following this idea, this review of current approaches was focused in the search of existing methods to calibrate simultaneously absolute and relative permeabilities.

2.1 The beginnings

The beginnings of the studies about multiphase flow were developed in the field of petroleum engineering. One of the very first works published about this issue was the one of Buckley and Leverett (1942). Buckley and Leverett presented the basic equation that describe the movement of two immiscible fluids in one dimension. When petroleum is displaced by water, the Buckley and Leverrett's theory gives the equation to calculate the velocity of a constant water shock that is moving across a lineal medium. Buckley and Leverett found an analytical solution for the one dimensional horizontal flow, considering zero compressibility and no gravitational or capillary forces.

From the petroleum perspective, the starting research works about multiphase flow modeling in porous media were Douglas et al. (1959), Peaceman and Rachford (1962) and Coasts et al. (1967). Bear (1972) published the book *Dynamics of Fluids in Porous Media*, in which there is one chapter exclusively dedicated to the description of the physical phenomena related with multiphase flow in porous media. The paper of Morel-Seytoux (1973) had crucial relevance to merge the advances reached by petroleum engineers and hydrogeologists, in parallel until that moment. In Morel-Seytoux's study, it was shown that air and water fluxes in unsaturated porous media can be seen as a multiphase system. Thus, it was possible to apply petroleum experience to better

understand multiphase flow problems in hydrology.

In late seventies and early eighties, several seminal books dealing with the description of the multiphase flow, from a petroleum perspective, were published. The most relevant were: Dake (1978), Aziz and Settari (1979), and Marle (1981).

Because of the increasing concern over the environmental impact of nonaqueous phase liquids spilled into the subsurface, modeling multiphase systems has now become relevant for environmental and hydrogeology fields. The first works in this direction were Abriola and Pinder (1985a and 1985b) and Faust (1985).

After these initial studies there have been uncounted publications about multiphase flow from a petroleum and hydrogeologist point of view. Below there is a resume of the works that have been more significant for the development of the stochastic inverse simulation for multiphase flow.

2.2 Current numerical approaches for multiphase flow

The fundamental principles for multiphase flow are material and energy conservation. Each of the phases has its own properties and quantities such as viscosity and density and it is studied as if it filled all the medium, simultaneously with the other phase. Starting with this idea, the conservation equation can be directly applied to each of the phases. The mass-balance equation is derived by equating the rate of mass change, corresponding to a component, in a given control volume (Bear, 1979):

$$\frac{\partial\left(\phi\rho_l S_l\right)}{\partial t} + \nabla\cdot\rho_l\mathbf{u}_l = -q_l\rho_l \quad \text{para } l = o, w \tag{2.1}$$

where the subscripts w and o are phase qualifiers corresponding, respectively, to wetting (water) and non-wetting (oil) phases. The subscript l is a phase qualifier, $\mathbf{u}_l$ is Darcy's velocity of the phase $[L/T]$, S_l is the saturation (volume fraction of the total void space occupied by the phase l, with no dimensions), ϕ is the porosity (with no dimensions), ρ_l the phase density $[M/L^3]$, q_l is the injection/production rate per unit volume $[T^{-1}]$ and t is the time $[T]$. For injection the rate will be negative, while for production it will be positive. Equation (2.1) can also be used to describe a pseudo-three-phase system in which the third phase is assumed to be at constant pressure.

Darcy's law is an empirical expression that describes the relation between the flux and the fluid pressure. Since its discovery last century, it has been derived from the momentum balance equations (Dullien, 1979). Although Darcy's law was originally developed for one fluid that completely saturates the medium, it can also be applied to

describe the flow of each of the immiscible fluids, which move simultaneously. In this case, the permeability concept that defines the flow of one fluid, has to be modified depending on the quantity of the other fluid. Assuming that density and porosity are constant, and negligible gravitational effects, Darcy's equation for each of the phases l, can be expressed as:

$$\mathbf{u}_l = -\frac{\mathbf{k}k_{rl}}{\mu_l}\nabla p_l \tag{2.2}$$

where $\mathbf{k}$ is the absolute permeability $[L^2]$ of the porous medium, k_{rl} is the relative permeability of the phase l (no dimensions), μ_l is the phase viscosity $[M/LT]$ of the phase l, and ∇p_l is the pressure gradient $[M/L^2T^2]$. Relative permeability concept isolates mathematically the physical phenomena that explains the interference of each fluid phase with the flow of the other. The relative permeabilities are normally taken to be scalar functions of phase saturations, ranging between 0 and 1.

Substituting equation (2.2) into mass conservation equation (2.1), the formula to express the movement for each of the phases is:

$$\frac{\partial\left(\phi\rho_l S_l\right)}{\partial t} - \nabla\cdot\left[\rho_l\frac{\mathbf{k}k_{rl}}{\mu_l}\nabla p_l\right] = -q_l \quad \text{para } l = w, o \tag{2.3}$$

This generalization was introduced in the petroleum field rejecting the gravitational effects, and thus the equations appear in function of the pressure function gradient ∇p_l and not in function of the potential or piezometric heads. describes two-phase immiscible flow, these equations are completed with the next auxiliary relations:

1. Continuity of fluid saturations and pore volume,

$$S_w + S_o = 1 \tag{2.4}$$

   which simply says that the pore space is completely occupied by the two fluid phases.

2. Capillary pressure-saturation relationships,

$$P_c(S_w) = p_o - p_w \tag{2.5}$$

   P_c is the capillary pressure $[M/LT^2]$ function. It reflects the fact that two immiscibly mixed fluids will have different pressures due to surface tension.

3. Relative permeability-saturation relationships,

$$k_{rl} = k_{rl}(S_w) \tag{2.6}$$

Other assumptions taken for two-phase immiscible flow formulation, include unique functional relations for $P_c(S_w)$ and $k_{rl}(S_w)$, ignoring hysteresis and organic liquid entrapment. Non linearities inherent in the above system of equations (2.5) are due to capillary pressure P_c and relative permeabilities k_{rl}, which can be approximated as functions of saturation. The relative permeability dependence with saturation is commonly represented by either a set of tabled values or in a functional form such as those described by van Genuchten (1980) and Brooks and Corey (1966).

These partial differential equations (2.3)-(2.6) are the basic equations used to describe the flow of two immiscible fluid phases in underground reservoirs. The state quantities are pressures and saturations for each fluid phase, as a function of position and time.

There are two main methods to solve the system of equations (2.3)-(2.6). Analytical methods (Buckley and Leverett, 1942; Morel and Seytoux, 1973) have been used for more than a century to deal with differential equations. On the other hand, numerical approaches have also existed for many years, but they were not fully exploited until the development of computers to solve approximate forms of the governing equations (Aziz and Settari, 1979). The main power of the analytical methods is their capability in many cases to produce exact solutions in terms of the controlling parameters. The analytical methods provide an insight into how the processes control flow, at the same time that can be used to check on the accuracy of numerical methods, which can be subjected to a variety of different errors. To solve real problems analytical methods are not useful as only work under very restrictive conditions on the geometry and the medium and fluid properties. Hence, equations for multiphase flow have to be solved with numerical approximations complemented with a suitable set of initial and boundary conditions. As it has been mentioned in the introduction, in addition there are hybrid methods of numerical and analytical solutions (e.g., Douglas, 1983; Dahle et al., 1990; Langlo and Espedal, 1994), but they also have the limitation of being applicable only under certain circumstances.

2.2.1 The choice of primary variables

The system of equations (2.3)-(2.6) is very difficult to solve because of two main reasons: the highly non linear nature of the coupled partial differential equations governing the system, and the lack of reliable constitutive data for these problems. These difficulties have led many researches to explore alternative forms of the governing equations, and to seek specialized numerical algorithms that can improve the computational performance of the simulators. These studies have identified that the different choices of primary variables not only impact on the computational performance of a numerical code, but

may also determine the feasibility of a numerical modeling study in field applications (Forsyth et al., 1995; Forsyth et al., 1998).

Recent studies regarding general recommendations for selecting primary variables in the mathematical formulation for the multiphase flow modeling through porous media are the ones of Wu and Forsyth (2001) and Kees and Miller (2002). Wu and Forsyth (2001) propose a dynamic variable switching or variable substitution scheme, in order to achieve optimal numerical performance and robustness.

The most common possibilities for the election of the solution variables are (Aziz and Settari, 1979, Kiss and Miller, 2002): two fluid pressure, pressure and saturation or fractional flow approximations. Let's describe these three approximations.

Two fluid pressures approximation

The governing equations are written in terms of the fluid pressures. Expanding the accumulation derivatives in terms of capillary pressure, equations (2.3) can be rearranged as (Abriola and Rathfelder, 1993):

$$\begin{aligned}\phi\rho_l C_l\left[\frac{\partial p_o}{\partial t}-\frac{\partial p_w}{\partial t}\right]+\phi\rho_l S_l\beta_l\frac{\partial p_l}{\partial t}+\frac{1}{2}\rho_l S_l\phi^0\beta_m\left[\frac{\partial p_o}{\partial t}+\frac{\partial p_w}{\partial t}\right]-\\ -\nabla\cdot\left[\frac{\mathbf{k}k_{rl}}{\mu_l}\nabla p_l\right]=-q_l\end{aligned} \tag{2.7}$$

where β_l and β_m are the l-fluid and matrix compressibilities LT^2/M ,ϕ^0 is the porosity at the reference pressure, and $C_l = \partial S_l/\partial P_c$ is the l-fluid capacity coefficient. This pressured-based approximation can easity consider the matrix and fluid compressibility effects. Anyway, these effects are often neglected in typical contaminant hydrology applications (Faust, 1985; Kaluarachchi and Parker, 1989; Kueper and Frind, 1991; Abriola and Rathfelder, 1993), as, for example, they are neglected in this dissertation. This approach has been used very often in hydrology and nowadays it is adopted by a considerable number of authors (i.e., Pinder and Abriola, 1986; Kaluarachchi and Parker, 1989; Sleep and Sykes, 1989; Abriola and Rathfelder, 1993; Schrefler and Xiaoyong, 1993). This formulation is limited to situations where both phases are present through the domain (Abriola and Rathfelder, 1993), i.e., this method is unable to handle situations often involved in environmental simulations, when one of the phases disappears and the pressure of that phase is poorly defined.

Pressure and saturation approximation

It is possible to reformulate the governing equations in terms of a saturation and pressure of whichever phase is present throughout the simulation. The second phase

pressure can then be removed from the equations by expressing it in terms of the saturations and pressures of the other phase, using equations (2.4) and (2.5) the system (2.3) is:

$$\begin{aligned} \phi\frac{\partial S_w}{\partial t} - \nabla\cdot\left[\frac{\mathbf{k}k_{rw}}{\mu_w}(\nabla p_o - \nabla P_c)\right] &= -q_w \\ -\phi\frac{\partial S_w}{\partial t} - \nabla\cdot\left[\frac{\mathbf{k}k_{ro}}{\mu_o}\nabla p_o\right] &= -q_o \end{aligned} \tag{2.8}$$

The importance of this method is its suitability for problems where one fluid completely saturates the medium and the other one disappears. In the formulation of equations (2.8) this would mean $S_o = 0$, because S_o does not appear explicity. The pressure-saturation formulation has been employed by several authors (Faust, 1985; Kueper and Frind, 1991a and 1991b; Forsyth et al. 1995; Binning and Celia, 1999).

Fractional flow approximation

This approach is motivated almost exclusively by the petroleum reservoir simulation. One of its main characteristics is that it is necessary to formulate streamline simulators. The basic idea of the fractional flow definition, f_w, is to treat the total multiphase flow as a single mixed fluid, and then describe individual phases through fractions of the total flow,

$$f_w = \frac{\mid \mathbf{u}_w \mid}{\mid \mathbf{u}_T \mid} \tag{2.9}$$

Total flux $\mathbf{u}_T$, can be defined as the sum of the phase volumetric fluxes:

$$\mathbf{u}_T = \mathbf{u}_w + \mathbf{u}_o \tag{2.10}$$

Under the assumption that fluids are incompressible, if (2.4) and (2.10) are applied to (2.1), divergence of total Darcy's velocity is obtained:

$$\nabla\cdot\mathbf{u}_T = -(q_o + q_w) = -q_T \tag{2.11}$$

In one dimesion this equation has the particularly simple solution that the total flux is constant in space and it is determined by boundary conditions.

P is the total (or global) fluid pressure. It is defined as the pressure that would produce the flow of a fluid of a mobility (k_{rl}/μ_l) equal to the sum of the flows of fluids w and o,

$$\mathbf{u_T} = -\mathbf{k}\left(\frac{k_{rw}}{\mu_w} + \frac{k_{ro}}{\mu_o}\right)\nabla P \tag{2.12}$$

the use of this variable reduces the coupling between pressure and saturation equations.

With these definitions the water flux can be expressed as a function of the total flux with the help of the fractional flow function:

$$\mathbf{u}_w = \mathbf{u}_T f_w \tag{2.13}$$

Using this formulation (2.13), the mass-balance equation (2.1) for the water can be expressed as:

$$\phi \frac{\partial S_w}{\partial t} + \nabla \cdot (\mathbf{u}_T f_w) = -q_w \tag{2.14}$$

developing the second term,

$$\phi \frac{\partial S_w}{\partial t} + \mathbf{u}_T \cdot \nabla f_w + f_w \nabla \cdot \mathbf{u_T} = -q_w$$

Substituting the equation (2.11) and assuming that f_w is function of saturation ($\nabla f_w = \frac{df_w(S_w)}{dS_w} \nabla S_w$), equation for the two-phase flow in function of the fractional flow is:

$$\phi \frac{\partial S_w}{\partial t} + \mathbf{u}_T \cdot \frac{\partial f_w}{\partial S_w} \nabla S_w = f_w q_T - q_w \tag{2.15}$$

Total Darcy's velocity $\mathbf{u_T}$ is derived from the solution to the total pressure field (equation (2.10)).

This approach leads to two equations: a saturation equation (2.15), that is parabolic for S_w and it has an advection diffusion form, and a global pressure equation ((2.10) and (2.12)) whose form is elliptic for P. The advective term is nonlinear and usually leads to shock formations.

Examples about the use of this approximation can be found in Douglas (1983), Morel-Seytoux and Billica (1985a y 1985b), Dahle et al. (1990) Wagen (1993), Langlo and Espedal (1994) and Chen et al. (1995). The principal drawbacks of the fractional flow approach are: complex to be applied in three dimensions, poor performance for general boundary conditions, and difficult performance in more general problems involving heterogenous material properties (Binning and Celia, 1999). On the contrary, the great advantage is its low computational costs.

2.2.2 Numerical approximation

Numerical simulation of multiphase flow, expressed with any of the mentioned approximations, can be performed with several techniques:

- **Finite differences:** This is the method addopted in this dissertation, so it will be explained in detail along next chapter. Examples of its applications are

Abriola (1985), Morel-Seytoux and Billica (1985), Faust (1985) and Kueper and Frind(1991).

- **Finite elements:** It overcomes the difficulties in the treatment of complicated geometry and boundary conditions. It has been applied by a high number of authors like Li et al. (1990), Schrefler and Xiayong (1993) Forsyth et al. (1995), Chen et al. (1995) and Kim et al. (1996)).

- **Techniques based on the characteristics method for the saturations equation:** This method is used when the equations are expressed in function of fractional flow (Douglas, 1983; Dahle et al., 1990; Langlo and Espedal, 1994).

- **Streamline simulators:** Streamline based methods have received significant attention over the last years. Nowadays they are accepted to be an effective and complementary technology to more traditional flow modeling techniques as finite differences and finite elements. A comprehensive review of the theoretical basis for streamline simulation technology can be found in Batycky (1997) and Thiele (2001). The key principles are to express the mass conservation equation in terms of the time of flight and to reproduce the 3D solution by combining one dimensional solutions along streamlines. One benefit of streamline simulators is its inherent memory and computational efficiency, being for many problems 2 to 3 order of magnitude faster than conventional finite difference simulators. Applications of streamline simulators in different cases have been performed by Batycky and his team (e.g., Batycky et al., 1996a and 1996b; Batycky, 1997).

Several works comparing the different behavior of the different approaches can be found in the literature. Young (1984) compares the sensitivity to the grid size and orientation. Ewing (1991) reviews numerical techniques for the solution of the pressure equations in the fractional flow approach, and demonstrates the importance of accurate determination of velocities. Abriola and Rathfelder (1993) analyse the mass balance errors, and Binning and Celia (1999) study the advantages and disadvantages of the characteristics method. Recently, the control volume finite element method and the control volume function approximantion (Li et al., 2003) have been developed to enforce the conservation property and get accurate fluid velocities using finite element methods.

For temporal discretization there are also several choices, being the fully-implicit time stepping the dominant approach in hydrology, while in traditional petroleum engineering literature the predominant approach is the explicit or semi-explicit.

Anyway, it should be pointed out that a non mass conservative numerical scheme may still give accurate and correct solutions with mass conservative results as long as

both spatial and temporal discretization are sufficiently small. A mass conservative solution may not guarantee the accuracy of the solution. In other words, the ability of a numerical model to conserve mass is a necessary but no sufficient condition for convergence (Cella et al., 1990).

When the working scale is large a great computational time is required. There has been a huge advance in new computational algorithms for solving the problem faster and with better discretization. This fact, and the extraordinary advances in computer hardware have resulted in quite good algorithms and codes that allow to perform fairly efficiently the multiphase flow simulation. Although, it is always desirable to obtain more speed and capacity for computing to achieve better model discretization and characterization. Consequently, numerical simulation of multiphase flow remains a challenging task. In Wu et al. (2002) there is a review of the last advances, and the presentation of a new technique that allows to improve the compute efficiency with the parallel-computing method (Larsen and Bech, 1990).

2.3 Inverse stochastic simulation

2.3.1 Stochastic framework

Until the eighties decade, most reservoir descriptions employed in simulation models consisted of a layered system, where along each layer the petrophysical and flow properties (permeability, porosity, dispersivity, etc.) were homogeneous. This view of modeling a reservoir suffered a major revolution with the recognition that it can be impossible to characterize the natural variability in a deterministic way (Freeze, 1975). This natural heterogeneity of the medium properties affects significantly the flow behavior through porous media (i.e., Miller et al., 1998 and its references). Unfortunately, it is quite difficult to characterize the heterogeneity of the different properties because they are sampled at few locations, they are defined at laboratory scale, and they must be specified at every location represented in the numerical model by smooth interpolating the data at sampled locations. For example, porosity is generally less variable than permeability, and can be measured fairly directly by well logging or experiments on reservoir core samples, but permeability is much more heterogeneous, and difficult to measure.

Stochastic analysis revealed to be a method that permits to model the spatial variability of heterogeneous hydraulic properties, by a space random function characterized by its multivariate distribution (Matheron, 1973; Freeze, 1975; Smith, 1981; Hoeksema and Kitanidis, 1985a; Dagan, 1986; Sudicky, 1986). In the stochastic framework, with a few selected statistical parameters of the subsurface properties such as mean and

variance, the overall variability of the flow processes can be determine. Geostatistical techniques provide efficient tools to generate equi-probable distributions of unknown fields from sampled data.

2.3.2 Inverse modeling problem

With the stochastic analysis the model can be established, in a relatively easy way, to generate plausible reservoir models that reproduce static data such as well logs, core analysis, stratigraphic interpretations, geostatistical data analysis, seismic data, analog studies, outcrop information and geological setting models. However, it is far more difficult to generate plausible reservoir models that reproduce dynamic data such as transient pressures, saturations, and flow rates. The origin of the lack in the reproduction of dynamic data is the non linear connection between parameters and production data (e.g., relative permeabilities and saturation data in a heterogeneous reservoir). Classical inverse modeling techniques consisted on the modification of relative permeabilities, porosity and permeability at each grid block. The results of the classical inverse modeling is that the reservoir model no longer matches the geologic interpretation, the log data, or the core data. Thus, once the flow equations and the stochastic model are established still remains the problem of estimating the properties from the available data in such a way that the historical data are reproduced.

Traditionally, permeability estimates have been obtained from well-tests. Well-tests are essentially reservoir-scale experiments in which the fluid pressures at wells are observed in response to a perturbation in the flow rate. Historically, well-tests have been interpretted using simplified solutions, assuming uniform properties, and with graphically-based procedures. Well-test analysis provides good insight into the average properties of the reservoir at the vicinity of a well.

Calibration (also termed parameter estimation, history matching or inverse modeling) of the numerical model using the observations of the response of the system has revealed to be a much efficient technique than well-testing. This technique permits to integrate the heterogeneity pattern of the system given by the dynamic variables. These type of data differ from well-tests in that they are usually available over a longer period of time, and may include a number of wells. The flow encountered in these situations is usually much more complex than in the controlled well-test. Integration of dynamic data has revealed its importance in constructing more realistic geological models. For example, pressure data carry important information on the spatial variation of reservoir permeability (Wen et al., 1996) or tracer data on the connectivity features in the underlying permeability field (Harvey and Gorelick, 1995).

Reservoir history matching is a difficult problem, which has historically been carried

out with trial and error processes. Nowadays the automatic history matching is used to achieve a solution to the inverse problem. Automatic inverse modeling is based on minimizing an objective function, J, which includes a sum of squared production data mismatch terms:

$$J = \sum_{t=1}^{T_s} \sum_{i=1}^{N_s} w_{s,i} (S_{i,t}^{SIM} - S_{i,t}^{MEAS})^2 + \sum_{t=1}^{T_p} \sum_{i=1}^{N_p} w_{p,i} \left(p_{i,t}^{SIM} - p_{i,t}^{MEAS}\right)^2 \tag{2.16}$$

N_s and N_p are, respectively, the number of saturation and pressure measured points. T_s and T_p are, respectively, the number of times in which saturation and pressure are measured, and the indexes SIM and $MEAS$ are referred to simulated and measured values. $w_{s,i}$ and $w_{p,i}$ are weighting terms.

Minimization is done based on least squares methods (linear or non linear multiple variable regression) or optimization routines, which due to the non linearity of the parameters requires the usage of iterative processes.

One of the first works presented for automatic history matching was the one of Jacquard and Jain (1965). They applied the gradient method to the estimation of permeability in a two dimensional reservoir from pressure data obtained under single-phase flow conditions. They based their procedure on the computation of sensitivity coefficients, using an electric-circuit analog, and used zonation to limit the number of parameters to be estimated. Later, motived by Jacquard and Jain's ideas, Carter et al. (1974) presented a derivation of the method to compute sensitivity coefficients for two dimensional single-phase flow problems. This procedure can be applied to compute sensitivity of simulator grid block pressures to all grid block permeabilities and porosities. Despite their efficiency, these initial studies are limited by the fact that they are restricted to linear problems and consequently are not applicable to multiphase flow problems.

2.3.3 Ill-posedness

The minimization problem is said to be ill-posed as its solution does not guarantee the following properties (Carrera and Neuman, 1986a; Sun, 1994):

- **Existence:** The observation error (or noise) of state variables cannot be avoided. As a result, an accurate solution of the inverse problem may not exist.

- **Uniqueness:** Different combinations of hydrogeologic conditions may lead to similar observations of production variables. Hence, it is impossible to uniquely determine the particularities of the reservoir by only observing the state variables.

- **Stability:** Instability frequently results due to poor degree or lack of one-to-one-ness in the pertinent operator. This feature produces a flat objective function surface around minima.

For example (Watson et al., 1994), the estimation of the absolute permeability $\mathbf{k}(\mathbf{x})$ (equation (2.2)) from pressure data taken at a well $p(\mathbf{x_0}, t)$. The estimation of $\mathbf{k}(\mathbf{x})$ in two or three dimensions cannot be appropriately done from the one dimensional data $p(\mathbf{x_0}, t)$. This feature results in non uniqueness in the solution. It is also possible that no minimum of the objective function exists, or that two different sets of $\mathbf{k}$ give two different $p(\mathbf{x_0}, t)$ which are close. This makes inversion to be unstable.

In order to mitigate or eliminate these problems more information, apart from the state variable observations, can be used. The technique known as regularization is a way of alleviating the ill-posedness of inverse problems through the incorporation of prior constrains or information into the objective function (Sun, 1994). Carrera and Neuman (1986a, 1986b and 1986c) used prior information to modify the likelihood function and showed that the use of prior information reduces the ill-posedness of the problem. In this sense, the introduction of prior data is similar to a regularization of the ill-posed problem as reduces the non uniqueness, but also reduces the instability in the computational algorithms (Chu et al., 1995).

2.3.4 Optimization algorithms

There are a number of strategies to find parameter combinations that yield smaller values of the objective function, eventually identifying a local or hopefully global minimum. The available algorithms can be classified as follows (Sun, 1994):

- **Search methods:** In this kind of methods the objective function is evaluated for different parameter combinations, mapping out the objective function in the n-dimensional parameter space, looking for the minimum. While no derivatives of the objective functions with respect to the parameters must be calculated, these methods usually require many function evaluations and are therefore inefficient. Examples of search methods include trial-and-error, Fibonacci section search, golden section search and quadratic interpolation method. Detailed discussions about these methods can be found in any textbook on numerical optimization (e.g., Scales, 1985).

- **Gradient based methods:** For this set of methods it is required the calculation of the gradient of the objective function with respect to the parameter vector, along the direction given by the gradient. The procedure is robust, but time expensive. The basic gradient method is steepest descent method, which uses the

negative gradient direction as the search direction in each iteration. However, steepest descent usually terminates far from the solution due to round-off effects. Instead, a conjugate gradient method as the one of Fletcher and Reeves allows to find the minimum more efficiently (Carrera and Neuman, 1986b). For conjugate gradient methods the computational requirement for each iteration is relatively low, but the number of iterations required can be large, especially for multiphase flow problems (Makhlouf et al., 1993). Other possibility is the adjoint method, which is very efficient because the flow problem and the adjoint sensitivity problem have the same form, hence the calculation of the sensitivity coefficients is straightforward. The adjoint method has also been applied to multiphase flow problems, altough in many cases it resulted to be high computationally cost. Carrera and Neuman (1986b) studied the convergence when switching from one method to another when the former slows down or fails to convergence. Their conclusion is that changing the optimization algorithm, an improvement in the rate of convergence can be obtained.

- **Second order methods:** When the method is based on the Hessian matrix, instead of the gradient, the approach is known as second order method. The computational cost of calculating the second derivatives is compensated with a rather efficient stepping in the parameter space. Examples of second-order methods are Newton method, Gauss-Newton method and Levenberg-Marquardt method. Standard implementations of these algorithms require calculation of sensitivity coefficients, which formally represents the derivative of predicted variables with respect to the model parameters. An excellent review of methods for computing sensitivity coefficients and solving inverse problems was presented by Yeh (1986). Chu et al. (1995) presented an efficient method of computing sensitivity coefficients. Additional information can be incorporated when it becomes available. This method yields a smoothed version of the true distribution. Wu et al. (1999) presented a good review about the calculation of sensitivity coefficients, and developed an algorithm to use the adjoint method to get the sensitivity matrix for a two-phase flow problem, in a way that the Gauss-Newton method can be used for inverse modeling. The drawback is that the adjoint approximation needs storage of pressures and saturations for all the nodes and times of discretization. There exist analytical developments of sensitivity parameters for the multiphase flow like the ones of Ates and Kelkar (1998) or Vasco et al. (1999). Applications of Gauss-Newton method and the calculation of sensitivity coefficients in the integration of well-test information, production history and time-lapse seismic data can be found in the work of Landa (1997 and 2001).

- **Heuristic methods:** The most common are simulated annealing (Hegstad et al., 1994) or genetic algorithms (Romero et al., 2000). These methods sample a much larger solution space than gradient methods and increase the likelihood of obtaining global minimums to the objective function. However, their convergence is reached quite slowly.

2.4 Inverse modeling methods

Depending on the assumptions taken, the optimization algorithm, the way the parameters are estimated, or the strategy for inversion, there are many different kind of methods for inversion. The most extended methods are the ones that calibrate perturbing non calibrated realizations of the model. For this type of methods the efficiency depends on the way realizations are perturbated. For an extensive and comprehensive review about the existing methods for integration of production data in reservoir models, it is recommended to look at Wen et al. (1997), Oliver et al. (2001) or Hendricks-Franssen (2001), and the references contained therein. In this section it is presented a brief resume of the principal methods, developed until present time, that integrate dynamic variables through inverse modeling. In Zimmerman et al. (1993) there is a complete study comparing some of the inverse approaches described here. The main conclusion achieved on this study was the importance of the appropriate selection of the variogram and the time and experience devoted by the user of the method in analyzing and modeling the observed data.

2.4.1 Cokriging method

Cokriging is a geostatistical tool for estimating two or more random fields together by using their measurements, when they are correlated. This method was applied to inverse groundwater modeling by Dagan and Rubin (Dagan, 1985; Rubin and Dagan, 1987a; Rubin and Dagan 1987b; Dagan and Rubin, 1988) and Hoeksema and Kitanidis (Hoeksema and Kitanidis, 1984; Hoeksema and Kitanidis, 1985b). The unknown transmissivity value at a point is estimated by a weighted linear combination of the observed transmissivity and pressure. Dagan (1985) and Rubin and Dagan (1987b) showed that when the random transmissivity and pressure fields are jointly Gaussian with known mean and covariance, the cokriging estimate and cokriging covariance are equivalent to the conditional mean and conditional covariance of the new joint probability distribution function conditioned on the measurements. The statistical parameters are estimated by the maximum likelihood method that includes linearizations of the steady state flow equations. Analytical expressions of cross-covariances of permeabi-

lity and pressure are obtained assuming uniform flow and infinite domain. Harvey and Gorelick (1995) have applied the cokriging method to flow and tracer transport integrating tracer arrival time data, concluding that it improves the accuracy of the permeability estimation.

As transmissivity and pressure are non linearly related, the classical cokriging method needed a modification. To overcome this problem Yeh et al. (1996) proposed an iterative stochastic inverse method to estimate transmissivity and pressure fields that account for transmissivity and pressure data. It first estimates a transmissivity field by cokriging from the available transmissivity and steady state pressure data. The flow equation is then solved numerically to obtain a pressure field. The covariance and cross-covariance of transmissivity and pressure are then updated and a new transmissivity field can be obtained by again cokriging using the updated covariance and cross-covariance. This process is continued until the variance of estimated transmissivity stabilizes. Later the method has been changed in the sense that a Monte Carlo simulation approach is adopted (Hanna and Yeh, 1998) to account for the mass conservation of the approach. The method requires significant computational effort, while its advantages are that it is very simple to implement and has not suffered from convergence problems.

2.4.2 Fast Fourier transform method

This method was developed by Gutjahr (Gutjahr, 1989; Gutjahr et al., 1993), and allows to condition to both transmissivity and pressure data by using linearization and fast Fourier transform method. The covariance and cross-covariance are represented as functions of the spectral and cross-spectral density. Transmissivity realizations conditioned to the pressure data are constructed by adding the difference between the unconditional simulation and kriged values of the unconditional simulation to the kriged values using the field data. The key assumption is the linearized flow equation as in the linearized cokriging method. Later this method has been extended to account for the non linear relationship between transmissivity and pressure in the computation of the pressure covariance and the pressure-transmissivity cross-covariance using an iterative approach (Gutjahr et al., 1994). This technique is very efficient and is capable to generate many realizations with modest computing resources over times on the order of minutes.

2.4.3 Pilot point method

The pilot point method (de Marsily et al., 1984) reproduces pressure data by calibrating the transmissivity field. The method starts by generating a conditional simulation of the transmissivity field with geostatistical techniques. Then, the generated field is modified by adding other transmissivity data at some select locations (called pilot points). Adjoint sensitivity analysis is used to determine the locations where additional transmissivity data should be included in order to improve the reproduction of the pressure data. The new transmissivity data at the selected pilot points are treated as local data, a new conditional realization of transmissivity is then generated, and, the flow model is run again. The iteration of adding pilot points is continued until a least-squared error criterion is met or the addition of more pilot points does not improve the calibration. One of the disadvantages of this method is that is very CPU intensive.

Lavenue and Pickens (1992) and Ramarao et al. (1995) applied the pilot point method to reproduce pressure data. In their work, they generated a selected number of conditionally simulated transmissivity fields and calibrated each of the fields to reproduce the pressure data.

2.4.4 Self-calibrated method

This method is also an iterative geostatistical based inverse technique, which reduces the parameter space to be estimated in the optimization process. The conditioning to pressure is done by solving the groundwater flow equation, not through any linearization. It was introduced by Sahuquillo et al. (1992), and developed later by Gómez-Hernández and others (Gómez-Hernández et al.,1997; Capilla et al., 1997; Capilla et al., 1998). It was the first inverse stochastic simulation method to construct multiple equiprobable transmissivity fields honoring single-phase historical pressure data.

In the self-calibrated method the spatially variable transmissivity values are parameterized as the sum of a seed transmissivity field, obtained by standard geostatistical techniques, plus a perturbation of the entire field, which is expressed as a linear function of the perturbations at a selected number of locations referred to as master blocks. This approach can also account for uncertainty in flow boundary conditions (pressure or flowrate).

The self-calibrated method basic ideas and numerical schemes will be addopted in this dissertation for the development of a two-phase inverse modeling method, therefore, more details about the self-calibration method can be found in the following chapters.

In Wen et al. (1998) the self-calibrated method was extended to integrate production data, such as fraction flow rate data and pressure at production wells. To

reach this aim a streamline based multiphase flow simulator was adapted for fast flow simulation. One dimensional single-phase analytical streamline solution was utilized for fast calculation of fractional flow sensitivity coefficients.

The self-calibrated method has also been extended by Hendrics-Franssen (2001) to handle transient groundwater flow, joint conditioning of transmissivity and storativity fields, and to couple inverse modeling of groundwater flow and mass transport (the objective function also includes the mismatch corresponding to concentration data).

An application of the self-calibrated method to two-phase flow has been presented by Wen et al. (2002), using multiphase production data to estimate the spatial distribution of lithofacies in 2D.

2.4.5 Maximum likehood method

This is a general non linear technique that estimates reservoir parameters using prior estimates along with transient or steady state pressure data. Early development of this method was presented in a series of three papers of Carrera and Neuman (Carrera and Neuman, 1986a; Carrera and Neuman, 1986b; Carrera and Neuman, 1986c). Parameter estimation is performed using the maximum likelihood theory, incorporating the prior information into the likelihood function. The non linear flow equation is solved by a numerical method.

The likelihood function expresses how likely are the parameteres to have producted the observed data. The method of maximum likelihood consists of finding the specific value of the parameter that is most likely to have produced the data. The inverse problem solution is obtained iteratively. The most important characteristic of the method is that aquifer parameters are estimated for a limited number of zones which partition the aquifer. Different parameteres can be estimated for each zone such as, values and directions of principal hydraulic conductivities in anisotropic media, specific storage, boundary conditions, or recharge rates. This method is also computationally intensive in the optimization process.

2.4.6 Markov Chain Monte Carlo Method

In the Bayesian approach, parameters are taken as random and through the differential equation the state variables are also random, yielding the same results as conceptualized from the geostatiscal approach. The method has been proposed by the team at the Norwegian University of Science and Technology to integrate historical production data (Hegstad et al., 1994; Omre and Tjelmeland, 1997; Tjelmeland and Omre, 1997; Hegstad and Omre, 1997). This team was one of the pioneers in the applications of

Markov chain Monte Carlo methods to the earth science for generating realizations from a specified (but unnormalized) probability density function in reservoir characterization. Inspired by their work, Oliver and others (Oliver et al., 1996; Oliver et al., 1997) employed the Markov chain Monte Carlo method for the generation of reservoir models that are conditional to transient pressure data. The most probable model (the maximum a posteriori estimate) conditioned to both prior information and pressure data is obtained by minimizing an objective function derived directly from the a posteriori probability density function. The decision to accept or reject the resulting history matched realization is made on the basis of the Metropolis-Hastings algorithm. As in most of the methods mentioned until this point, with the exception of the fast Fourier method, in many applications the computational demands of the simulator can greatly restrict the number of forward simulations that can be carried out. Consequently, the Markov chain Monte Carlo method is hard, or even impractical, to implement. One way to overcome this difficulty is to us the multi-scale computational model. Slightly following the ideas suggested by Celia et al. (1993), Higdon et al. (2002) speed up the forward simulator by running it on a smaller, coarsened version of the original inputs. Then, use the resulting posterior simulation output to guide and speed up the posterior simulation on the original, fine-scale specification.

2.4.7 Simulated annealing method

Simulated annealing has its basis in statistical theory, being a flexible and generally applicable heuristic optimization technique (Hegstad et al., 1994). It does not require neither a functional form for the covariances, nor gradient calculations. A perturbation is applied in a set of grid blocks and an energy objective function is evaluated. The decision of wether accepting or not the perturbation is based on the change of energy caused by this perturbation. Its extensive use arises from the fact that additional data constraints can be incorporated by a simple modification of the objective function and its success in generating parameter fields that give a good approximation to the global minimum of the objective function. The computational costs become immense if the objective function includes production data that must be generated at each iteration by solution of a forward problem using a reservoir simulator. It belongs to the class of Markov chain Monte Carlo techniques, but when it is used without careful consideration of the stopping temperature, the results will not be random realizations from the correct probability density function.

Datta-Gupta et al. (1995) were able to use the simulated annealing method to generate stochastic permeability fields conditioned to both spatial statistics and tracer data. They also applied it to water-oil displacement calculations. Several examples of

simulated annealing usage for estimating model parameters in order to solve remediation management problems are provided in Finsterle and Pruess (994).

2.4.8 Genetic Algorithms

In the same way that simulated annealing is applied to address the optimization problem, the genetic algorithms have been used for reservoir engineering in several works, including those by Romero et al. (2000), Romero et al. (2000b) and Romero and Carter (2001). Genetic algorithms are a class of optimization methods which draw on ideas from natural evolution and genetics. They are randomized search algorithms based on an analogy to the mechanics of natural selection according to the Darwinian evolutionary theory and the survival of the fittest principle. In the case of Romero et al. (2000) and Romero and Carter (2001) the genetic algorithms has been applied to optimize the inversion problem in which the pilot points method (de Marsily et al., 1984) is used. Like the simulated annealing method the genetic algorithm has a slow rate of convergence and is computationally inefficient. The main attractions of simulated annealing and genetic algorithm formulations are their simple integration of static data and their ability to converge to the global minimum of the objective function whereas in the gradient based methods it is common to end up in a local minima or a saddle point.

2.4.9 Two-step inversion for multiphase flow

A two step inversion method was developed by Vasco et al., 1999. This method utilizes a multiphase streamline simulator as a forward model. The parameter sensitivities are formulated in terms of one dimensional integrals of analytic functions along the streamlines. The integration of dynamic data is then performed using a two-step iterative inversion: (1) match the breakthrough times at the producting wells and (2) matching the production history. The pressure and streamlines are recalculated for each iteration during inversion. The approach follows from an analogy between streamlines and ray tracing in seismology. One advantage is that sensitivities for all the reservoir parameters require a single simulation. Yoon et al. (1999) have extended this approach to multiscale, relying on a hierarchical parameterization and a scale-by-scale inversion of the production response. With this extension, they are able to account explicitly for varying data resolution.

Another two-step approach was presented by Wang and Kovscek (2000). However, their method does not compute sensitivity coefficients nor is their formulation of the inverse problem similar to Vasco et al's approach. Their basic idea is to relate the

fractional flow curve at a producer to the water breakthrough of individual streamlines. By adjusting the effective permeability along streamlines, the breakthrough time of each streamline is found that reproduces the reference producer fractional-flow curve. The second step is to map the streamline permeability modification onto the grid blocks. Then, flow simulation is performed to check the match and the process is iterated until convergence. Argarwal and Blunt (2001) have extended the method proposed by Wang and Kovscek (2000) to compressible models with gravity. However, Argawal and Blunt (2001) consider gravity and compressibility only for the forward streamline simulator, and do not take them into account to find the permeability perturbation.

2.4.10 Gradual Deformation

Developed very recently (Roggero and Hu, 1998; Hu, 2000a; Le Ravalec-Dupin, et al., 2000), gradual deformation is a parameterization method that reduces considerably the unknown parameter space of stochastic models. The method is based on the fact that linear combinations of multi-Gaussian random functions remain multi-Gaussian random functions. It consists in iteratively optimize combinations of independent realizations of a stochastic model until the constrains are satisfied. This method, initially developed for Gaussian stochastic models, has been extended to non Gaussian realizations (Hu, 2000b).

The gradual deformation method has been developed by combining independent realizations, the different features of the procedure using dependent realizations have been recently analyzed by Hu (Hu, 2002). This new formulation improves the numerical stability of the method, at the same time that explicitly takes into account the numerical dependence between realizations, allowing the deformation of conditional realizations. However, this procedure is limited to global deformations with fixed structural parameters. The modification of the gradual deformation algorithm made by Ying and Gómez-Hernández (2000) allows to honor the well data while preserving the permeability variogram. In the paper mentioned above by Wen et al. (2002), Ying and Gómez-Hernández's algorithm is modified to invert lithofacies distribution from production data within the framework of truncated Gaussian simulation.

2.4.11 Fractal simulation method

This method treats the spatial distribution of reservoir permeability as fractal (Grindrod and Impey, 1993). The fractal parameters are estimated from field data (permeability and pressure) by maximum likelihood estimation method. Reservoir models conditional to the pressure data are constructed through a linear superposition of un-

conditional fields, as in the linearized fast Fourier transform method with randomly generated phase and amplitude coefficients. A linear superposition of the unconditioned fields is used to condition them to observed data, minimizing the difference between the variance of the final field and the data.

2.4.12 Neural networks

Artificial neural networks can be trained to predict the outcome of the flow code. For example, Rogers and Dowla (1994) trained an artificial neural network to predict the mass of contaminant removed during 50-year simulation period, and then they used the neural network to optimize a groundwater remediation plan. The principal advantage that this technique gives for history matching is its potential to be implemented in parallel processes in order to improve the speed of flow simulations.

2.5 Uncertainties

Having defined the parameters to be used in the reservoir model, the way to minimize the objective function and the inversion approach, the result is a reservoir model which is conditioned to both static and dynamic data. This model is then used to forecast the future behavior of the reservoir. Traditional inversion techniques result in a single best reservoir model that minimize the differences between the observed and simulated historical data. But this prediction is affected by errors or uncertainties, as the error in the input parameters lead to errors or uncertainties in the model predictions. Integrations of additional data reduces the uncertainty of the model (Wen et al., 1998), but the resulting best model is usually oversmooth compared to the real reservoir. either this parameter uncertainty at unsampled locations is quantified. When using the reservoir model for prediction, the next step is to quantify the forecast uncertainty. The purpose of inverse modeling is not only to estimate best parameters for a given model structure, but also to reduce and estimate the parameter uncertainty.

Uncertainty quantification in the dynamic reservoir modeling is one of major challenges facing reservoir modeling. There are mainly two approaches to quantify the flow-prediction uncertainty using the simulation methods described.

One of the methods to solve this problem is the Monte Carlo approach. This method, as it has been explained in the section above, consists in performing a high resolution flow simulation for each of a large number of realizations of the reservoir description. It is based on the fact that the resultant distribution is an equal likely representation. The dependent variables are averaged over many realizations to obtain statistical moments, or probability distribution functions of the model prediction.

Since it is a statistical postprocessing of deterministic flow simulations, the Monte Carlo simulation approach is flexible. However, because of computational expense, sometimes it can be very difficult to generate sufficient conditional realizations to evaluate uncertainty. Often, only few realizations are generated; for example, in the PUNQ (production forecast uncertainty quantification) study, comparing several uncertainty quantification methods for production forecasting, most participants generated 10 realizations (Floris et al, 2001). Another drawback of the Monte Carlo approach is that the ensemble of realizations could provide a poor representation of uncertainty because of a defect in the model or the sampling algorithm. The advantages are that any distribution function can be chosen, the non linearities are taken into account and the results have a physical meaning.

One class of Monte Carlo techniques is the Markov chain Monte Carlo method (Hegstad and Omre, 1997), which has been explained before. In Hegstad and Omre (1998) an application to that approximation was shown and in Omre (2002) several algorithms for the sampling of the posterior model were presented. One of that algorithms to estimate the uncertainty of the model predictions is described in Oliver et al. (1996) and Oliver et al. (1997), employing the Markov chain Monte Carlo technique to generate a set of realizations. In Oliver's approach a sample is drawn from the prior reservoir model. Concurrently, a sample is also drawn from the production data. This production sampling is done because the production data contains observation errors and the reservoir model contains modeling error. Pairs of prior reservoir samples and production samples are subsequently history matched. The matching criterion is formed by both the mismatch between the production sample and the simulated production data and the deviation of the reservoir model from the sampled prior reservoir model used as starting point for the optimization. Applications of Oliver's approach to full-field reservoir problems can be found in Wu et al. (1999) and Floris and Bos (1998).

As it has been mentioned before the self-calibrated method (Sahuquillo et al., 1992; Gómez-Hernández et al., 1997; Capilla et al., 1997; Capilla et al., 1998; Hendrincks-Franssen, 2201) was the first method to use inverse modeling techniques in the context of generating multiple realizations. The self-calibrating method uses stochastic approximation to solve single-phase inverse flow problem. For example, in Gómez-Hernández et al. (1997) inverse modeling is applied to a number of stochastic reservoir models and the range of forecasts is used as a quantification of uncertainty. In Ramarao et al. (1995) there is an application of pilot point method and Monte Carlo techniques for the quantification of uncertainty.

To avoid the computation of a high number of realizations, there is an alternative

to the Monte Carlo methods, this technique consists in solving the statistical moment equations of the interest variables (Zhang and Tchelepi, 1999; Zhang et al., 2000). The stochastic differential equations that describe the flow process are averaged to obtain the equations governing the statistical moments of the dependent variables. Then the moment differential equations are solved either analytically or numerically. The moment differential equations are commonly derived under the assumption that small perturbation and with some kind of closure approximation. Zhang and Techelepi's work presents analytical solutions for simple 1D and 2D non linear problems, but is limited to uniform mean flow in unbounded domains. Zhang et al. (2000) have extended the Lagrangian statistical moment approach to more complex domains and flow patterns due to the presence of wells. Huang et al. (1996) presented one of the first attempts to quantify uncertainties for multiphase systems. They showed that secondary production performance uncertainty is more affected by the iner-well variation of the permeability field than primary production. Thus, descriptions obtained based on matching primary performance are inadequate for secondary production performance matching. Other studies as the one of Wen et al. (1998) have pointed out that the uncertainty is highly influenced by the flux conditions of the system, for example the production state in the wells.

To finish with the review about methods for estimation the parameter and model uncertainties, gradual deformation method applications are analyzed. Le Ravalec et al. (2000) presented a study proving that the realizations constructed with the gradual deformation method do not reflect properly the posterior probability density function. Hence, their conclusion was that the gradual deformation method cannot be used to infer the uncertainty. At the same time, in this work it is proposed an improved gradual deformation method. In this extension additional conditions for the objective function were considered, allowing to investigate the conditioned realizations space from the calibrated realizations, and then to obtained a measure for the uncertainty.

2.6 Relative permeability

History matching makes possible to build a reservoir model that satisfies static as well as dynamic data. Integration of dynamic data centers its attention in the estimation of absolute permeabilities. Relative permeability functions are generally estimated by interpreting flow data collected from laboratory displacement experiments in which one fluid is injected into a core sample that is saturated with another fluid or fluids. Typically the data consist of time dependencies of the differential pressure across the core sample and the cumulative production of the fluid displacement. The interpretation

of displacement data is usually based on the application of semi-analytical approaches (Mitlin et al., 1999) or numerical simulations. The minimization of the objective function in the semi-analytical method developed by Mitlin et al. (1999) is ensured by using the simulated annealing method. They improved the model accounting for presssure drop data before breakthrough in the laboratory experiments. Over the last decade numerical inverse algorithms have been developed for the estimation of relative permeabilities at core scale (Watson et al., 1994; Grimstad et al., 1997). Considerable progress has been made in the methodology for interpretting core flow experiments and recent experimental advances are providing exciting prospects for even more effective solutions on the laboratory scale. However, relatively little attention has been directed to the estimation of these properties at reservoir scale. The values obtained in the laboratory can be very different to the ones corresponding to the conceptual and numerical model, mainly due to the scale effects (Frykman and Lindgaard, 1997) and differences in reservoir conditions and laboratory conditions. In the study presented by Smith (1991) the influence of heterogneities on average relative permeability functions is analyzed. However, this study is performed for steady state conditions. Hastings et al. (2001) presented a streamline simulator that permits to calculate multiphase flow taking into account both heterogeneities of absolute and relative permeabilities at reservoir scale. They apply the inverse method in order to calculate the uncertainties of these parameters nor to the simultaneous estimation of absolute and relative permeabilities. Alpak et al. (2001) is another of the few articles for the estimation of two-phase relative permeabilities at reservoir scale. The problem of their application to two-phase flow is that they use a single-phase inversion algorithm. Their idea was to detect radial variability in the water saturation profile from the corresponding profile of relative permeabilities.

During last years several works about the estimation of absolute and relative permeabilities with inverse techniques have been published (Watson et al., 1994; Kulkarni and Datta-Gupta, 1999; Ates and Kelkar, 2000; Valestrand et al., 2001). In these works different approaches are used, for different scales, but always considering homogeneous relative permeability curves all over the study area. Kulkarni and Datta-Gupta (1999) used the streamline based method developed by Vasco et al. (1999) to estimate relative permeabilities from production data at reservoir scale for homogeneous relative permeability curves. They concluded that the water front is highly sensitive to the end-point water relative permeability. They also showed that water breakthrough data are not sufficient to derive reliable estimates of both absolute and relative permeabilities, and pressure information needs to be added. Valestrand et al. (2001) developed an inverse method for simultaneous determination of absolute and relative permeabi-

lities, but at core scale and for homogenous relative permeabilities. In their method the relative permeabilities are estimated first by utilizing the harmonic mean value of the absolute permeability. Then the absolute permeability is estimated, keeping the relative permeabilities fixed at their first estimate. The procedure is repeated until convergence. Some examples in 1D are presented.

Different analytical expressions have been developed for relative permeability curves. B-Splines (Kulkarni and Datta-Gupta, 1999; Valestrand et al., 2001) or potential functions (Mitlin et al., 1999; Ates and Kelkar, 2000; Akin, 2001) are frequently used. For this dissertation, the conventional Corey functional representations are used to approximate water relative permeability, k_{rw}, and oil relative permeability, k_{ro}:

$$\begin{aligned} k_{rw} &= k^0_{rw}\left(\frac{S_w - S_{rw}}{1 - S_{rw} - S_{ro}}\right)^{n_w} \\ k_{ro} &= k^0_{ro}\left(\frac{S_o - S_{ro}}{1 - S_{rw} - S_{ro}}\right)^{n_o} \end{aligned} \tag{2.17}$$

k^0_{rw} and k^0_{ro} are the end-point relative permeability curves, S_{rw} and S_{ro} the residual saturations, and n_w and n_o the shape exponents, for water and oil respectively.

Depending on which expressions for relative permeability curves are selected, the parameters for the calibration change. For example, Ates and Kelkar (2000) used the Corey function representations. They applied the method of the double loop (Ates and Kelkar, 1998) for optimizing both relative and absolute permeabilities. They study the sensibility of breakthrough with respect to the end-point relative permeability ratio (k^0_{ro}/k^0_{rw}) and the exponents (n_w and n_o). The conclusion of the work is that, in synthetic cases, their method can produce adequate descriptions of both absolute and relative permeabilities. Bennet and Graf (2002) studied various parameters affecting pressure and breakthrough performance, like permeability multipliers and end-point water relative permeability.

To summarize, it has been shown that at present time there exist enough tools and techniques to perform simultaneous absolute and relative permeabilities inverse modeling at reservoir scale. Besides, the need to real characterize the reservoir properties through heterogeneous absolute and relative permeabilities, can be done similarly to the existing stochastic inverse techniques. However, to the best of our knowledge, this kind of problems have not been performed yet, and this is the target of this dissertation. In the following chapters a new technique to characterize the spatial distribution of absolute and relative permeability curves is going to be described and applied.

Chapter 3

Two-phase flow numerical approach

In this section the equations for immiscible flow of two phases, already presented in last chapter, are expanded and approximated numerically. In general these equations have important petroleum and hydrology applications. For example, it is often the case that oil is found in geological formations together with water, the presence of which must be accounted for in the modeling process. Moreover, improved oil recovery techniques usually involve the injection of fluids such as water into the reservoir with goals of maintaining reservoir pressure and sweepping the oil to production wells. Some of the most popular models of groundwater flow (e.g., Richards equation) are based on certain simplifications of the multiphase model. For more complex hydrological applications such as cleanup of hazardous water, it is often necessary to remove some of the simplifying assumptions leading to Richards equations and return to more complete multiphase models. It should be noted that in both the petroleum and groundwater remediation contexts, there may arise more complex situations in which mass transfer between phases and chemical reactions can occur. This creates the need for generalizations of the multiphase immiscible flow model not presented here. However, the formulation presented here is the basis for mathematically simulating two-phase flow in a wide range of very important applications, and hence are used in this dissertation.

3.1 Governing equations

If a porous medium is saturated with one fluid and a second fluid, immiscible with the first one, is introduced in the medium, the fluid that initially was filling the medium suffers a displacement. For the petroleum engineering the two fluids are oil and water (or gas and oil) while for hydrology are, for example, water and air (or a non aqueous contaminant and water). To simplify, it can be assumed that there is an interphase between the two fluids which moves changing its configuration depending on the flow.

The curvature of the interphase is given by the heterogeneity of the medium and the fluid properties.

The mathematical formulation of the multiphase system in a porous, or fractured formation, is developed here assuming that the system is composed of two phases: water and oil. Altough each of these two phases contains a number of components, they are treated a a single pseudo-component with averaged properties of the fluids. The processes of interphase transfer are not considered, and the two fluid components of water and oil are assumed to be present only in their associate phases. Each phase flows in response to its pressure, gravitational, and capillary forces according to the multiphase extension of Darcy's law. In an isothermal system containing two mass components, two mass-balance equations are needed to fully described the system for flow. Let's consider a very small part of the reservoir, called a control volume (see Figure 3.1). The three sides are of lengths dx, dy and dz, respectively. The area of the face normal to the x-axis is $dydz$, the area of the face normal to the y-axis is $dxdz$ and the area of the face normal to the z-axis is $dxdy$ (figure 3.1). The mass balance equation for both phases is normally formulated for standard conditions, requiring that the rate of change of mass within the control volume ($\frac{\partial(\phi\rho_l S_l)}{\partial t}$) is equal to the net rate at which the fluid is entering in the control volume through the control surface ($-\nabla \cdot \rho_l \mathbf{u}_l$, see Figure 3.1) plus the net rate at which the mass is produced ($-q_l\rho_l$) within the control volume:

$$\frac{\partial\left(\phi\rho_l S_l\right)}{\partial t} = -\nabla \cdot \rho_l \mathbf{u}_l - q_l\rho_l \quad \text{for } l = o, w$$

where subscripts w and o refer, respectively, to water (wetting phase) and oil (non-wetting phase). $\mathbf{u}_l$ is the volumetric flux vector or Darcy's velocity $[L/T]$ for phase l, S_l is the saturation (volume fraction of the total porous space occupied by the phase l: $S_w + S_o = 1$), ϕ is the porosity (dimensionless parameter), ρ_l is the fluid density $[M/L^3]$, q_l is the injection or production rate per unit volume $T^{-1}]$ and t is the time $[T]$. For the injection case, the term q_l is negative, while in the production case is positive.

Rearranging the different terms for each fluid phase l, the mass balance equation may be written as:

$$\frac{\partial\left(\phi\rho_l S_l\right)}{\partial t} + \nabla \cdot \rho_l \mathbf{u}_l = -q_l\rho_l \quad \text{for } l = o, w \tag{3.1}$$

The air-water system could be treated in the same manner, simply substituting subscript o (oil) by a (air). It was shown in chapter 2 that this equation (3.1) can be written in many ways with different dependent variables and constitutive relations.

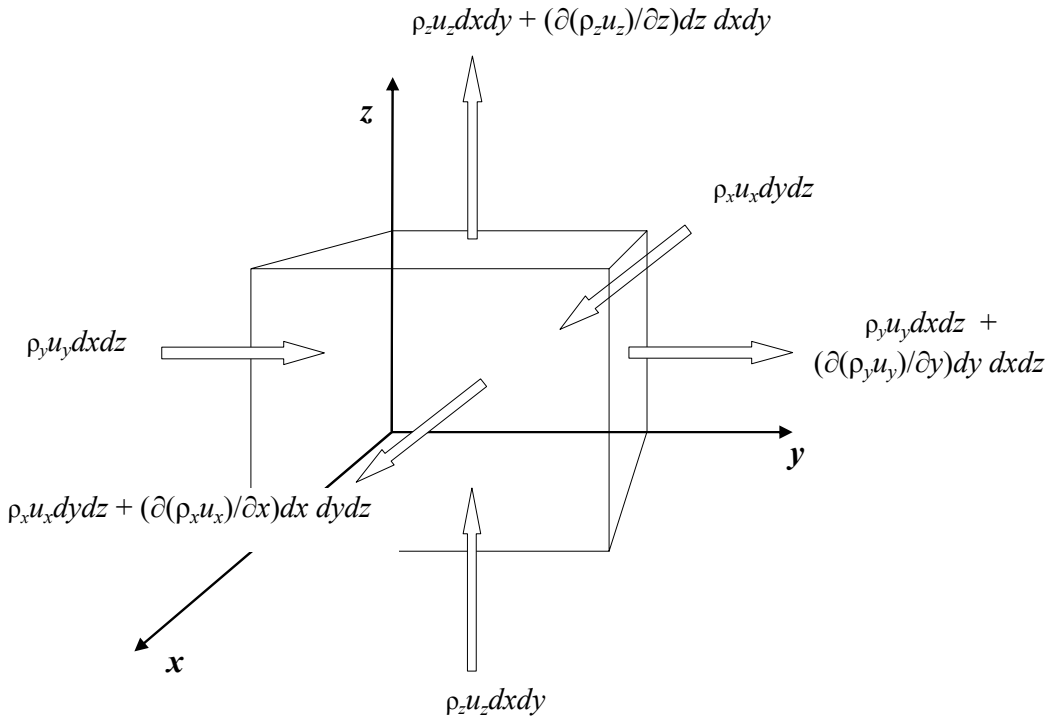

Figure 3.1: Control volume flow through a reservoir.

In the same way that the mass balance equation has been employed for each of the fluids, Darcy's law, originally developed for a single fluid completely saturating the medium, can be applied to describe the flow of each of the immiscible fluids simultaneously moving. Darcy's law is a linear relation between the gradient of fluid pressure and the fluid flux. It is valid for viscous dominated flow which occurs at low velocities. At higher fluid velocities, slip flow, or non zero flux along the pore walls is increasingly important and Darcy's law must be modified to include additional terms.

For multiphase flow the concept of permeability, which defines the flow for a single fluid, has to be modified depending on the quantity of the other fluid that is present. For the purposes of this dissertation all fluids, as well as the solid matrix, will be considered to be incompressible (constant porosity and density), as well as the absence of gravity. Darcy's law for each of the fluids l is:

$$\mathbf{u}_l = -\frac{\mathbf{k}k_{rl}}{\mu_l}\nabla p_l \tag{3.2}$$

where ∇p_l is the pressure gradient of phase l. The product of the absolute permeability tensor (also called intrinsic permeability), $\mathbf{k}$ $[L^2]$, by the dimensionless relative permeability, k_{rl}, is known as the effective permeability $\mathbf{k_{efec}}$ $[L^2]$. The absolute permeability depends exclusively on the porous medium properties. The relative permeability is

function of the saturation, the rock properties and the fluid properties, although it is possible to approximate the relative permeability as a function of saturation (Bear, 1972).

Substituting the mass conservation equation (3.1) in Darcy's equation (3.2) the equation for the flow of each fluid is obtained (3.3). This generalization was introduced in the oil field rejecting the gravitatory component in the fluid potential, resulting the equations in function of the pressure gradient and not in function of the potential or the piezometric head:

$$\frac{\partial\left(\phi\rho_l S_l\right)}{\partial t} - \nabla\cdot\left[\rho_l\frac{\mathbf{k}k_{rl}}{\mu_l}\nabla p_l\right] = -q_l \quad \text{for } l = w, o \tag{3.3}$$

The equation system for the incompressible two-phase flow of water and oil, assuming absolute permeability is isotropic ($\mathbf{k}$ is a scalar, k), is:

$$\begin{aligned} \phi\frac{\partial S_w}{\partial t} - \nabla\cdot\left(\frac{kk_{rw}}{\mu_w}\nabla p_w\right) &= -q_w \\ \phi\frac{\partial S_o}{\partial t} - \nabla\cdot\left(\frac{kk_{ro}}{\mu_o}\nabla p_o\right) &= -q_o, \end{aligned} \tag{3.4}$$

where p_w and p_o are respectively the water and oil pressures $[M/LT^2]$.

Auxiliary relations have to be included in order to solve the system of equations. These relations are the capillary pressure between the aqueous and non-aqueous phases ,P_c $[M/LT^2]$, and the continuity of fluid saturations and pore volume:

$$\begin{aligned} P_c = p_o &- p_w \\ S_w + S_o &= 1 \end{aligned} \tag{3.5}$$

The equations (3.4) and (3.5) define the differential equation system which describes the two-phase immiscible flow, where the unknowns are the pressures p_o and p_w, and the saturations S_w and S_o. Given this set of equations, boundary and initial conditions must be supplied to complete the mathematical description. They are usually given as known pressures, saturations or fluxes for each of the fluid phases. Many different combinations of these boundary conditions occur in practical problems. An important criteria for acceptance of a solution method is that it must be able to solve the governing equations for the wide variety of possible boundary conditions. This fact and the non linear nature of the problem make difficult to find an analytical solution for this system of equations ((**??**) and **??**)).

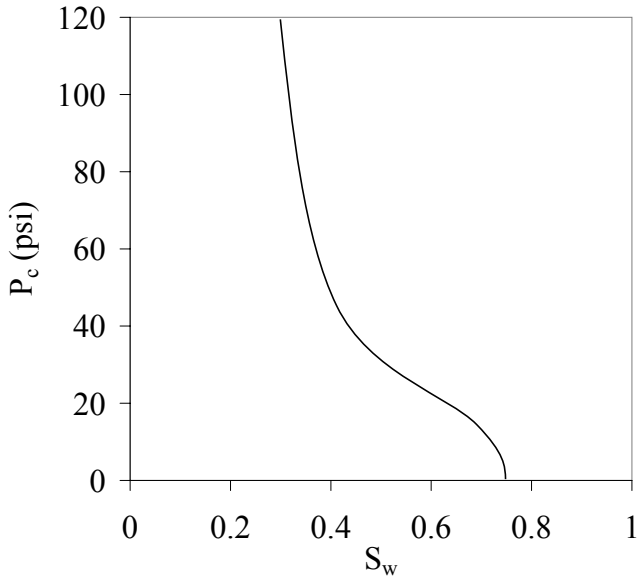

Figure 3.2: Typical capillary pressure dependence with water saturation, for a water-oil system.

Capillary pressure, P_c, is the physical variable to describe the pressure difference in the interphase between the two fluids that are in contact. An expression can be established to calculate capillary pressure at any point in the interphase, in function of the saturation (S_w). This relation, P_c-S_w, can be measured in the laboratory, resulting in a series of curves, similar to the one shown in Figure 3.2. For a complete description of the functions P_c-S_w, hysteresis effects have to be taken into account. This means that capillarity depends on the wetting fluid saturation and direction of saturation change (drainage or imbibition curve). As is shown in Figure 3.3, the capillary pressure curve for an imbibition process is different from the drainage curve, and terminates at a different saturation. Anyway, in most situations the direction of flow can be predicted and only one set of capillary pressure curves is required. Capillary pressures are often ignored in large-scale reservoir displacement studies, because their effect is small in relation to the numerical dispersion associated with the large grid blocks in the reservoir model. In the development of this dissertation this assumption has been adopted.

3.2 Relative permeability functions

Let's now take a look to the behavior of the functions that have most interest in this dissertation, relative permeability functions. In general, when studying the flow in porous media for more than one fluid the permeability is defined with the effective

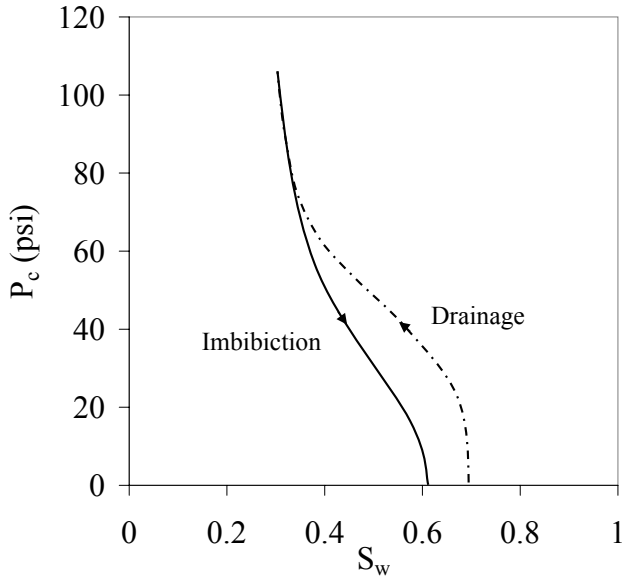

Figure 3.3: Typical drainage and imbibition capillary pressure functions.

permeability. The effective permeability of the medium to each fluid is the product of the absolute permeability times the relative permeability of each phase ($\mathbf{k_{efec}} = \mathbf{k}k_{rl}$). The relative permeabilities are dimensionless and vary with the void ratio for a saturated soil and the void ratio and degree of saturation (or water content) for an unsaturated soil. In many situations, the change in void ratio may be of secondary importance and the coefficient of permeability can be satisfactorily defined as a function of degree of saturation (or water content). For example, k_{rw} is the water relative permeability which varies from 0.0 (for a completely dry soil) to 1.0 (for a fully saturated soil). For each particular soil, the relations $k_{rl}(S_w)$ are either predicted by models based on some more or less realistic capillary assumptions or experimentally determined in laboratory as well as in field conditions. The result is a series of curves $k_{rl} - S_w$, like the schematic oil-water relative permeability curve given in Figure 3.4 (other examples in Lake, 1989). For further information about oil and water relative permeabilities curves (water-oil system), or water and air relative permeability curves (water-air system), the reader is referred, respectively, to Holm et al. (1965) and Brooks and Corey (1966).

The relative permeability of one fluid decreases when the saturation of this fluid is also decreasing. However, the relative permeability of one fluid disappears at a point in which the saturation of this fluid is different from zero (Figure 3.5). This saturation is called residual saturation (S_{rw} and S_{ro}), due to the zero relative permeability of this fluid at this point. At residual saturation the fluid cannot move any more and the saturation cannot be further reduced. Apart from the residual saturation there

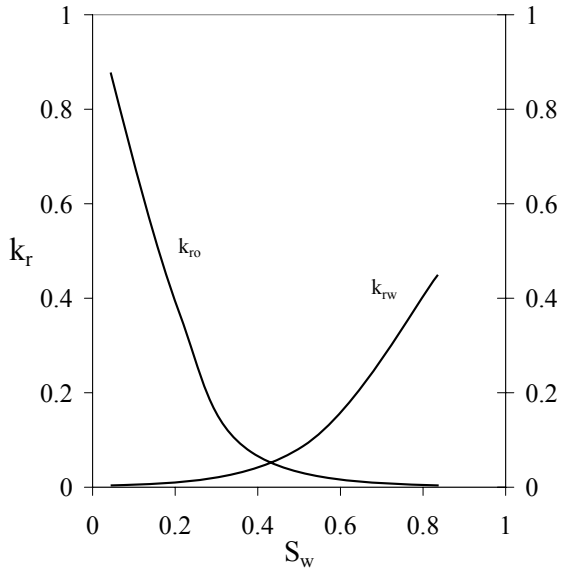

Figure 3.4: Typical saturation dependent relative permeabilities for water-oil systems.

are another two points that characterize the length of the curves, they are known as the end-points (k^0_{rw} y k^0_{ro}). These points correspond to the residual saturations of the other fluid. The end-points are a measure of wettability, being the end-point of the wettable fluid smaller than the corresponding the non wettable fluid. In the case of water and oil, the water relative permeability, k_{rw}, has a value less than one for the residual saturation S_{ro}, however k_{ro} takes a value close to one for the saturation S_{rw}. This means that the presence of water has little influence in the oil flow, while the presence of oil highly interferes in the water flow. The sum of the water and oil relative permeabilities for the same saturation is always less than 1. This implies that for multiphase flow, the total capacity through a porous medium is reduced.

Although there is not a theoretical expression for the relative perpermeability functions, there are several empirical functions for the water-oil curves. When analytical expressions are needed, B-splines or potential expressions are used. The potential formulation given by Brooks and Corey (1996) are:

$$\begin{aligned} k_{rw} &= k^0_{rw}\left(\frac{S_w - S_{rw}}{1 - S_{rw} - S_{ro}}\right)^{n_w} \\ k_{ro} &= k^0_{ro}\left(\frac{S_o - S_{ro}}{1 - S_{rw} - S_{ro}}\right)^{n_o} \end{aligned} \tag{3.6}$$

where n_o and n_w are the shape indexes. These equations are adjusted in most experimental cases and separate explicitly the modeling of the curvature through the

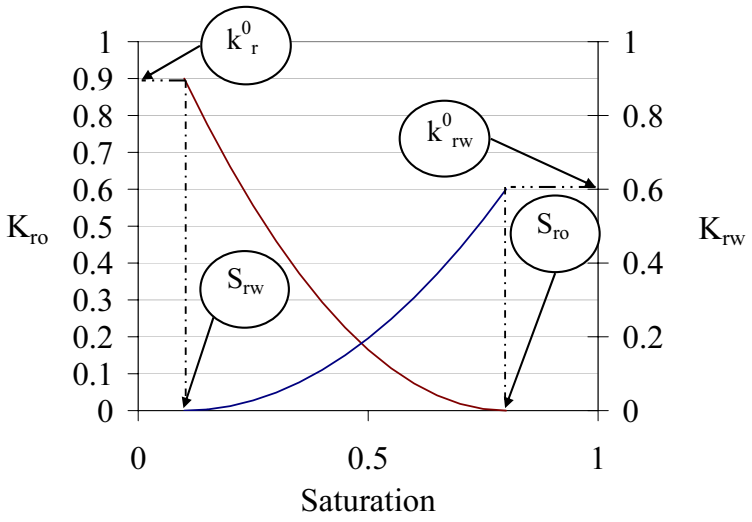

Figure 3.5: Water and oil relative permeability curves.

exponents. In Figure 3.5 indexes n_w and n_o are equal to 2.

Wettability also has a great influence on the shape of relative permeability curves. Residual oil saturation decreases and the water relative permeability increases as the system becomes more oil-wet. For systems with preferential wettability, the relative permeability for the non-wetting phase and the capillary pressure function exhibit hysteresis effects, depending on wether the saturations are increasing or decreasing. In this dissertation hysteresis effects of relative permeability functions are also neglected.

3.3 Fractional flow formulation

The fractional flow approach was first developed by petroleum engineers, but it has also been used by hydrologists. This approximation appeared due to its possibilities from a numerical point of view.

In chapter 2 it has been already developed the deduction of the fractional flow approximation for two-phase flow (equations (2.9) to (2.15)). In any case, some of these concepts should be reminded here, as they are needed for the development of the numerical approach. Fractional flow is an adimensional variable defined as the ratio between the module of water Darcy's velocity and the module total Darcy's velocity:

$$f_w = \frac{\mid \mathbf{u}_w \mid}{\mid \mathbf{u}_T \mid} \tag{3.7}$$

Following the assumptions taken is this dissertation capillarity, gravity forces, and

compressibility are neglected, resulting the fractional flow variable as:

$$f_w = \frac{k_{rw}/\mu_w}{k_{rw}/\mu_w + k_{ro}/\mu_o} \tag{3.8}$$

With these assumptions, and provided that oil displacement occurs at a constant temperature, oil and water viscosities have fixed values and relative permeabilities are strictly function of water saturations, the fractional flow is as well function of saturation. For a typical set of relative permeabilities, fractional flow can take the shape shown in Figure 3.6, with values ranging between 0 to 1. The shape of this curve varies with the viscosity ratio of oil to water.

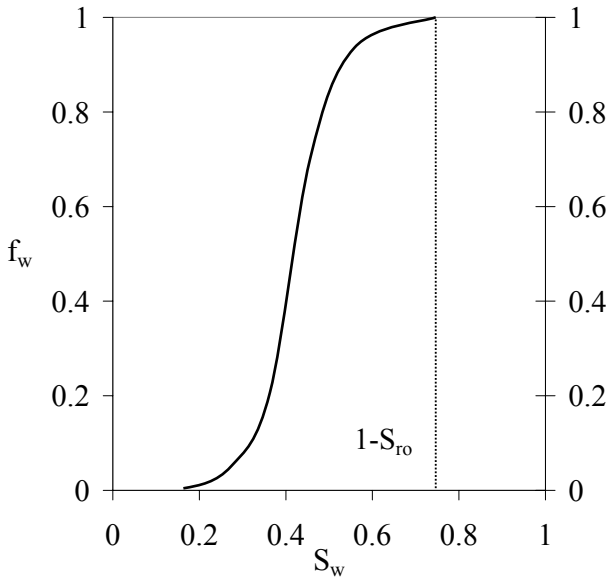

Figure 3.6: Typical fractional flow curve as a function of water saturation.

When flow is consider incompressible and the gravity term is rejected, the mass conservation equation (3.1) can be written like:

$$\phi \frac{\partial (S_l)}{\partial t} + \nabla \cdot \mathbf{u}_l = -q_l \quad \text{para } l = w, o \tag{3.9}$$

As in equation (3.2), Darcy's law for the water (w) and oil (o) are respectively written in the following form:

$$\mathbf{u}_w = -\frac{\mathbf{k} k_{rw}(S_w)}{\mu_w} \nabla p_w \quad \mathbf{u}_o = -\frac{\mathbf{k} k_{ro}(S_o)}{\mu_o} \nabla p_o$$

being $\mathbf{u}_T$ the total flux, defined as the sum of the phase-volumetric fluxes:

$$\mathbf{u}_T = \mathbf{u}_w + \mathbf{u}_o$$

and its divergence:

$$\nabla \cdot \mathbf{u}_T = -(q_T + q_w) = -q_T \tag{3.10}$$

In one dimesion this equation has a simple solution, the total flux is constant in space and determined by the boundary conditions. This equation is obtained adding both equations (3.9) and applying the second of the equations (3.5). If in the equations (3.9) there are no terms of production or injection, the divergence of $\mathbf{u}_T$ will be zero.

The water flux can be written in function of the total flux with the help of the fractional flow:

$$\mathbf{u}_w = \mathbf{u}_T f_w \tag{3.11}$$

Applying this expression (3.11), equation (3.9) for the water is:

$$\phi \frac{\partial S_w}{\partial t} + \nabla \cdot (\mathbf{u}_T f_w) = -q_w$$

$$\phi \frac{\partial S_w}{\partial t} + \mathbf{u}_T \cdot \nabla f_w + f_w \nabla \cdot \mathbf{u_T} = -q_w$$

Substituting the equation (3.10) and taking into account that fractional flow f_w is only function of saturations ($\nabla f_w = \frac{df_w(S_w)}{dS_w} \nabla S_w$), the formulation of the two-phase immiscible flow formulation with the fractional flow is the following:

$$\phi \frac{\partial S_w}{\partial t} + \mathbf{u}_T \cdot \frac{\partial f_w}{\partial S_w} \nabla S_w = f_w q_T - q_w \tag{3.12}$$

The solution to this equation for the saturation $S_w(\mathbf{x}, t)$ needs to solve first the equation (3.10) for the total flux $\mathbf{u}_T$, which solution is trivial only for the one dimensional case. Buckley and Leverett (1942) found an analytical solution for the equation (3.12) using the fractional flow values measured experimentally. In the appendix A solution given by Buckley and Leverett is described in detail.

S_w has been taken as the state variable, but it is also possible to take S_o as $S_w + S_o = 1$ and $f_w + f_o = 1$. Neglecting capillary forces, f_w can be expressed in function of S_w through the relative permeabilities relations. In fact, the shape of f_w-S_w is the principal factor to determine the fluid displacement.

The source term, $q_w - f_w q_T$, will be zero if it represents production, being for this case $q_w = f_w q_T$ by the Darcy's law. However, for injection the source term can be different from zero, for example when only water is injected, $q_T = q_w$, and $q_w - f_w q_T = (1 - f_w) q_w \neq 0$.

The volumetric flow for oil and water given by Darcy's law (equation (3.2)) is respectively inverse proportional to the viscosities μ_o and μ_w. The dependence of both viscosities on temperature, they decrease with increasing temperature, is ignored in the present study. The oil is normally more viscous than water. behave

3.4 Discrete equations in 1D

The equation for two-phase flow in function of fractional flow has been derived (equation (3.12)), resulting in a differential partial equation of first order. In one dimension this equation is expressed:

$$\phi \frac{\partial S_w}{\partial t} + u_T \cdot \frac{\partial f_w}{\partial S_w} \frac{\partial S_w}{\partial x} = f_w q_T - q_w$$

where ∇S_w is represented by $\frac{\partial S_w}{\partial x}$.

The solution to this equation for one injection and one production well, situated in the extremes of the domain, is the so called two-phase Buckley-Leverett displacement (see appendix A and Figure 3.7). This problem can be solved numerically or by the characteristics method. The characteristic method reduce the partial differential equation system to a system of ordinary differential equations. It has been already mentioned in the literature review that there are several possibilities to numerically approximate this equation. In this dissertation the approach addopted is the finite differences.

The spatial derivative is approximated with the following finite difference expression:

$$\frac{\partial f_w}{\partial S_w} \frac{\partial S_{w,i}}{\partial x} \simeq \frac{f_{w,i+1/2} - f_{w,i-1/2}}{\Delta x}$$

where Δx is equal to the grid spacing between nodes $i-1$ and i (see Figure 3.8). The one point upstream weighting scheme, used in this dissertation, approximates the value of f_w at faces $i+1/2$ and $i-1/2$ with the value in the grid block on the upstream side, in this case a smaller value of x:

$$\frac{\partial f_w}{\partial S_w} \frac{\partial S_{w,i}}{\partial x} \simeq \frac{f_{w,i} - f_{w,i-1}}{\Delta x} \tag{3.13}$$

Figure 3.8 illustrates the block centered grid that is commonly used in reservoir simulation. The dependent variable is defined at the center of the grid block and the fluxes are evaluated across the faces separating the grid blocks. The divergence of the flux in grid block i expressed with finite differences is the net efflux from the grid block. The developments presented here are for equal grid spacing, for unequal grid spacing

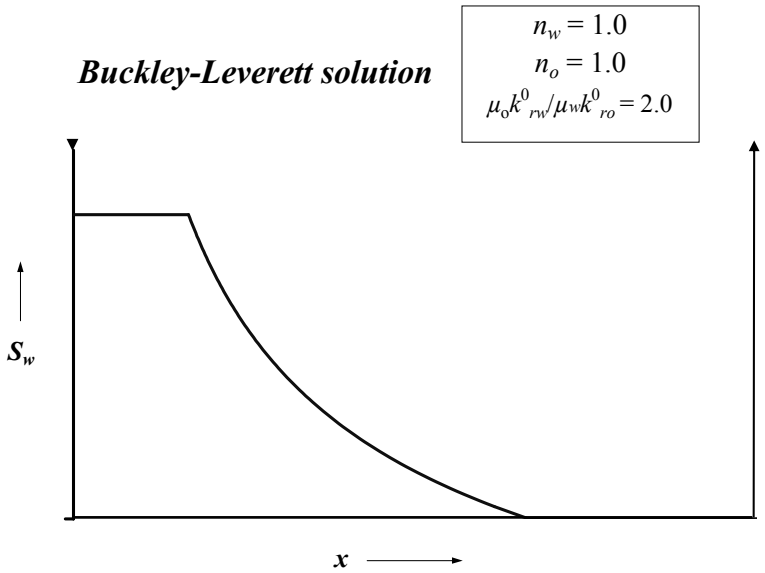

Figure 3.7: Water saturation distribution as a function of distance, prior to breakthrough in the producing well. Result given by the Buckley-Leverett solution. The values taken for the parameters of relative permeability functions, equation (3.6), are the following: the final points $k^0_{rw} = k^0_{ro} = 1.0$, residual saturations $S_{rw} = S_{ro} = 0.0$, indexes $n_1 = n_2 = 2.0$ and viscosity ratio $\mu_o/\mu_w = 2.0$.

the concepts are the same but the equations would need to be expressed with more details.

The accuracy of the finite difference approximation for the time derivative and the stability of the procedure is dependent on the time level at which the flux terms in the conservation equation is evaluated. The formulation taken here is said to be the implicit procedure. This formulation evaluates the spatial differences for the flux terms on the new time level, $t + 1$, using the yet unknown values of the dependent variable. Thus, the difference approximation in time couples the finite difference equation backwards in time to the known value of the dependent variable at the old time level, t. Each finite difference equation has several unknown values of the dependent variable at the new time level. Since the dependent variable at the new time level has to be computed by solving a system of equations, this formulation is said to be an implicit procedure. With this temporal discretization the temporal derivative is equal to:

$$\frac{\partial S^{t+1}_{w,i}}{\partial t} \simeq \frac{S^{t+1}_{w,i} - S^{t}_{w,i}}{\Delta t} \tag{3.14}$$

being t the calculation time step and Δt the increment between two time steps.

The total flux is given by equation (3.10). In one dimension it is equal to $u_T =$

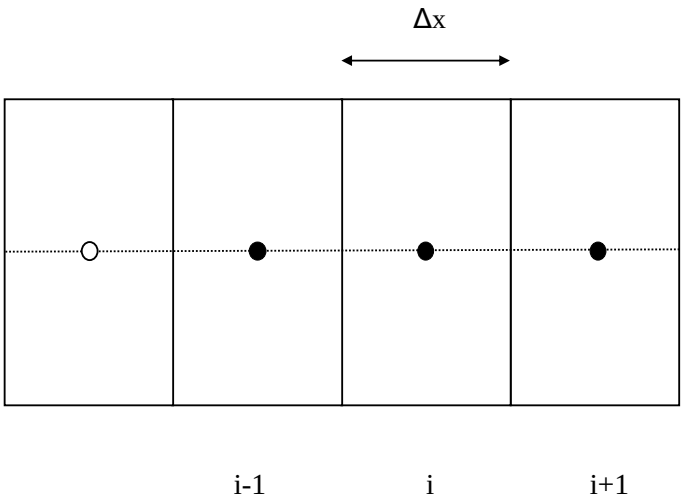

Figure 3.8: Block centered grid.

Q_T/A. By using the approximations in equations (3.13) and (3.14), the two-phase flow equation in one dimension can be discretized, obtaining the following expression:

$$\frac{\phi}{\Delta t}\left(S_{w,i}^{t+1} - S_{w,i}^{t}\right) + \frac{Q_T}{A \cdot \Delta x}\left[f_{w,i}^{t+1} - f_{w,i-1}^{t+1}\right] = f_{w,i}^{t+1} q_T - q_w^{t+1} \tag{3.15}$$

The terms in the right term disappeared in case inside the block there are not neither injection nor production wells, or in case a production well is located. Multiplying by $A\Delta x$, where A is the transversal area and Δx is the spatial increment, equation (3.15) can be expressed as:

$$\frac{V_i}{\Delta t}\left(S_{w,i}^{t+1} - S_{w,i}^{t}\right) + Q_T\left[f_{w,i}^{t+1} - f_{w,i-1}^{t+1}\right] = f_{w,i}^{t+1} Q_T - Q_{w,i}^{t+1} \tag{3.16}$$

where V_i is the cell volume multiplied by porosity, $V_i = \phi A \Delta x$, and Q is the production term, $Q = A\Delta x q$.

Rearranging the terms of equation (3.16), the system of equations that results, for each time step, is:

$$\frac{V_i}{\Delta t} S_{w,i}^{t+1} - \frac{V_i}{\Delta t} S_{w,i}^{t} = -Q_T\left[f_{w,i}^{t+1} - f_{w,i-1}^{t+1}\right] - Q_{w,i}^{t+1} + f_{w,i}^{t+1} Q_T \tag{3.17}$$

and the matrix form for each iteration time is:

$$[\mathbf{A}]\left(\{S^{t+1}\} - \{S^{t}\}\right) = \{Q^{t+1}\} \tag{3.18}$$

The matrix [**A**] is equal to:

$$[\mathbf{A}] = \begin{bmatrix} A_1 & 0 & 0 & 0 & \dots \\ 0 & \ddots & 0 & 0 & \dots \\ 0 & 0 & A_i & 0 & \dots \\ \vdots & \vdots & 0 & \ddots & \dots \\ \vdots & \vdots & \vdots & 0 & A_N \end{bmatrix}$$

being N the number of nodes which are used to discretize the work domain. The definition of the matrix components is:

$$A_i = \frac{V_i}{\Delta t} \tag{3.19}$$

Saturations vector $\{S^t\}$ and production vector $\{Q^t\}$ for time t are expressed:

$$\{S^t\} = \begin{Bmatrix} S^t_{w,1} \\ \vdots \\ S^t_{w,i} \\ \vdots \\ S^t_{w,N} \end{Bmatrix} \quad \{Q^t\} = \begin{Bmatrix} Q^t_1 \\ \vdots \\ Q^t_i \\ \vdots \\ Q^t_N \end{Bmatrix}$$

the components of the production term vector $\{Q\}$ are equal to:

$$Q^t_i = Q_T f^{t+1}_{w,i-1} - Q^{t+1}_{w,i} \tag{3.20}$$

To solve a problem similar to the one of Buckley and Leverett the medium is supposed to be initially occupied by oil with a saturation equal to $S_o = 1 - S_{rw}$, being $S_w(x, 0) = S_{rw}$. At point $x = 0$ water is injected with a constant rate of q_w. Following the former notation S_{rw} and S_{ro} are respectively water and oil residual saturations.

The injection term is a boundary condition, its saturation is constant and it is not necessary to calculate. This makes that for every node the right term of equation (3.16) is equal to zero. Because of that, and to simplify the equations from now on, the right term of equation (3.16) is ignored.

Considering all the equations for the whole discretized time space, it is possible to write the system of equations in a compact form:

$$[\mathcal{A}]\{\mathcal{S}\} = \{\mathcal{Q}\} \tag{3.21}$$

the matrix $[\mathcal{A}]$ is constituted by a series of submatrices $[\mathcal{A}^{lt}]$ with size NxN. Coefficients t and l take the values $1, ...T$, where T is the final discretization time. Matrix $[\mathcal{A}]$ will have the following non zero submatrices:

$$[\mathcal{A}] = \begin{bmatrix} \mathcal{A}^{00} & 0 & 0 & 0 & \dots \\ \mathcal{A}^{01} & \mathcal{A}^{11} & 0 & 0 & \dots \\ 0 & \mathcal{A}^{12} & \mathcal{A}^{22} & 0 & \dots \\ \vdots & 0 & \ddots & \ddots & \ddots \\ \vdots & \vdots & 0 & \mathcal{A}^{T-1T} & \mathcal{A}^{TT} \end{bmatrix}$$

where

$$\mathcal{A}_{ii}^{tt} = \tfrac{\phi}{\Delta t} \quad \mathcal{A}_{ii}^{t-1,t} = \tfrac{\phi}{\Delta t}$$

$$\mathcal{A}_{ij}^{tt} = 0 \quad \mathcal{A}_{ij}^{t-1,t} = 0 \qquad \text{if } i \neq j$$

$\{\mathcal{S}\}$ and $\{\mathcal{Q}\}$ vectors are given by:

$$\{\mathcal{S}\} = \begin{Bmatrix} \mathcal{S}^0 \\ \mathcal{S}^1 \\ 0 \\ \vdots \\ \mathcal{S}^T \end{Bmatrix} \quad \{\mathcal{Q}\} = \begin{Bmatrix} \mathcal{Q}^0 \\ \mathcal{Q}^1 \\ 0 \\ \vdots \\ \mathcal{Q}^T \end{Bmatrix}$$

The N size vectors $\{\mathcal{S}^t\}$ and $\{\mathcal{Q}^t\}$ correspond to the unknown saturations and the production term:

$$\mathcal{S}_i^t = S_{w,i}^t \qquad \mathcal{Q}_i^t = \frac{Q_T}{A\Delta x}\left(f_{w,i}^t - f_{w,i-1}^t\right)$$

Once the system of equations (3.21) is solved, saturations for each time step at every node are available, and consequently pressure values could easily be deduced from equation (3.9).

3.5 Discrete equations in 2D

The formulation with fractional flow, saturation as the only dependent variable, can be used for one dimensional problems but can not be extended to two or three dimensions. The total flux is no longer known in advance for dimensions higher than one. An alternative is to calculate the total flux field and calculate stream tubes in which the fluid flows as if the displacement is one dimensional within the stream tube. This approach, known as streamline method, is valid if the total flux field does not change with time. However, the total flux changes if relative well rates change or the displacement is not a unit mobility ratio displacement ($k_{rw}^0\mu_o/k_{ro}^0\mu_w \neq 1$).

In 2D is necessary to include pressure as dependent variable. The typical formulation in reservoir engineering for finite differences is the implicit pressure and explicit saturation (IMPES method). Its basic idea is to obtain a single pressure equation by a combination of the flow equations. After the pressure has been advanced in time, the saturations are updated explicitly.

The finite difference approach applied to the equations of multiphase flow (3.4), using the spatial and temporal discretization defined before and the definition $\lambda_l = \frac{kk_{rl}}{\mu_l}$, results for 2D in the following equations:

$$\begin{aligned}\phi\frac{S_{l,ij}^{t+1} - S_{l,ij}^{t}}{\Delta t} &- \frac{\lambda_{l,(i+1/2)j}\left(p_{l,(i+1)j}^{t+1} - p_{l,ij}^{t+1}\right) - \lambda_{l,(i-1/2)j}\left(p_{l,ij}^{t+1} - p_{l,(i-1)j}^{t+1}\right)}{(\Delta x)^2} \\ &- \frac{\lambda_{l,i(j+1/2)}\left(p_{l,i(j+1)}^{t+1} - p_{l,ij}^{t+1}\right) - \lambda_{l,i(j-1/2)}\left(p_{l,ij}^{t+1} - p_{l,i(j-1)}^{t+1}\right)}{(\Delta y)^2} \\ &= -q_{l,ij} \quad \text{for } l = w, o\end{aligned}$$

where i and j are respectively row and column indexes. This system of equations has to be complemented with capillary pressure and saturation continuity equations (3.5). The coefficient λ_l can be upstream weighted as it was explained before. This means that $\lambda_{l,(i+1/2)j}$ is approximated by $\lambda_{l,ij}$ and $_{l,(i-1/2)j}$ by $\lambda_{l,(i-1)j}$, and similarly with the column indexes j. With the upstream approach 2D equations are equal to:

$$\begin{aligned}\phi\frac{S_{l,ij}^{t+1} - S_{l,ij}^{t}}{\Delta t} &- \frac{\lambda_{l,ij}\left(p_{l,(i+1)j}^{t+1} - p_{l,ij}^{t+1}\right) - \lambda_{l,(i-1)j}\left(p_{l,ij}^{t+1} - p_{l,(i-1)j}^{t+1}\right)}{(\Delta x)^2} \\ &- \frac{\lambda_{l,ij}\left(p_{l,i(j+1)}^{t+1} - p_{l,ij}^{t+1}\right) - \lambda_{l,i(j-1)}\left(p_{l,ij}^{t+1} - p_{l,i(j-1)}^{t+1}\right)}{(\Delta y)^2} \\ &= -q_{l,ij} \quad \text{for } l = w, o\end{aligned} \tag{3.22}$$

If the IMPES method is used to solve this system of equations, the capillary pressure definition, P_c, is used to express both equations (3.22) in function of P_c and the pressure of one of the fluids, p. Done that, the IMPES solution consists of two steps, first with P_c evaluated explicitly p^{t+1} is evaluated implicitly, and second S_l^{t+1} is solved explicitly.

In this study the flow formulation in two dimensions is taken from the code TOUGH2 (Pruess and Oldenburg, 1999). The modified version of TOUGH2, T2VOC module (Falta et al., 1995) has been taken to solve the two-phase flow equations in 2D. In the TOUGH2 code the equations are discretized in space using the integral finite difference method. For systems of regular grid blocks, the integral finite difference method results

identical to a conventional finite difference formulation (equations (3.22)), but the derivation of the finite differential equations is based on a discrete conservation principle. This method does not need the partial differential equations (3.4) to derive the numerical approximation. All that is needed is a physical problem involving a density of some material and a rule for the flux of that quantity. For the two-phase flow problem that it is studied here, the governing mass balance equation for each component can be written in the following integral form:

$$\frac{\partial}{\partial t}\int_V M_l dv = \int_\Gamma \mathbf{F}_l \cdot \mathbf{n} d\Gamma + \int_V q_l dv$$

The integration is over an arbitrary subdomain V of the flow system, which is bounded by the closed surface Γ, with inward normal vector $\mathbf{n}$. M_l is the mass accumulation term for fluid l, $\mathbf{F}_l$ is the mass flux term, and q_l is a term representing sinks and sources. The mass accumulation term is (Finsterle and Pruess, 1995)

$$M_l = \phi \sum S_l \rho_l$$

thus, M_l is the total mass fraction of component l present per unit volume. The mass flux term, neglecting gravity effects, is equal to:

$$\mathbf{F}_l = -\frac{k k_{rl}}{\mu_l}\rho_l(\nabla p_l)$$

The time discretization is carried out with an implicit finite difference scheme. The resulting discrete non linear equations used in TOUGH2, derived with the technique of integral finite differences with regular spacing discretization, are similar to equations (3.22).

3.5.1 Numerical solution scheme

The code TOUGH2 is programmed to solve the discrete non linear system (3.22) by Newton-Raphson iteration, which is implemented as follows. Let's first write equations (3.22) in a residual form as:

$$R_{ij}^{l,n+1} = - \phi \frac{S_{l,ij}^{t+1} - S_{l,ij}^{t}}{\Delta t} + \frac{\lambda_{l,ij}\left(p_{l,(i+1)j}^{t+1} - p_{l,ij}^{t+1}\right) + \lambda_{l,(i-1)j}\left(p_{l,ij}^{t+1} - p_{l,(i-1)j}^{t+1}\right)}{(\Delta x)^2} + \frac{\lambda_{l,ij}\left(p_{l,i(j+1)}^{t+1} - p_{l,ij}^{t+1}\right) + \lambda_{l,i(j-1)}\left(p_{l,ij}^{t+1} - p_{l,i(j-1)}^{t+1}\right)}{(\Delta y)^2} - q_{l,ij} \tag{3.23}$$

for $l = w, o$

For a two-phase flow system, $2 \times N$ coupled non linear equations must be solved (N= number of grid blocks), with two equations at each node for water and oil flow equations. The unknowns are the independent primary variables which completely define the state of the flow system at a given time. In this work the two primary variables are fluid pressure and saturation, and the rest of the dependent variables, such as relative permeability, as well as non selected pressure and saturation, are treated as secondary variables. In general the unknowns, can be expressed as $\xi_i \quad i = 1, \ldots, 2N$.

An iteration index κ is introduced and the residuals $R_n^{l,t+1}$, for node n, in equations (3.23) at iteration step $\kappa + 1$ in a Taylor series in terms of those at index κ are:

$$R_n^{l,t+1}(\xi_{i,\kappa+1}) + \sum_i \left.\frac{\partial R_n^{l,t+1}}{\partial \xi_i}\right|_\kappa (\xi_{i,\kappa+1} - \xi_{i,\kappa})) + \cdots = 0 \tag{3.24}$$

Retaining only terms up to first order, the following set of linear equations for the increments $(\xi_{i,\kappa+1} - \xi_{i,\kappa})$ is obtained:

$$-\sum_i \left.\frac{\partial R_n^{l,t+1}}{\partial \xi_i}\right|_\kappa (\xi_{i,\kappa+1} - \xi_{i,\kappa})) = R_n^{l,t+1}(\xi_{i,\kappa}) \tag{3.25}$$

All terms $\frac{\partial R_n}{\partial \xi_i}$ in the Jacobian matrix are evaluated by numerical differentiation. Equation (3.25) is solved by sparse direct matrix methods or iteratively by means of preconditioned conjugate gradients. Iteration is continued until the residual, $R_n^{l,t+1}$, for solving changes in primary variables, $\xi_{i,\kappa+1}$, over an iteration is reduced below a present convergence tolerance ε,

$$\left|R_n^{l,t+1}\right| \leqslant \varepsilon \tag{3.26}$$

3.6 Convergence and Stability

Likewise in single phase flow numerical solvers, spatial and temporal truncation error estimation have to be included in multiphase flow solution approaches (Kees and Miller, 2002). The numerical solution of the governing equation has only finite precision and may suffer from discretization errors such as numerical dispersion. While care must be taken when choosing the numerical scheme, errors from the numerical model are usually smaller than errors made by using wrong parameter values, which in turn are small compared with the errors from using an inappropriate conceptual model.

The beginnings of the research work for this dissertation encountered a curious and important feature of the numerical approach taken for 1D fractional flow equations. Here a resume of these results is submitted as these results are important to take into account when performing 1D two-phase flow simulations expressed with the fractional flow approach.

To commence with the research about the two-phase flow numerical approach, several 1D studies to reproduce the Buckley and Leverett displacement were planed. Fractional flow approximation was taken for that exercises, while it was not yet decided what numerical approximation for two-phase flow was the most suitable for the inversion method to be developed. The first possibility considered was the spatial numerical approximation suggested by Aziz and Settari (1979):

$$\frac{\partial f_w}{\partial S_w}\frac{\partial S_{w,i}}{\partial x} \simeq \frac{f'_{w,i}S_{w,i} - f'_{w,i-1}S_{w,i-1}}{\Delta x} \tag{3.27}$$

where $f'_{w,i}$ is the fractional flow derivative with respect water saturation S_w. This approximation differs from the one described in section 3.4, given by equation (3.13), which ended up to be much more appropriate. Let's see what happens when approximation (3.27) is used instead of approximation (3.13).

Equation (3.27) is common in petroleum engineering for cases in which the system of equations for multiphase flow is given in terms of pressure and saturation, or for the two-pressure approximation. Taking this spatial approach and the time discretization given by equation (3.14), the two-phase flow equation in one dimension is:

$$\frac{V_i}{\Delta t}\left(S_{w,i}^{t+1} - S_{w,i}^{n}\right) + Q_T\left[f_{w,i}'^{\,t+1}S_{w,i}^{t+1} - f_{w,i-1}'^{\,t+1}S_{w,i-1}^{t+1}\right] = 0 \tag{3.28}$$

This equation is the equivalent to formula (3.17), but with spatial discretization corresponding to (3.28). The way it was deduced is equivalent, and compressibility, gravitary and capillary forces are neglected.

To check the behavior of this approach the next step was to compare the numerical results given by expression (3.28) with the analytical solution given by Buckley and

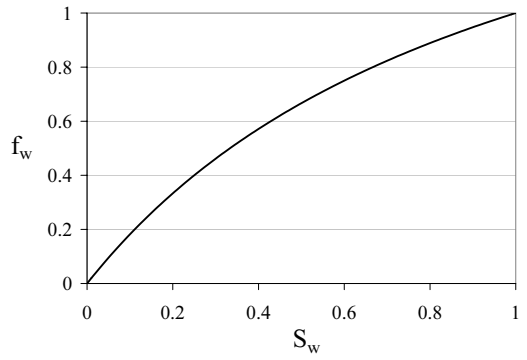

(a) Case A

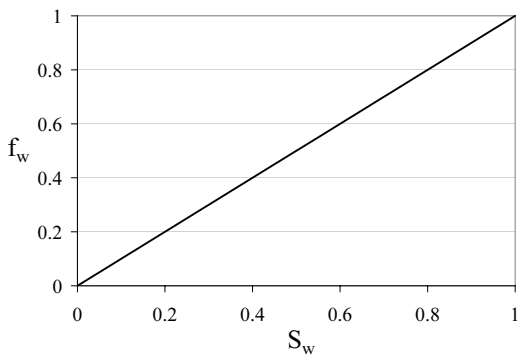

(b) Case B

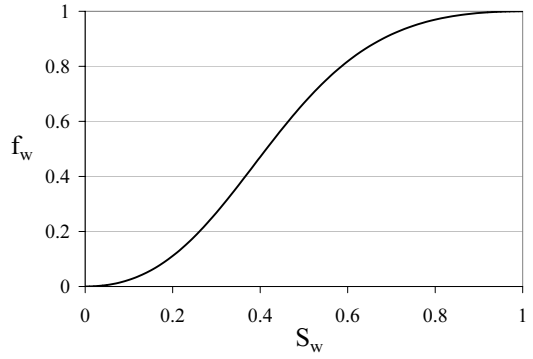

(c) Case C

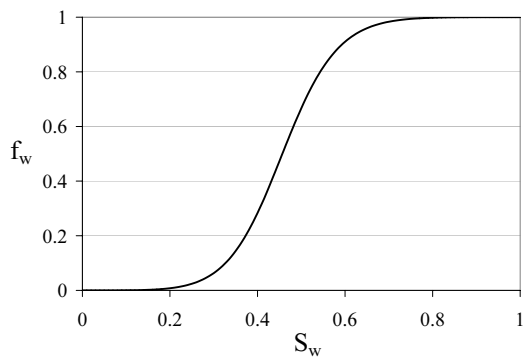

(d) Case D

Figure 3.9: f_w in function of S_w for cases A, B, C and D. In equation (3.29) case A: $n_o = n_w = 1.0$ and $\mu_o k^0_{rw}/\mu_w k^0_{ro} = 2.0$, case B: $n_o = n_w = 1.0$ and $\mu_o k^0_{rw}/\mu_w k^0_{ro} = 0.5$, case C: $n_o = n_w = 2.0$ and $\mu_o k^0_{rw}/\mu_w k^0_{ro} = 2.0$ and case D: $n_o = n_w = 2.0$ and $\mu_o k^0_{rw}/\mu_w k^0_{ro} = 0.5$.

Leverett (e.g., Figure 3.7) described in appendix A. The work domain consisted of 500 discretization nodes and the time domain was discretized with 500 time steps. The results are given in function of adimensional spatial coordinate x_D and adimensional time t_D, both defined following the analytical formulation given by Buckley and Leverett (see appendix A).

Comparing equation (3.28) with equation (3.17), fractional flow derivative appears instead of fractional flow. This new variable, saturation dependent, is analytically calculated. Substituting analytical expressions for relative permeability curves given by equations (3.6) in the fractional flow equation (3.8), the fractional flow in function of saturation is:

$$f_w = \frac{1}{1 + \frac{\mu_w k^0_{ro}}{\mu_o k^0_{rw}} \frac{(1-S)^{n_o}}{S^{n_w}}} \tag{3.29}$$

where S is the water reduced saturation:

$$S = \frac{S_w - S_{rw}}{1 - S_{rw} - S_{ro}}$$

The fractional flow derivative with respect saturation is:

$$f'_w = \frac{\frac{\mu_w k^0_{ro}}{\mu_o k^0_{rw}}\, n_w (1-S)^{n_o} S^{n_w - 1} + \frac{\mu_w k^0_{ro}}{\mu_o k^0_{rw}}\, n_o (1-S)^{n_o - 1} S^{n_w}}{\left(S^{n_w} + \frac{\mu_w k^0_{ro}}{\mu_o k^0_{rw}}\,(1-S)^{n_o}\right)^2 (1 - S_{ro} - S_{rw})} \tag{3.30}$$

Assuming immiscible displacements, the shape presented by the fractional flow curve has an important influence on the numerical results (Young 1984). Four different fractional flow curves were used, varying the values of the two indexes n_w and n_o and the mobility ratio $\mu_o k^0_{rw}/\mu_w k^0_{ro}$. The four curves f_w-S_w are drawn in Figures 3.9(a) to 3.9(d). The four cases are going to be called case A for f_w in Figure 3.9(a) $n_o = n_w = 1.0$ $\mu_o k^0_{rw}/\mu_w k^0_{ro} = 2.0$, case B in Figure 3.9(b) $n_o = n_w = 1.0$ $\mu_o k^0_{rw}/\mu_w k^0_{ro} = 0.5$, case C in Figure 3.9(c) $n_o = n_w = 2.0$ $\mu_o k^0_{rw}/\mu_w k^0_{ro} = 2.0$ and case D in Figure 3.9(d) $n_o = n_w = 2.0$ $\mu_o k^0_{rw}/\mu_w k^0_{ro} = 0.5$.

Numerical approach given by equation (3.28) resulted in the saturation fronts graphed in Figures 3.10(a) to 3.10(d), corresponding respectively to cases A to D. Analytical and numerical solutions for time $t_D = 0.5$ are shown in these figures. In cases A and B it is found quite good reproduction of the analytical solution, but in cases C and D the match is not good enough. So, it can be concluded that numerical approximation given by equation (3.28) does not converge to the analytical solution for some fractional flow curves.

However, if instead of using approximation (3.28) equation (3.17) is used, the results are good for all the four fractional flow curves tested. These results are shown in Figures 3.11(a) to 3.11(d) for the four cases A, B, C and D, also for $t_D = 0.5$. Hence, the results suggest that this discretization is more appropriate when studying the fractional flow approximation.

It has been already mentioned that it is very important to choose spatial and temporal increments small enough to converge the numerical approach. The temporal increments have to be taken such as the maximum change of saturation is not too big. Aziz and Settari (1979) affirm that to make the solution stable the temporal increment has to follow this relation:

$$\triangle t < \frac{\phi}{u_T f'_{wi}} \triangle x. \tag{3.31}$$

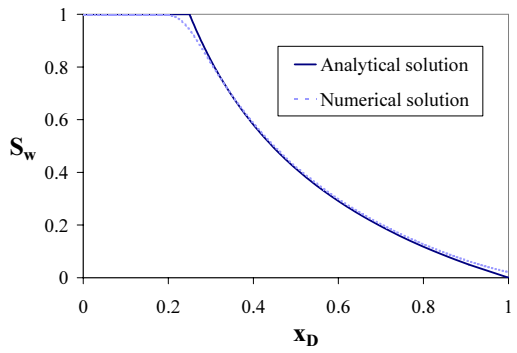

(a) Case A

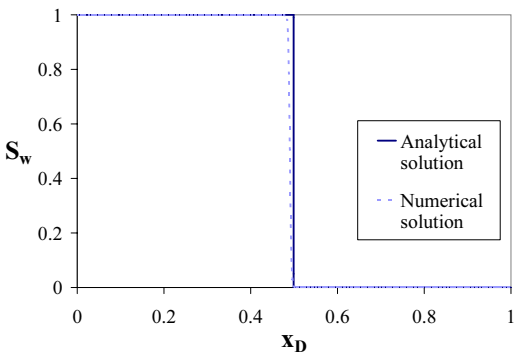

(b) Case B

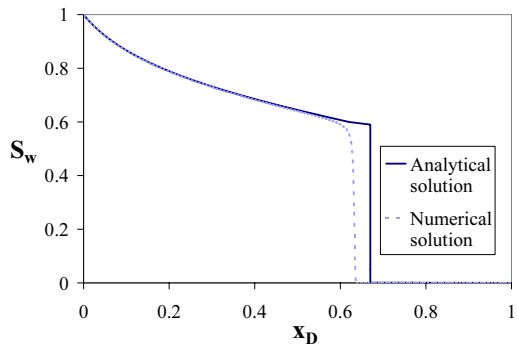

(c) Case C

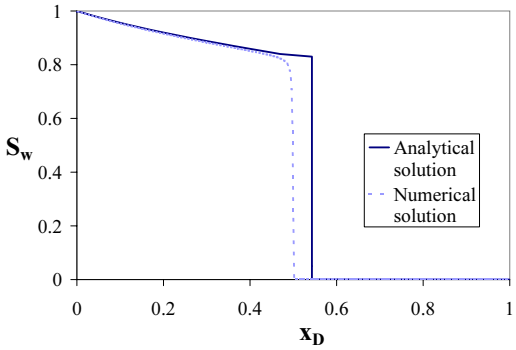

(d) Case D

Figure 3.10: S_w in function of x_D for time $t_D = 0.5$. $f_w - S_w$ curves are given in Figures 3.9 for cases A, B, C and D. Numerical approach for the discretization is equation (3.28) case A: $n_o = n_w = 1.0$ and $\mu_o k^0_{rw}/\mu_w k^0_{ro} = 2.0$, case B: $n_o = n_w = 1.0$ and $\mu_o k^0_{rw}/\mu_w k^0_{ro} = 0.5$, case C: $n_o = n_w = 2.0$ and $\mu_o k^0_{rw}/\mu_w k^0_{ro} = 2.0$ and case D: $n_o = n_w = 2.0$ and $\mu_o k^0_{rw}/\mu_w k^0_{ro} = 0.5$.

This guarantees that the saturation front advances with a velocity of, at least, a grid block per unit time step.

Using different spatial discretization that obey relation (3.31), several two-phase flow runs have been performed. The results are represented in Figure 3.12. The spatial discretization that represent almost exactly the Buckley and Leverett analytical solution are $\Delta x_D = 0.002$ y $\Delta x_D = 0.004$, while for $\Delta x_D = 0.05$ the convergence is not good enough. In all the runs the mobility ratio is taken as $\mu_o k^0_{rw}/\mu_w k^0_{ro} = 2.0$. These results mark the need to use adequate spatial and temporal discretization (Aziz and Settari, 1979) at the same time that show the applicability of the 1D fractional flow numerical approximation in order to reproduce the analytical solution of the saturation

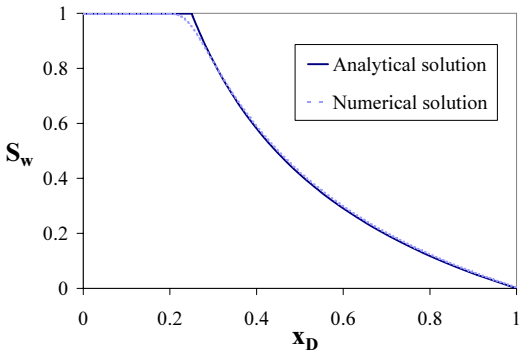

(a) Case A

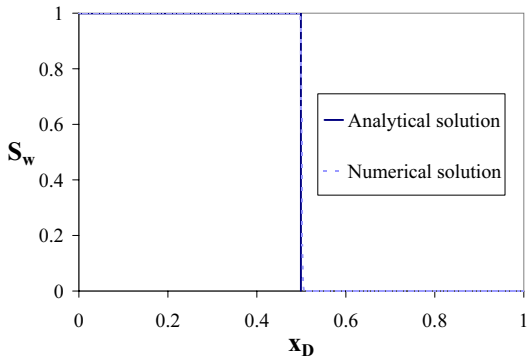

(b) Case B

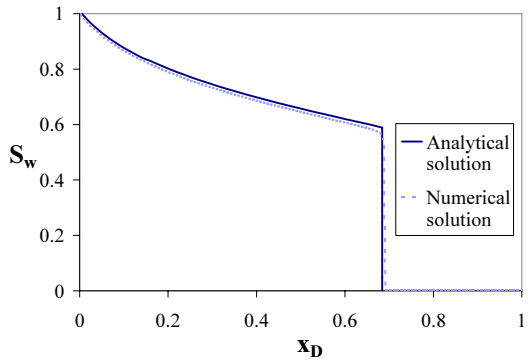

(c) Case C

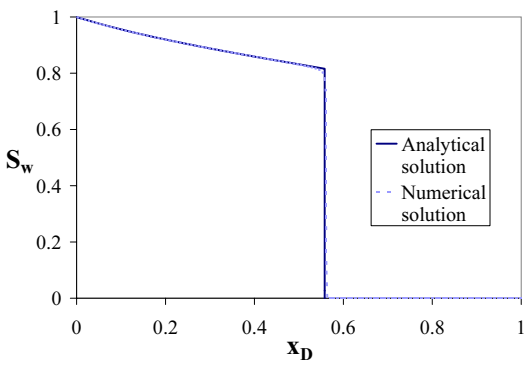

(d) Case D

Figure 3.11: S_w in function of x_D for time $t_D = 0.5$. $f_w - S_w$ curves are given in Figures 3.9 for cases A, B, C and D. Numerical approach for the discretization is equation (3.17) case A: $n_o = n_w = 1.0$ and $\mu_o k^0_{rw}/\mu_w k^0_{ro} = 2.0$, case B: $n_o = n_w = 1.0$ and $\mu_o k^0_{rw}/\mu_w k^0_{ro} = 0.5$, case C: $n_o = n_w = 2.0$ and $\mu_o k^0_{rw}/\mu_w k^0_{ro} = 2.0$ and case D: $n_o = n_w = 2.0$ and $\mu_o k^0_{rw}/\mu_w k^0_{ro} = 0.5$.

front.

3.7 Applying numerical two-phase flow solver

To give an idea of the applicability of the numerical scheme taken for the two-phase flow solver in 1D an 2D, a series of examples are presented. At the same time, the relevance of heterogeneities in relative permeability curves is going to be shown for both one and two dimensional cases.

All numerical studies were run on dedicated machines running Suse Linux 8.0 with 1800+AMD processors, 1 Gb of RAM. The code was compiled with gcc/ifc and -O3

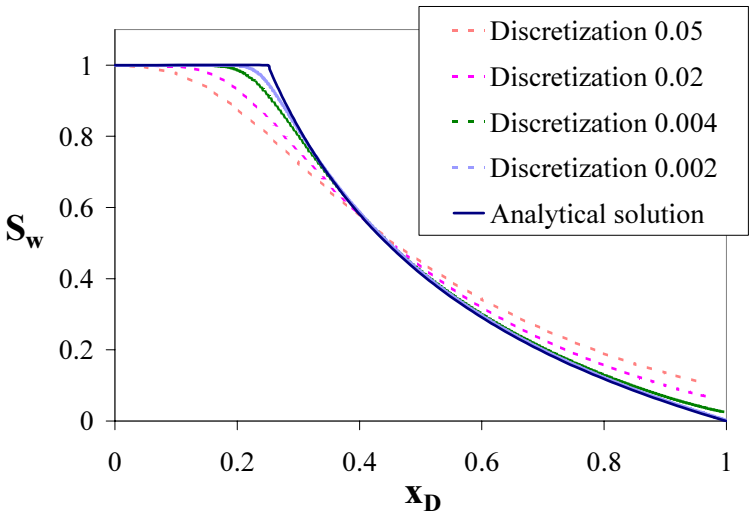

Figure 3.12: Comparison between Buckley and Leverett analytical solution and numerical solution using different spatial discretization. The problem is similar to the Buckley and Leverett displacement problem where water is injected in the left node ($x_D = 0.0$) and is pumped in the right node ($x_D = 1.0$). The different discretizations used are: $\Delta x_D = 0.05$, $\Delta x_D = 0.002$, $\Delta x_D = 0.004$ y $\Delta x_D = 0.002$, and the mobility ratio taken is equal to $\mu_o k^0_{rw}/\mu_w k^0_{ro} = 2.0$.

optimization.

As the goal of this dissertation is to take into account the heterogeneity of both absolute and relative permeabilities it was necessary to modify the code T2VOC (Falta et al., 1995) in order to be able to input absolute permeabilities and relative permeability curves for each of the nodes, or at least, for a number of zones in which the domain can be divided.

3.7.1 Spatial parameters estimation

Remember the diagram in chapter 1 (Figure 1.1), ones the conceptual model is built, the parameter values have to be assigned (step II in Figure 1.1). Here the parameters subjected to study are absolute and relative permeabilities, and their spatial distribution has to be estimated. Geostatistics has given a wide variety of techniques for spatial data analysis, estimation and simulation. Kriging is the basic geostatistical tool in order to interpolate measured data, for mapping application purposes. Kriging, and in general all estimation techniques have several drawbacks. Estimation produces a smooth map of the variable, and moreover this smoothing is not uniform (e.g., a map of kriging estimates displays artifact structures). Instead of estimating, simulation techniques give a possible solution to the estimation drawbacks. Simulation techniques

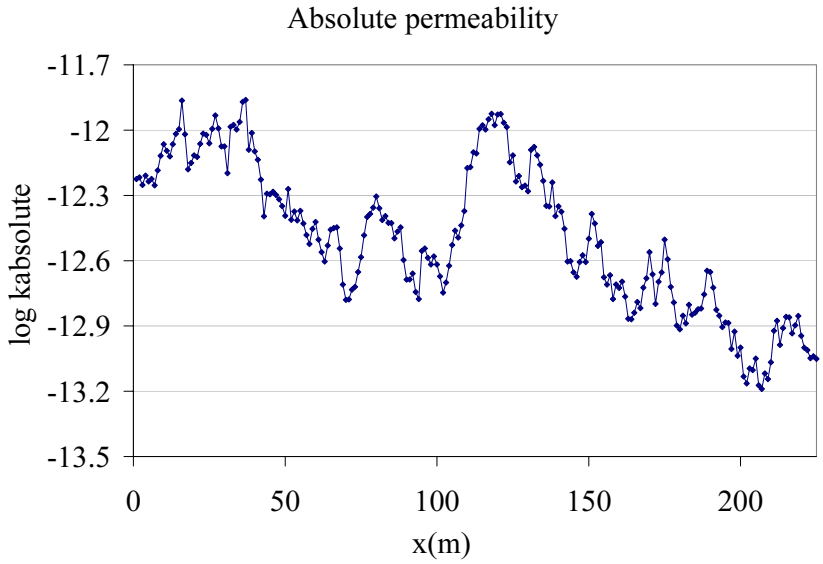

Figure 3.13: One dimensional example of the logarithm of absolute permeability field. This field is the result of performing a sequential Gaussian simulation for 225 nodes.

go further than just estimating a permeability field, they can generate multiple equally likely realizations of permeability fields with the desired geostatiscal features. The idea of simulations is to build a representation of the field that is consistent with the data observed, as kriging is, but the result is one of the possible versions of the reality. There are many algorithms that can be applied to simulate spatial distribution of permeability: matrix approaches (LU Decomposition), turning bands, spectral methods using fast Fourier transforms, moving averages, probability-field simulation, simulated annealing, and sequential Gaussian simulation. This last method is the most common approach adopted in recent times for reservoir modeling applications. For more information about kriging and simulation algorithms the reader is referred to Armstrong and Dowd (1994), Goovaerts (1997), Chiles and Delfiner (1999) and Deutsch (2002).

Before performing the simulation, a structural analysis and a statistical parameter inference must be performed. The purpose of this stage is to identify different zones of permeability within each of which the spatial statistical properties (e.g., histogram and variogram) can be inferred from the available data. In some occasions, when the number of data available are not enough to infer a spatial structure, the variogram is imposed from similar data set or case studies. With the variogram model defined, the sequential Gaussian simulation consists of visiting each grid node in a random order and following next steps:

1. Look for nearby data and previously simulated grid nodes.

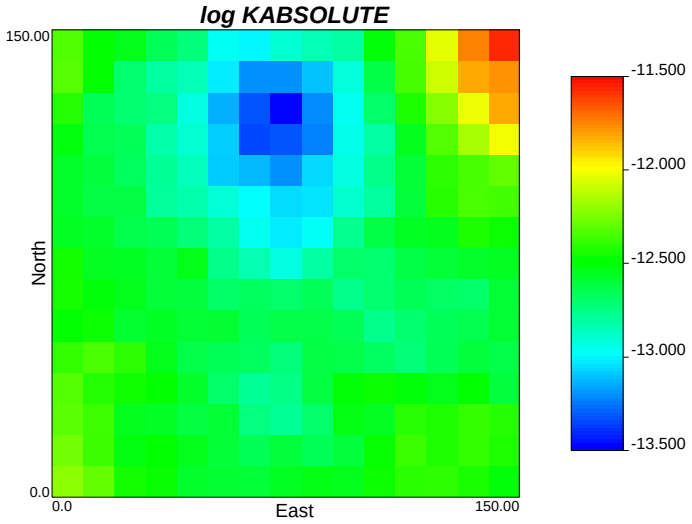

Figure 3.14: Two dimensional example of the logarithm of absolute permeability field. This field is the result of performing a sequential Gaussian simulation for 15x15 nodes.

2. Perform kriging and construct the conditional distributions calculating a mean and estimation variance by simple kriging.

3. Draw a simulated value from the conditional distribution (normal with mean and variance from step 2).

This entire procedure can be repeated with different random number of seeds to generate multiple realizations.

In the present study absolute permeability field is considered to be heterogeneous but isotropic. Conditional or unconditional simulations can be used to construct absolute permeability, which can be represented by a lognormal distribution with known mean and variance. Hence, it is also assumed that the spatial variability of absolute permeability is characterized by a known omnidirectional variogram. To generate simulated fields in this dissertation it was used the code GCOSIM3D (Gómez-Hernández and Journel, 1993). For 1D, the resulting simulated absolute permeability field could be the one shown in Figure 3.13, in which the total domain consists of 225 nodes. The graph in Figure 3.13 represents the logarithm of absolute permeabilities.

In 2D a simulation of absolute permeability values is represented in Figure 3.14. The heterogeneities are reflected by an area of low permeability and an area of high permeability, both of them quite close to each other.

To represent relative permeability functions power analytical expressions have been chosen. The formulas given in equations (3.6), corresponding to Brooks and Corey (1966), are taken for this dissertation. In the estimation of heterogeneous relative

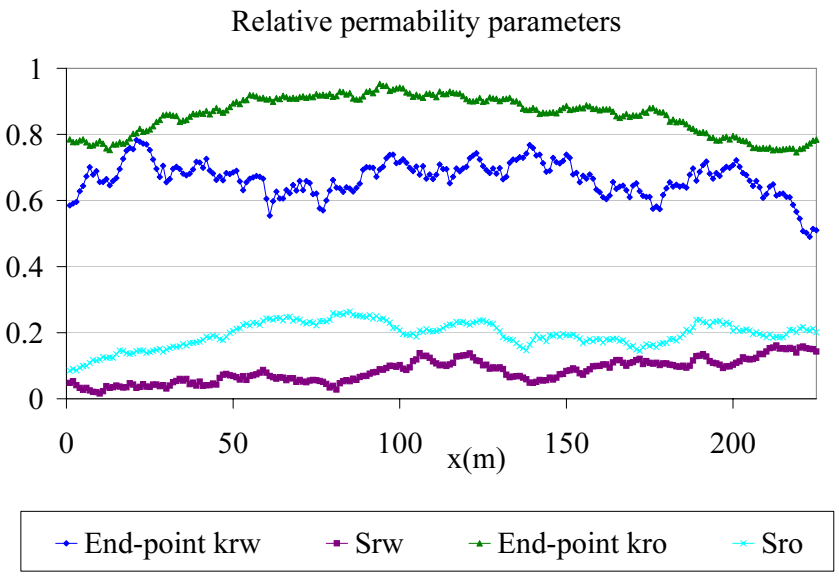

Figure 3.15: One dimensional example of S_{rw}, S_{ro}, k^0_{rw} and k^0_{ro} simulations. These parameters correspond to the relative permeability formulation given in equation (3.6). The total simulated field consists of 225 nodes.

permeabilities indexes n_w and n_o are assumed to be known, the two residual saturations S_{rw} and S_{ro}, and two end-points k^0_{rw} and k^0_{ro} for water and oil are assumed to be the parameters representing the heterogeneity. This means that to simulate heterogeneous relative permeabilities of water and oil, four simulations for S_{rw}, S_{ro}, k^0_{rw} and k^0_{ro} have to be run. The results for one case in 1D are shown in Figure 3.15. Four simulations has been carried out giving a simulated field for each of the parameters, S_{rw}, S_{ro}, k^0_{rw} and k^0_{ro}, at every node.

In 2D one possibility for relative permeability simulated fields is drawn in Figures 3.16(a) to 3.16(d). For absolute permeability fields the variogram taken to represent its spatial structure is spherical, while for the relative permeability parameters the variogram is Gaussian. Figure 3.16(a) corresponds to the end-point of water relative permeability, Figure 3.16(b) to water residual saturation, figure 3.16(c) to end-point of oil relative permeability and Figure 3.16(d) to oil residual saturation.

3.7.2 Flow results

Simulated fields for absolute and relative permeabilities are introduced in the numerical solver (step III in Figure 1.1) for two-phase flow. Initial and boundary conditions are also necessary to get a solution for the problem. In 1D, the problem that is going to be solved has one injector well at one extreme of the domain (node number 1) and one production well at the other extreme (node number 225). Constant mesh with block

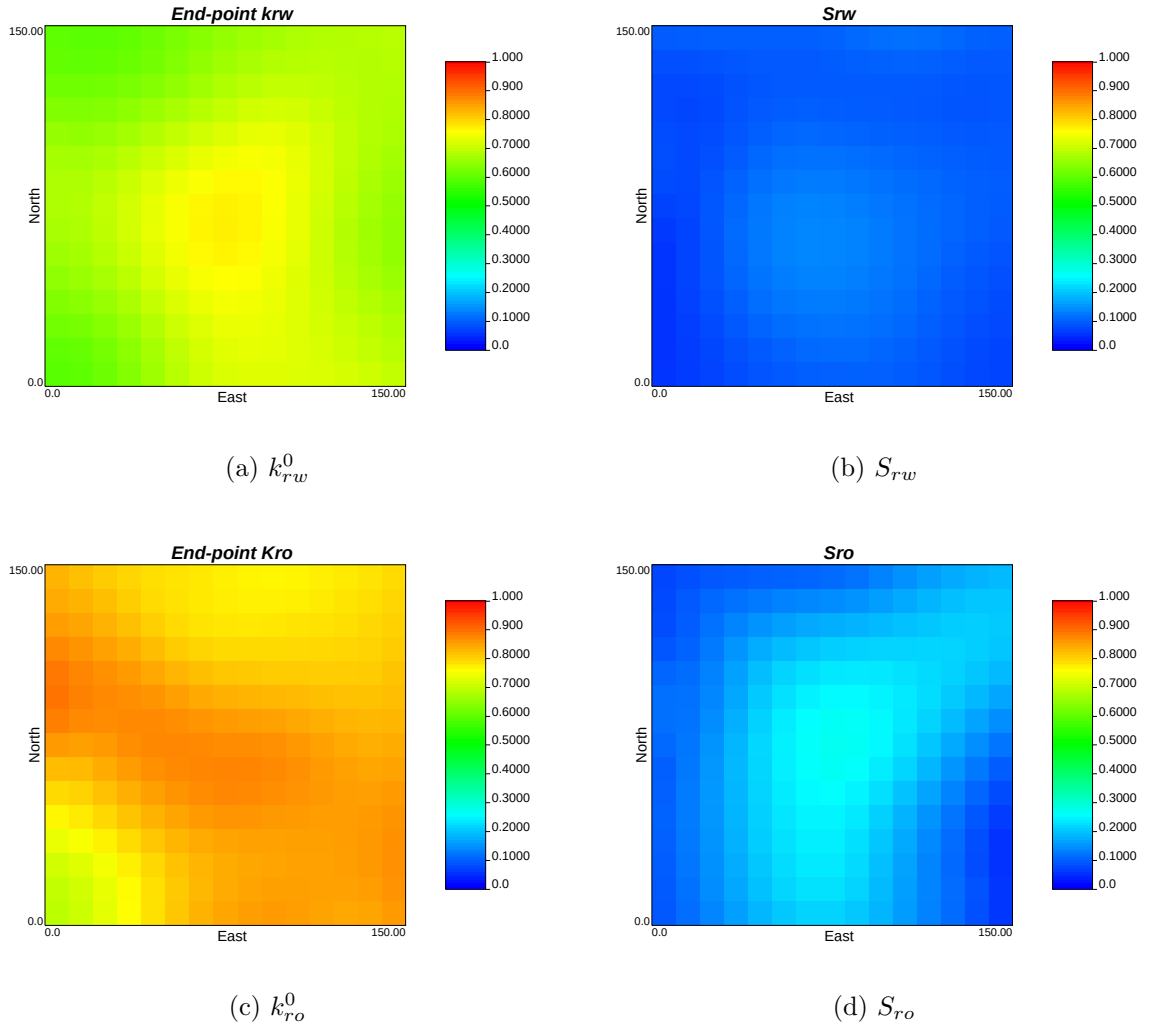

(a) k^0_{rw} (b) S_{rw}

(c) k^0_{ro} (d) S_{ro}

Figure 3.16: Two dimensional example of simulated values for k^0_{rw}, S_{rw}, k^0_{ro} and S_{ro} (equation (3.6)). 15x15 grid blocks.

grids of 1 meter length by 10 meter width is taken. The initial conditions are $S_w = 0.2$ and $P = 6.895e6$ Pa. The water is injected into the porous medium filled with oil and water. Water is injected at constant rate of 75×10^{-3}kg/s. For these examples mobility ratio is taken to be equal to one, $k^0_{rw}\mu_o/k^0_{ro}\mu_w = 1$. Constant 10.35 hour time steps are prescribed, an the simulation is run to 345.18 days.

Two different runs are performed, both of them with the absolute permeability field shown in Figure 3.9, but with different relative permeability fields. The first run is done assuming homogeneous relative permeabilities, so just one relative permeability curve for each of the fluids is taken. The parameters k^0_{rw}, k^0_{ro}, S_{rw} and S_{ro} are set to be equal to the average values taken to perform the simulations in Figure 3.11. These values are: $k^0_{rw} = 0.7$, $S_{rw} = 0.1$, $k^0_{ro} = 0.85$ and $S_{ro} = 0.2$. The second run is done

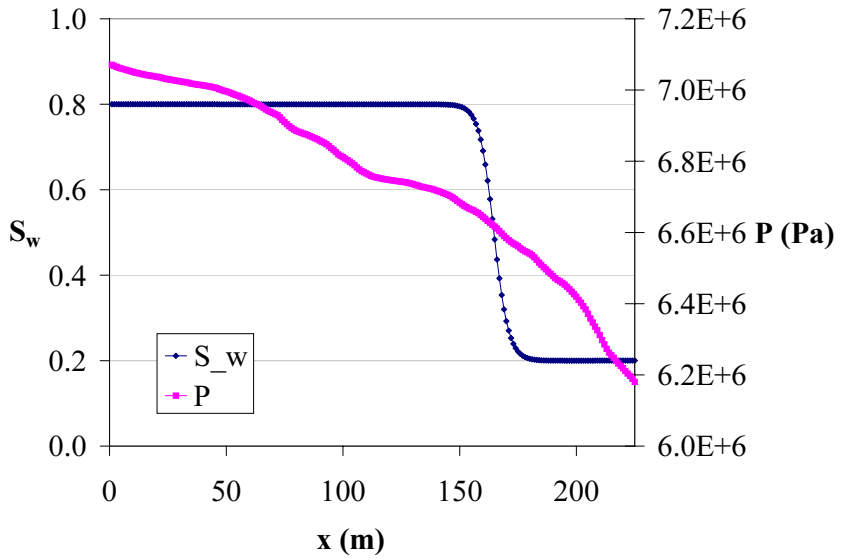

Figure 3.17: Saturation and pressure front corresponding to 1D two-phase flow when absolute permeability is taken heterogeneous, but relative permeability curves are homogeneous within all the domain. Injection water is applied in the grid block situated to the left.

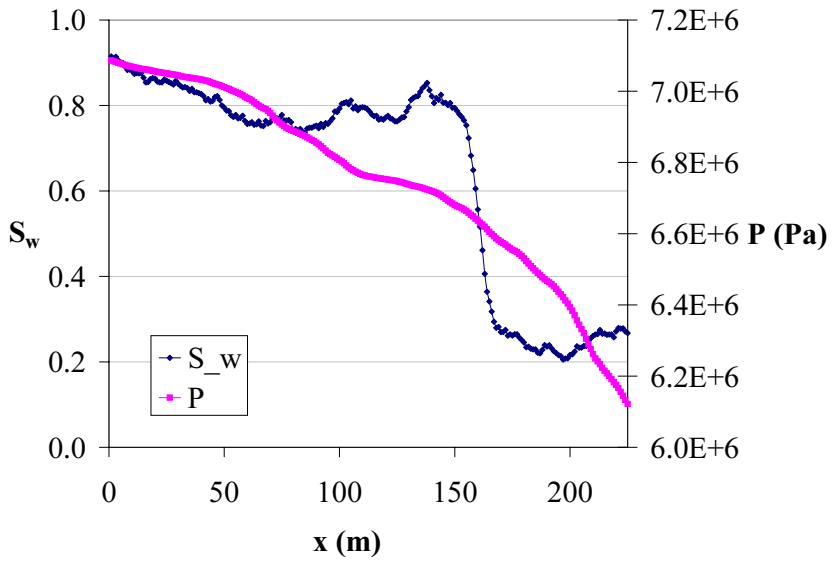

Figure 3.18: Saturation and pressure front corresponding to 1D two-phase flow when absolute and permeability are taken to be heterogeneous. Relative permeability parameters correspond to Figure 3.15. Injection water is applied in the grid block situated to the left.

with heterogeneous values for all four parameters represented in Figure 3.15. For both runs saturation and pressure fields are obtained all over the domain (Figures 3.17 and

3.18).

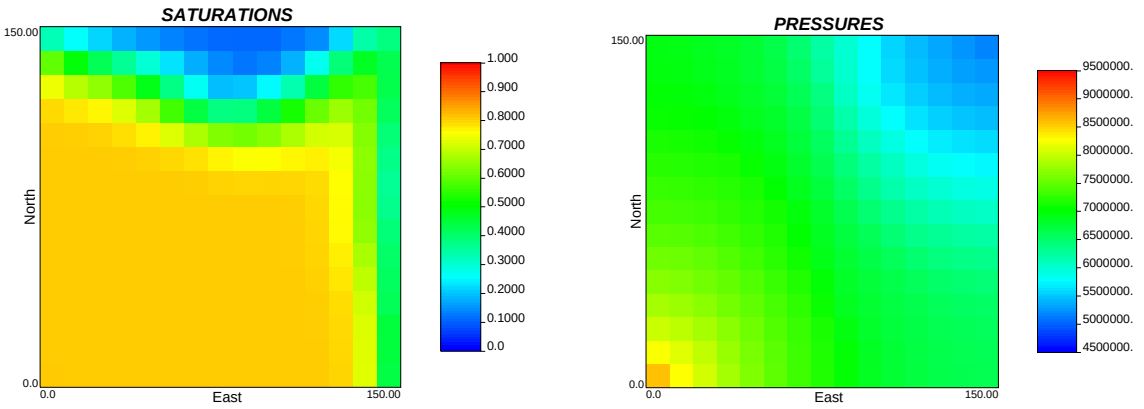

Figure 3.19: Saturation and pressure front corresponding to 2D two-phase flow when absolute permeability is taken heterogeneous, but relative permeability curves are homogeneous within all the domain. Injection water well is situated in the left lower grid block.

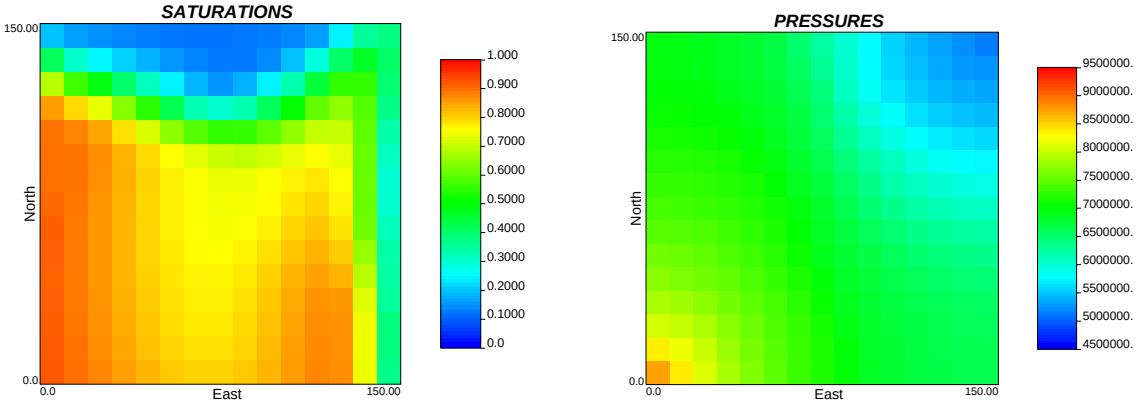

Figure 3.20: Saturation and pressure front corresponding to 2D two-phase flow when absolute and relative permeability are taken heterogeneous within all the domain. Relative permeability parameters are taken from figures 3.16(a) to 3.16(d). Injection water well is situated in the left lower grid block.

The main difference observed between Figure 3.17 and Figure 3.18 is that the saturation front for the heterogeneous relative permeability case presents some fluctuations in comparison to the homogeneous case. However, the pressure field does not present important differences when the absolute permeability field used is the same.

In the 2D case the parameters used are different. The grid sizes are 10mx10m, for a total of 15x15 grid blocks. The injector well is situated at the left lower corner, and the production well at the right upper corner. The initial conditions for the 2D run are $S_w = 0.1$ and $P = 6.895e6$ Pa. The water is injected into the porous medium filled

with oil and water. Water is injected at constant rate of 2.5kg/s. Constant 4.8 hour time steps are prescribed, an the simulation is run to 120 days.

In the same manner that it was done for the 1D case, two runs where carried out in 2D. One with homogeneous parameters for water and oil relative permeability curves (Figure 3.19) and the other with the heterogeneous field (figure 3.20). The heterogeneous parameters are given by Figures 3.16(a) to 3.16(d). The homogeneous relative permeability curves are described with the same parameter values than in the 1D case: $k^0_{rw} = 0.7$, $S_{rw} = 0.1$, $k^0_{ro} = 0.85$ and $S_{ro} = 0.2$

The results in 2D, as in the 1D case, show that for the same heterogenerous absolute permeability field the pressures do not reflect the heterogeneities of the relative permeability curves. The saturation is the variable that is highly influenced by the changes in the spatial distribution of the water and oil relative permeability curves.

In this chapter the forward two-phase flow numerical solver has been studied and adapted to take into account relative permeability heterogeneities. Numerical results have been compared with analytical solutions in 1D. The method has been applied in one and two dimensions to show the different characteristics when assuming homogeneous or heterogeneous relative permeability fields. The forward numerical solver needed is ready to be used, next chapter moves on the inverse modeling process and deals with the development of the inverse technique itself.

Chapter 4

Inverse method

When in chapter 1 numerical flow modeling was introduced, the explanation was assisted with the scheme given in Figure 1.1. Within the former chapter 3 both steps II and III of this scheme were described and detail instructions of the existing tools, for both parameter value assignment and numerical two-phase flow solution, were given. The next step, following Figure 1.1, is to apply the flow simulator to field cases. The results given by the two-phase flow solution has to be interpreted and used in order to predict how the reservoir in going to behave in the future. Before this can be done, it is very important to check if the model results are agree with all the available data. Following steps II and III it is guaranteed that the static parameter data are reproduced, but quite frequently it is found out that dynamic data are not. In this chapter the method already introduced as inverse modeling is going to be described in detail, in particular the inverse methodology followed and developed in this dissertation is going to be discussed. The basic ideas described in this chapter are very similar to the self-calibrated method (Hendricks-Franssen, 2001; Gómez-Hernández et al.,1997).

4.1 Self-calibrated method

Nowadays the generation of conditioned permeability fields in order to characterize an aquifer or a petroleum reservoir is a technique highly developed and of common usage. However, usually this initial model does not honor the production data when they are calculated with a numerical reservoir simulator under the same flow conditions. When the permeability field is going to be conditioned to such a dynamic data, the problem is the non linear relation given by the non linear differential equations (developed in chapter 3). The determination of the input parameters for the flow equations, in order to reproduce the saturation and pressure data, it is normally known as the inverse problem.

The main idea is based on the fact that saturations and pressures contain, indirectly, very important information about the properties in the reservoir. Thus, it is of vital importance that this information is incorporated in the characterization process. The calibrated parameters that reproduce the saturation and pressure data are closer to real values than those that cannot reproduce these dynamic data.

The self-calibrated method (Sahuquillo et al., 1992; Gmez-Hern ndez et al., 1997; Hendricks-Franssen, 2001) was developed to obtained real estimations of the piezometric heads in the aquifer. The estimation reflects the spatial variability corresponding to the model, at the same time that contributes with an uncertainty model. The self-calibrated method allows to integrate the most quantity of information that it is possible in order to condition the realizations of the reservoir attributes.

In this dissertation the self-calibrated method scheme is followed, adapting the method to two-phase flow equations described in chapter 3. The differential variation of water saturation is incorporated. The extension of the self-calibrated method presented here consists in the calibration of a parameter set that constitute the relative permeability functions. These parameters are chosen to characterize the heterogeneity of the relative permeability curves, and are: the end-points, k^0_{rw} and k^0_{ro}, and residual saturations S_{rw} and S_{ro}, for both water and oil phases, four values that control the length of the relative permeability curves when they are expressed in function of saturation.

The main steps of the iterative process, followed by the inversion technique developed, are resumed here. The loop from step 2 to step 7 is repeated until convergence is reached (see Figure 4.1). For each iteration ^{IT}:

1. Geostatistical techniques are used to generate a reservoir parameter model conditioned to local measurements of parameters, as it was explained in chapter 3. Simulations of the four parameters k^0_{rw}, k^0_{ro}, S_{rw} and S_{ro} and absolute permeability k are carried out. These values can be simulated in such a way that they only reproduce the spatial distribution taken to characterize the reservoir (unconditional simulations). Or, they can be simulated with additional constrains at the data points (conditional simulations). The built fields, conditional or unconditional, constitute the seed or initial input fields.

2. Initial model (created in setp 1) is input into the two-phase flow numerical solver. Saturation and pressure field are obtained for all the time steps at every grid block.

3. An objective function is defined as the squared difference of the simulated and observed saturation and pressures. Parameters are estimated by iteratively minimizing this objective function, which measures the deviation between the data

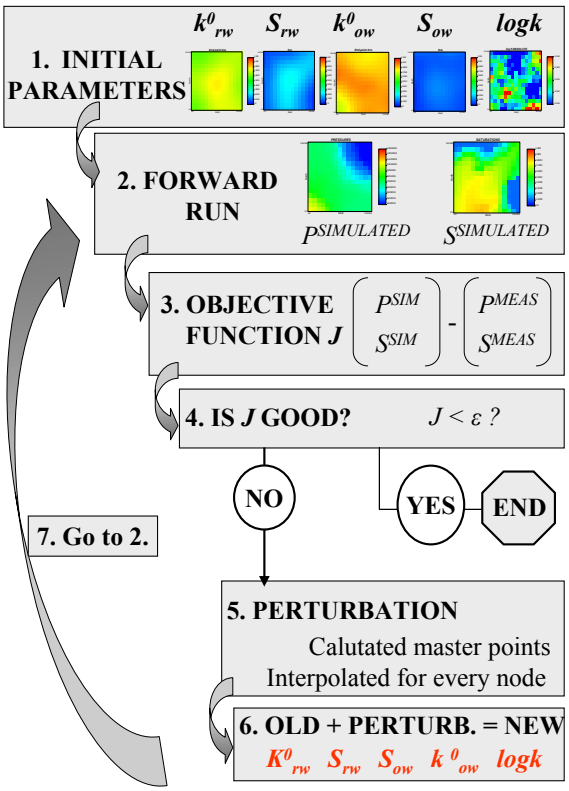

Figure 4.1: Self-calibrated method scheme.

and the model calculation:

$$J^{IT} = \sum_{t=1}^{T_s} \sum_{i=1}^{N_s} w_{s,i} \left(S_{i,t}^{SIM,IT} - S_{i,t}^{MEAS} \right)^2 + \sum_{t=1}^{T_p} \sum_{i=1}^{N_p} w_{p,i} \left(p_{i,t}^{SIM,IT} - p_{i,t}^{MEAS} \right)^2 \tag{4.1}$$

N_s and N_p are, respectively, the number of saturation and pressure data points. T_s and T_p are the number of times at which the measurements have been taken, for saturation and pressure respectively. Indexes ^{SIM} and ^{MEAS} indicate simulated and measured values. w_s and w_p are the weights that multiply the two terms in the objective function.

4. If J is smaller than a pre-determined value, the simulated permeability values are said to be conditioned to the measured saturation and pressure values, and the iterative loop stops. On the contrary, if J is not small enough, the optimization continues and k, k_{rw} and k_{ro} fields are perturbed. With this perturbation an

improvement in the saturation and pressure values is searched, in order to get them closer to the real ones (J smaller).

5. The optimization procedure determines the value of the perturbation that is applied to the initial field so that the objective function is reduced. In order to diminish the parameter dimension, the optimization is parameterized as a function of the perturbations of permeability at a few selected locations, called master points. If permeability measurements are assigned to master point positions, their perturbation is equal to zero when measurements do not have any error. When saturation and/or pressure is available at one point this point should be assigned to be a master point. In the case of absolute permeability the logarithm of absolute permeability, $log(k)$, is used for the optimization instead of k. For the method developed here, perturbations are computed from the gradient of the objective function. To explain the formulation, let's say that iteration ^{IT} is already finished and perturbations for iteration $^{IT+1}$ are going to be calculated. Parameter k^0_{rw} is taken to illustrate the equations in detail, with the rest of parameters the algorithm is equivalent. If the steepest descent optimization method is used, the element of perturbation vector $\{\Delta k^0_{rw}\}^{IT+1}$ at master point m is:

$$\Delta k^0_{rw}\big|_m^{IT+1} = -\alpha \quad g_{k^0_{rw}}\big|_m^{IT+1} \tag{4.2}$$

m represents any of the total number of master points, N_m. α is a step size along the gradient direction, which can be obtained using linear optimization. $g_{k^0_{rw}}\big|_m^{IT+1}$ is the gradient of the objective function with respect k^0_{rw} at point m for the iteration $^{IT+1}$ of the non linear optimization.

6. The resulting perturbations at the master points are extended throughout the entire reservoir domain by interpolation to obtain the perturbations that are going to be apply to the initial field to get a new field. The interpolation of the perturbations at every node is expressed with a linear combination of the perturbations at the master points. The perturbation $\Delta k^0_{rw}|^{IT+1}$ at any point i is equal to:

$$\Delta k^0_{rw}\big|_i^{IT+1} = \sum_m^{N_m} e_{i,m}\ \Delta k^0_{rw}\big|_m^{IT+1} \tag{4.3}$$

where $e_{i,m}$ could be ordinary kriging coefficients when estimating $\Delta k^0_{rw}|_i^{IT+1}$ from the values at master points, or the coefficients of a linear interpolation. In this dissertation inverse distance interpolation scheme is employed. If $D_{i,m}$ is the

distance between the point of interest i and the master point m, the weight $e_{i,m}$ is given by:

$$e_{i,m} = \frac{\frac{1}{D^b_{i,m}}}{\sum_{j=1}^{N_m} \frac{1}{D^b_{i,j}}}$$

where b is an appropriate constant. Once the perturbations are interpolated at every node, $\Delta k^0_{rw}|_i^{IT+1}$ in equation (4.3)), the new parameter field for iteration $^{IT+1}$ at point i is equal to:

$$k^0_{rw}\big|_i^{IT+1} = k^0_{rw}\big|_i^{IT} + \Delta k^0_{rw}\big|_i^{IT+1} \qquad i = 1, ..., N \tag{4.4}$$

With vector notation:

$$\left\{k^0_{rw}\right\}^{IT+1} = \left\{k^0_{rw}\right\}^{IT} + \left\{\Delta k^0_{rw}\right\}^{IT+1} \tag{4.5}$$

7. Go to step 2. The modified reservoir model, $\{k^0_{rw}\}^{IT+1}$, $\{S_{rw}\}^{IT+1}$, $\{k^0_{ro}\}^{IT+1}$, $\{S_{ro}\}^{IT+1}$ and $\{k\}^{IT+1}$, is input again into the reservoir simulator. The squared differences of simulated and observed saturations and pressures are re-evaluated (step 3), and the whole process continues until the solution of pressures and saturations corresponding to the numerical reservoir simulator is close to the observed data.

The equation that defines the objective function was given in step 3. The purpose and interpretation of the weights that appeared in equation (4.1), $w_{s,i}$ and $w_{p,i}$, could be explained with the next points:

- They scale data of different quality, that is, an accurate measurement obtains a higher weight than a more uncertain measurement.

- They scale observations of different types. For example, saturations and pressures have different units and usually differ by many orders of magnitude. They need to be scaled appropriately to be comparable in a formalize parameter estimation procedure.

- They weight the fitting error.

4.2 Computing the perturbations

Steps 1 to 7 described in former section summarized the whole process that is involved in the inversion. In step 5 the change directions are computed and the step size, α, that defines the perturbation is calculated. This process of searching the direction and module of the perturbation, in order to get a smaller objective function, is done with optimization methods. There exist various optimization algorithms, sorted in chapter 2. These are search methods, gradient methods and second order methods. In this dissertation, due the complexity of the non linear problem purposed, gradient methods are used. The objective of this section is to explain how the perturbations or variations are computed.

The basic gradient method is the steepest descent method, for which the search direction is equal to the negative gradient direction at each iteration ^{IT} (equation (4.2)). The optimal step size along this direction can be determined by a linear search. However, perturbation direction does not have to be equal to the negative gradient direction. One can avoid the gradient method using Quasi-Newton or variable metric methods. These are second order methods that require the computation of the Hessian matrix (which elements are the partial second derivatives of the objective function with respect to the perturbation parameters), or the sensitivity matrix. Other alternative is to use the adjoint methods to compute the gradient of the objective function or sensitivity of all production data to grid block permeability. Computation of the gradient of the objective function requires only the solution of a single adjoint system and thus requires no more computational time than one reservoir simulation run. Unfortunately, the implementation of these methods have resulted in slow convergence (Makhlouf et al. 1993). Wu et al. (1999) were the first to used the adjoint method in conjunction with the Gauss-Newton method to perform history matching. They implemented the adjoint method to compute the sensitivity of all production data to grid block permeabilities and porosities. The resulting calibrating process, however, is not practically feasible for the type of problems of interest to us where the sensitivity equations are too complex (see Appendix B). Because it is simple to implement, the so-called gradient method is chosen in this dissertation. This method needs the computation of the gradient of the objective function, $\{g\}$. In this section an explanation of how the components of the gradient are computed is given. To illustrate the procedure, let's say that the gradient of J is going to be computed with respect one of the five parameters, let's call it d. Parameter d could be k^0_{rw}, k^0_{ro}, S_{rw}, S_{ro} or $logk$.

The gradient of the objective function with respect d, is equal to:

$$\{g_d\} = \left\{ \frac{\partial J}{\partial d} \right\} \tag{4.6}$$

at the master point m:

$$g_d|_m = \left. \frac{\partial J}{\partial d} \right|_m \tag{4.7}$$

The forward model can be used to calculate J for any parameter. The component of the gradient $g_d|_m$ can be approximated by the forward finite difference approximation:

$$g_d|_m = \left. \frac{\partial J}{\partial d} \right|_m \approx \frac{J(d_m + \Delta d) - J(d_m)}{\Delta d} \tag{4.8}$$

where Δd is an increment of the parameter d. The value for the objective function $J(d_m + \Delta d)$ and $J(d_m)$ can be calculated by running the simulation model with the incremented parameter $d_m + \Delta d$ and the parameter d_m, respectively. Obviously, the gradient is more accurate if the increment Δd is small. Although, if it is too small, the round-off error may control the results. Sun (1994) suggests that for the numerical computation of the gradient of the objective function Δd can be taken to be directly proportional to d obtained in last iteration. The proportional factor can be determined by a trial-error procedure. The value for this proportional factor usually ranges from 10^{-5} to 10^{-2}. In this dissertation this value depends on the parameter that is considered to be perturbed. Effectively, the proportional factor is taken to be within this range, starting from 10^{-2} and making it smaller while the objective function is reducing its value.

Equation 4.8 is used to compute the gradient of the objective function. Thus, only for the computation of the gradient with respect each parameter, the forward simulation model has to be run N_m times in each iteration.

The calculation of the component, let's say M, of the gradient of the objective function with respect d is calculated following the next steps. Subscript m represents any master position, and can take the values $m = 1, ..., N_m$.

- A realization d is available from the last iteration, or from the seed field when the first iteration is performed. The corresponding objective function has been computed, J. The parameter value at the master point M is d_M, in the point where the component of the gradient of $\left. \frac{\partial J}{\partial d} \right|_M$ is going to be calculated.

- A perturbation of the parameter is assigned, Δd. This increment is interpolated with the increments for the rest of master points (equal to zero). The interpolation results in a set of increments for all master points $\{\Delta d\}$. The interpolation

can be performed with kriging or other interpolation methods. For this dissertation inverse distance interpolation method is applied.

- With the interpolated increments, the parameter field is changed $\{d\}+\{\Delta d\}$, at every master point. The rest of parameters remain unchanged. The resulting field is called $\{d\}_M$. Subscript $_M$ means that, at master point M, the perturbation is equal to Δd.

- The two-phase flow equation is solved for $\{d\}_M$ and the rest of parameters remain unchanged with respect the values obtained in last iteration.

- The objective function is computed with the output saturations and pressures at every measured node and time.

- The numerical approximation for the gradient of the objective function with respect d, at master point M in iteration ^{IT}, is approximated by equation (4.6).

$$g_d|_M = \left.\frac{\partial J}{\partial d}\right|_M \approx \frac{J(d+\Delta d)-J(d)}{\Delta d}$$

The process is repeated for every master point for all the parameters to obtain all the components of the gradient: $\left\{g_{k^0_{rw}}\right\}$, $\{g_{S_{rw}}\}$, $\left\{g_{k^0_{ro}}\right\}$, $\{g_{S_{ro}}\}$ and $\{g_{logk}\}$.

4.3 Optimization

In step 5 of the inversion model the steepest descent method was adopted for optimization. However, this method usually terminates far from the minimum. One possible solution is to use second order methods, which imply a considerable number of gradient evaluations. An alternative is to use conjugate gradient methods, for which the number of total evaluations of the objective function is higher, but the total amount of time is reduced. One of this methods was presented by Hestenes and Stiefel to solve linear systems (Scales, 1985), employing the conjugate search directions. This method for the optimization with respect k^0_{rw} is:

$$\begin{aligned}
\left\{\Delta k^0_{rw}\right\}^0 &= -\left\{g_{k^0_{rw}}\right\}^0 \\
\left\{\Delta k^0_{rw}\right\}^{IT} &= -\left\{g_{k^0_{rw}}\right\}^{IT} + \frac{\left(\left\{g_{k^0_{rw}}\right\}^{IT}-\left\{g_{k^0_{rw}}\right\}^{IT-1}\right)'\left\{g_{k^0_{rw}}\right\}^{IT}}{\left(\left\{g_{k^0_{rw}}\right\}^{IT}-\left\{g_{k^0_{rw}}\right\}^{IT-1}\right)'\left\{\Delta k^0_{rw}\right\}^{IT-1}}\left\{\Delta k^0_{rw}\right\}^{IT-1}
\end{aligned} \tag{4.9}$$

where $()'$ is the representation of the matrix transpose operator. Similarly equation (4.9) can be written for the rest of relative permeability parameters and the logarithm of absolute permeability.

Hestenes and Stiefel's method has been extended by Fletcher and Reeves to non linear optimization (Scales, 1985), using conjugate directions, which uses successive search directions:

$$\begin{aligned} \left\{\Delta k_{rw}^0\right\}^0 &= -\left\{g_{k_{rw}^0}\right\}^0 \\ \left\{\Delta k_{rw}^0\right\}^{IT} &= -\left\{g_{k_{rw}^0}\right\}^{IT} + \frac{\left\{g_{k_{rw}^0}\right\}'^{IT}\left\{g_{k_{rw}^0}\right\}^{IT}}{\left\{g_{k_{rw}^0}\right\}'^{IT-1}\left\{g_{k_{rw}^0}\right\}^{IT-1}}\left\{\Delta k_{rw}^0\right\}^{IT-1} \end{aligned} \tag{4.10}$$

where $\left\{g_{k_{rw}^0}\right\}'$ represents the transpose of the vector $\left\{g_{k_{rw}^0}\right\}$.

These two methods have the drawback that for non quadratic functions can end up with an updating direction almost orthogonal to the gradient. This will give no progress in the minimization at the next iterations. The Hestenes and Stiefel's variant of conjugate gradients corrects this feature by resetting the steepest descent direction of the current point (Scales, 1985). As suggested by Carrera and Neuman (1986c) the optimization algorithm implemented in the inverse method developed, switches these three methods described, steepest descent, Hestenes and Stiefel and Fletcher and Reeves. This alternation results in a faster convergence and avoids results far from the minimum.

4.4 Applying the inverse method

In this section an application of the developed inverse method, and the convenience of the study of the heterogeneities in relative permeability curves and absolute permeability is shown. Here it is considered the simultaneous calibration of absolute and relative permeability fields to saturation and pressure data. The problem configuration is an application of Buckley and Leverett displacement, having a 1D medium with a production well at one extreme, and an injection well at the other (Figure 4.2). The simulator described in last chapter is used to generate synthetic pressure and saturation data. The set of permeability values used to generate the well data are the truth case. This process has consisted in:

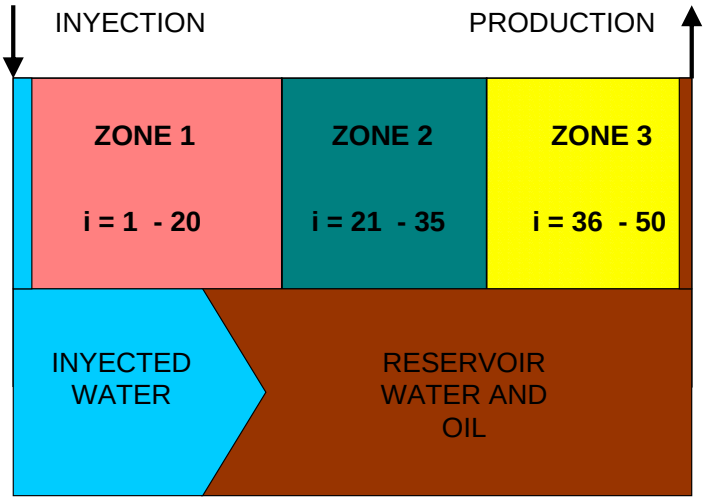

Figure 4.2: Buckley and Leverett displacement scheme. Water is injected at a well situated in the left extreme of the medium. At the right node there is a production well, in which water and oil are pumped.

- Construct a synthetic field for saturations and pressures from a set of parameters that are considered to be 'real'.
- Define the 'measurements'. Synthetic saturation and pressure fields are sampled for a set of times and points. These are considered to be the times and locations where data have been taken (as if they were well data).
- Build a set of initial parameters to start the calibration.
- Calibrate the parameters through the calculated objective function with the saturation and pressures data taken, the 'measurements'.

Zone	Nodes	k	S_{rw}	S_{ro}	k^0_{rw}	k^0_{ro}
1	1-20	1.0×10^{-13}	0.15	0.19	0.7	0.85
2	21-35	8.0×10^{-13}	0.20	0.22	0.8	0.87
3	36-50	1.0×10^{-12}	0.23	0.26	0.9	0.92

Table 4.1: Parameters that define the absolute and relative permeabilities for the three zones. These parameters are employed for the generation of synthetic saturation and pressure fields. These values are the saturations and pressures taken to be 'real'. Indexes n_w and n_o are equal to 1 for the three zones.

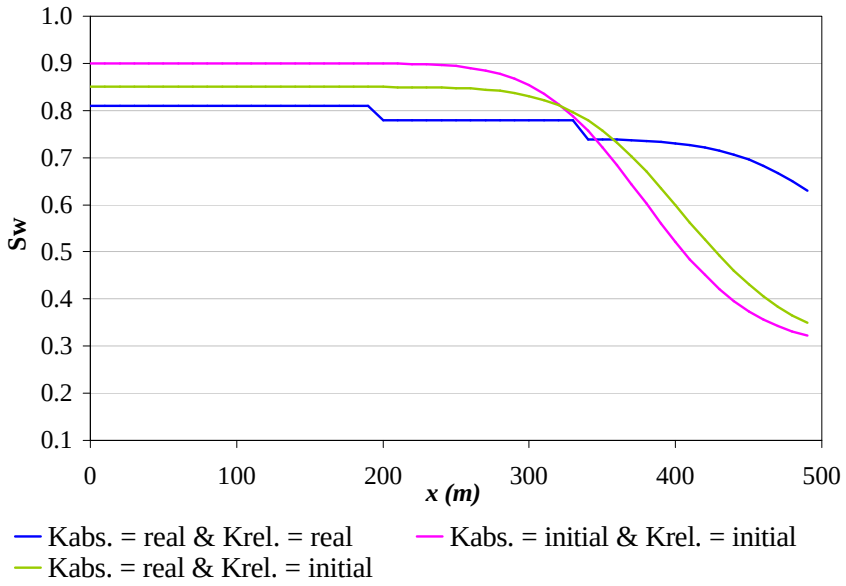

Figure 4.3: Saturation front corresponding to the numerical solution at the end of the simulation. The blue curve represents the real case, the pink curve the initial results, and the green curve the saturation front when using the real values for absolute permeability and the initial parameters for relative permeability curves.

The study area is discretized with a regular grid of 50 grid blocks. The medium has been divided in three zones, within each of them permeability is considered to be homogeneous. Grid blocks corresponding to each of the zones are graphed in figure 4.2. Parameters that describe the reality, which normally is not known, are resumed in Table 4.1. In this example heterogeneity for both absolute and relative permeability is built per zones. 500 time steps are used. The analysis is carried out assuming that there are three data points at grid blocks $i = 10, 25, 40$, one per zone, for 10 times (t = 50, 100, 150, 200, 250, 300, 350, 400, 450 and 500). These measurements are directly read from the synthetic results.

k	S_{rw}	S_{ro}	k^0_{rw}	k^0_{ro}
5.0×10^{-13}	0.10	0.15	0.68	0.70

Table 4.2: Initial parameters taken for the example calibration. These parameters define relative permeability curves and absolute permeability in the three zones in which the domain is divided. Indexes n_w and n_o are equal to 1 for the three zones.

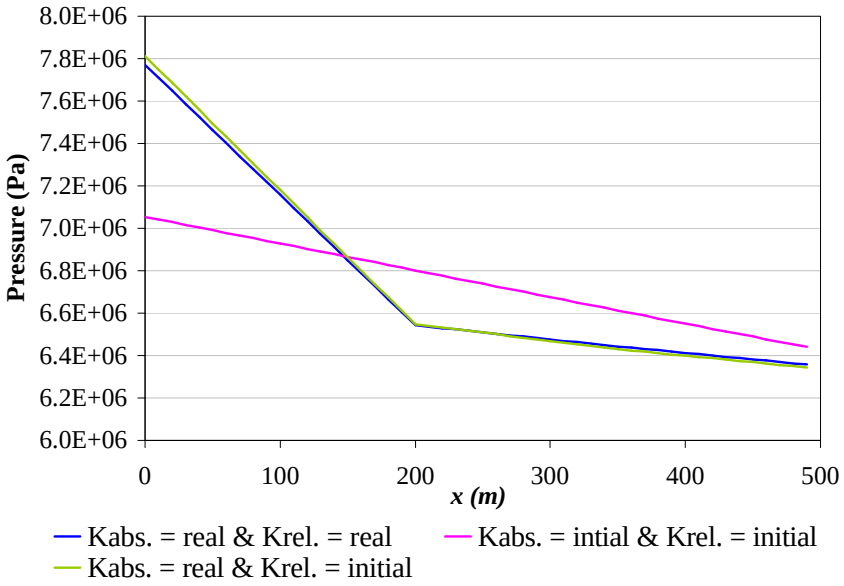

Figure 4.4: Pressure front corresponding to the numerical solution at the end of the simulation. The blue curve represents the real case, the pink curve the initial results, and the green curve the saturation front when using the real values for absolute permeability and the initial parameters for relative permeability curves.

For the calibration it is necessary to start from a set of initial values, summarized in Table 4.2. These parameters have been defined as homogeneous for all the domain. In the Figures 4.3 and 4.4 saturation and pressure are graphed for all the nodes at the last time step simulated. Blue curve represents the output values given by the two-phase numerical flow solver with real parameter values in Table 4.1. The pink curve corresponds to the numerical solution using initial parameter values in Table 4.2.

The objective of this exercise is to check the importance of calibrating or not calibrating relative permeability curves. The results are going to corroborate results shown in chapter 2, the saturation front is much more influenced by the relative permeability curves than the pressure front. Indeed, no calibration is necessary to arrive to that conclusion. If saturation and pressure fronts are computed with the forward two-phase flow simulator, assuming that absolute permeability is known, but relative permeability values are unknown and assigned to be equal to the initial values (Table 4.2), the result is very interesting. Saturation and pressure fronts are graphed in Figures 4.3 and 4.4 with the green curves. It can be seen that the pressure field does not change so much with respect the real values given by the blue curve, while the saturation front is highly affected. This property of relative permeabilities can be taken into account when the optimization algorithm is programmed. If the pressure term in the objective function

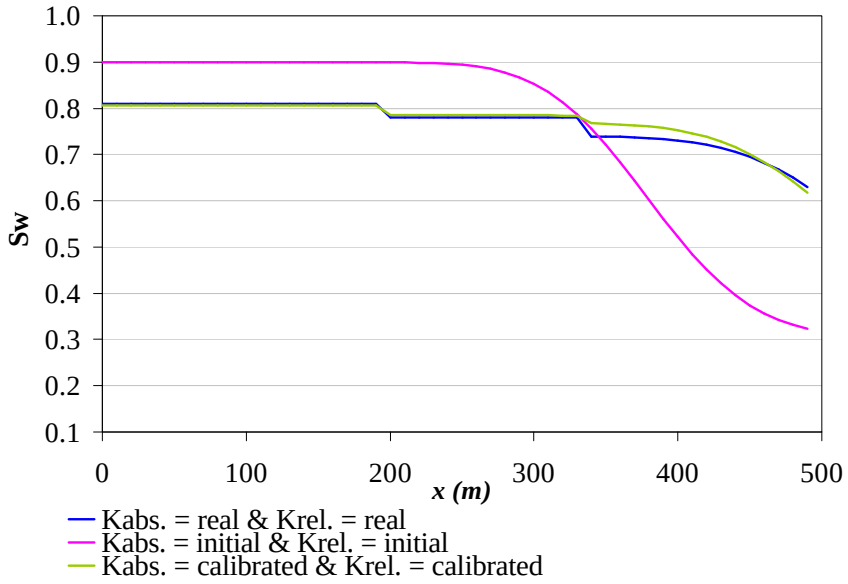

Figure 4.5: Saturation front corresponding to the calibrated parameters. Results for the last simulation time. The blue curve corresponds to real values, the pink one to the initial. The green curve is the result after the simultaneous calibration of relative and absolute permeabilities.

has been reduced considerably, but not for the saturation term, weight for pressures w_p can be assigned to be zero and optimization can continue only for parameters of relative permeability curves.

When the calibration is run the starting parameter values, given in Table 4.2, are modified iteratively to end up with the values given in Table 4.3. The saturation and pressure fronts given by the calibrated parameters are represented by the green curves in Figures 4.5 and 4.6. In the calibration presented here it was employed a weight for the pressures ($w_{p,i}$ in equation (4.1)) equal to 10^{-10}, obtaining with it an initial objective function value of 149.98. Saturation weights for all the examples taken in this dissertation are equal to 1. This means that saturation measurements are assumed to be free of any error. Saturation errors can be taken into account by just changing this value. The election of the pressure weight w_p in the objective function was made after several tries with different weights. The value chosen was the one that resulted in an objective function with an order of magnitude low enough to perform the inverse modeling. After 323 iterations the objective function resulted equal to 0.00176. The match was considered very optimum for both saturation and pressure fields (see Figures 4.5 and 4.6).

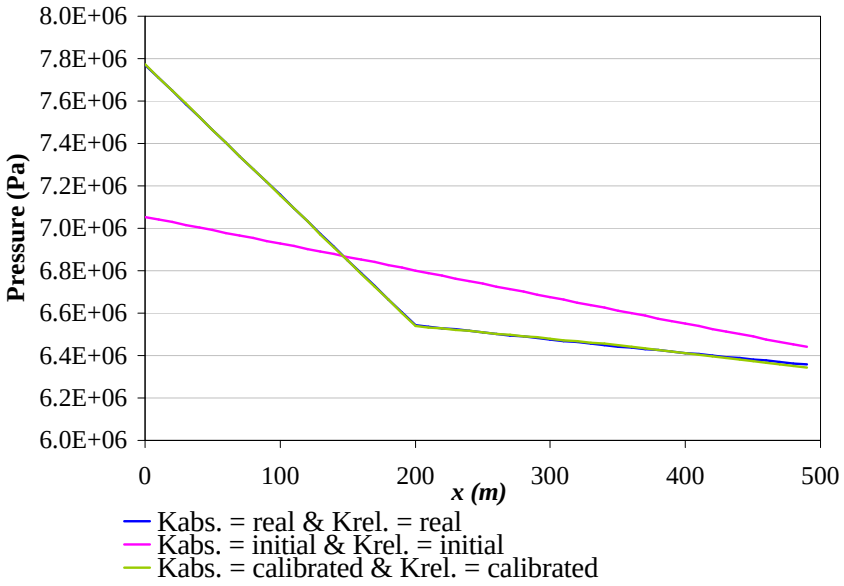

Figure 4.6: Pressure front corresponding to the calibrated parameters. Results for the last simulation time. The blue curve corresponds to real values, the pink one to the initial. The green curve is the result after the simultaneous calibration of relative and absolute permeabilities.

For this exercise the evolution of the objective function for the first 100 iterations has been graphed in Figure 4.7. The y axis corresponds to the objective function and it has been plotted in logarithm scale. For the first 5 iterations, when the objective function is bigger than 2, the weight value of the saturations has been set to zero, $w_s = 0$. This has been done because until that point the contribution for the objective function is mainly due to the pressure term. This avoids to compute the gradient for the relative permeability parameters for the first iterations.

Zone	Nodes	k	S_{rw}	S_{ro}	k^0_{rw}	k^0_{ro}
1	1-20	1.0×10^{-13}	0.145	0.194	0.608	0.738
2	21-35	8.0×10^{-13}	0.203	0.215	0.890	0.867
3	36-50	1.0×10^{-12}	0.211	0.230	0.759	0.827

Table 4.3: Parameter values obtained after the simultaneous calibration of relative and absolute permeability fields in the three zones.

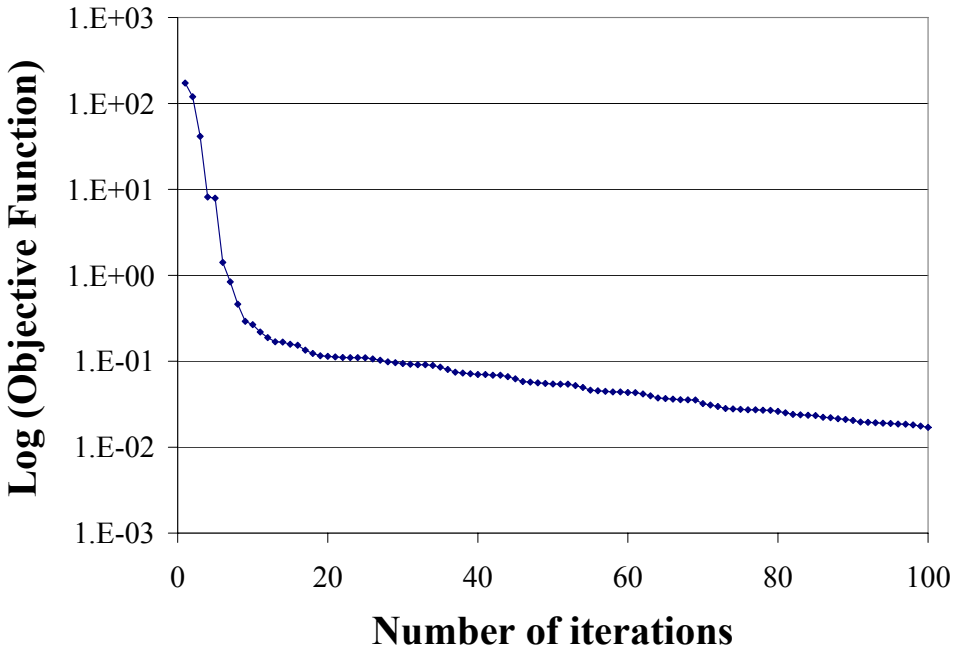

Figure 4.7: The objective function (in logarithm scale) is represented in function of the number of iterations for 1D example.

This simple example shows that the inverse method developed works and it is capable to match the production data. The technique is ready to be applied to more complex 1D and 2D cases, and to perform uncertainty analysis. Next chapters present these applications.

Chapter 5

Calibrating absolute and relative permeabilities in 2D

The main objective of this dissertation is to produce a technique that simultaneously calibrate (or inverse model) both absolute and relative permabilities, considering both parameters spatially variable within the reservoir. Former chapters have extensively described the most important basic concepts of the inverse method developed. The present chapter shows several applications of this method in one and two dimensions for different reservoir configurations. In first place, calibrations of absolute and relative permeability fields in two dimensions are shown. Also one calibration with seismic data as dynamic variable plus production data is analyzed.

In the following examples absolute permeability heterogeneity is closer to a real reservoir representation than the heterogeneities used for 1D cases. These heterogeneities are similar to the field presented in chapter 3 (Figure 3.14). Relative permeabilities are still assumed to be homogeneous within different areas in which the domain is divided in all the analyzed cases, except in one example. To make the hypothetical problem closer to a real case, extra data are supposed to be available, like absolute permeability measurements or seismic information. This additional information has a major importance for a good agreement between reality and calibrated results. First, three test problems were run: quarter five spot configuration with production data, quarter five spot configuration with production and seismic data and vertical section with production data. A final forth example was carried out with relative permeabilities varying all over the domain.

Discretization and size taken in the cases performed in this dissertation are chosen to make the problems easy to compute. It is the aim of this research to develope a new inverse technique, to test the possibilities to run it, and to see how this technique can improve reservoir characterization. Future research must look for optimization

techniques to speed up the forward and inverse simulator in order to perform more realistic cases with higher discretizations and domain size.

5.1 Relative permeability field given in zones: quarter five spot case.

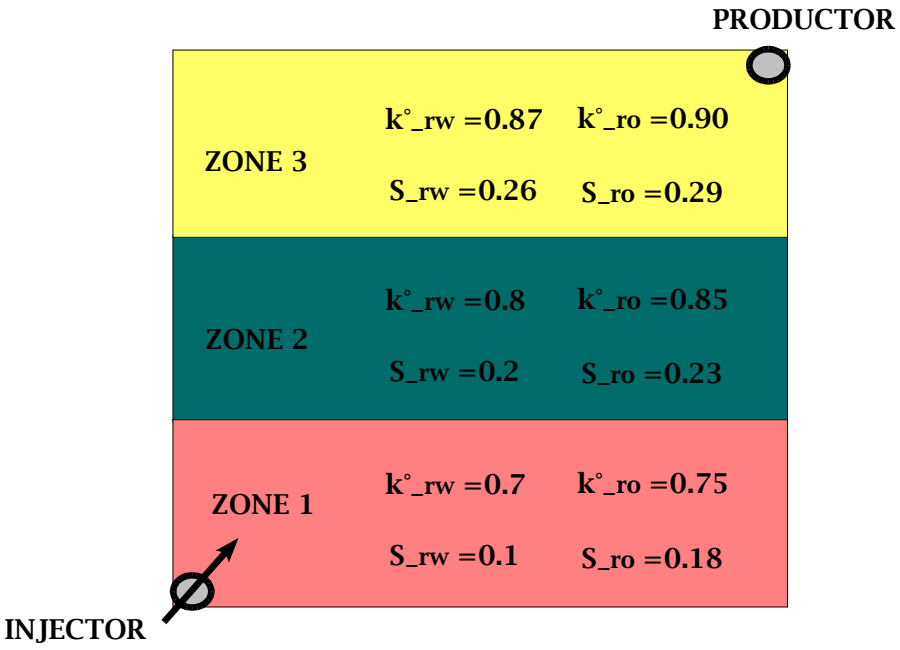

Figure 5.1: The quarter five spot scheme is represented in this figure, injector situated at lower left corner, and producer at upper right corner. The reservoir is divided into 3 different zones, within each of them the relative permeability parameters are assumed to be constant. The true values for the relative permeability parameters are also resumed in the figure.

The first example chosen for a 2D immiscible two-phase flow was the so called quarter five spot problem, which is a model problem in reservoir engineering. The spatial domain is a horizontal cut of an oil field, where a periodic arrangement of injection and production wells is considered. Figure 5.1 should clear the setting. In one space dimension this problem simplifies to Buckley-Leverett displacement problem, used in former chapters.

As in 1D, a synthetic case is created. 15 by 15 grid blocks are used to discretized the 2D domain with no flow boundaries. Reservoir performance was simulated using a uniform spatial grid with $\Delta x = \Delta y = 10$m. Remember that the objective of the

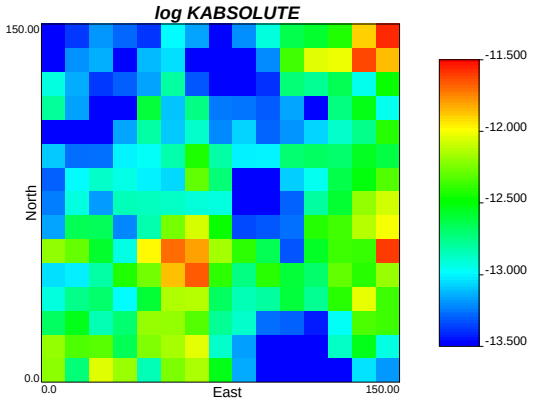

Figure 5.2: 2D heterogeneous absolute permeability field that is taken as the real absolute permeability field.

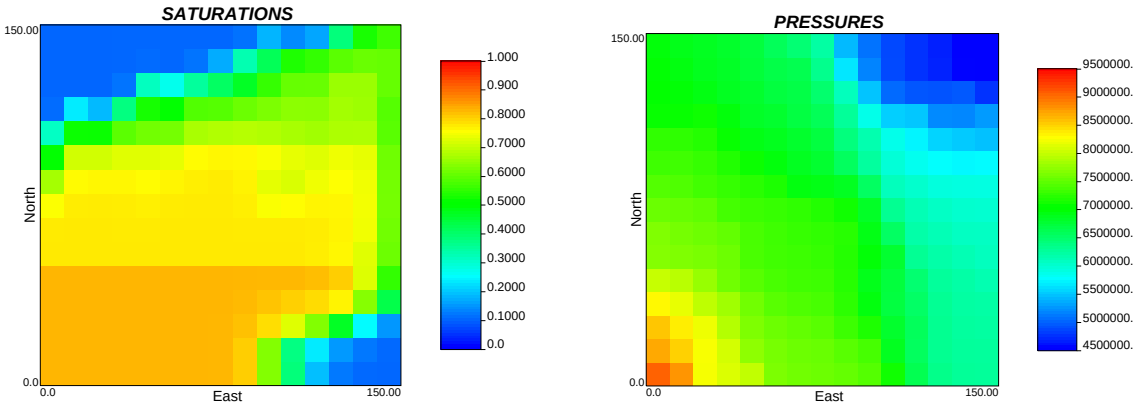

(a) Sw (b) P

Figure 5.3: When introducing real parameters in the two-phase flow simulator this is the saturation (a) and pressure (b) field obtained at the end of the simulation.

exercise is just to check the feasibility of the inverse technique, this is the reason why the discretization is so simple. Absolute permeability is heterogeneous all over the reservoir, but relative permeability is constant within some areas (schemed in Figure 5.1). No statistical correlation was considered between the five parameters (k, k^0_{rw}, S_{rw}, k^0_{ro} and S_{ro}). However, there is an implicit correlation as all the parameters are calibrated to the same set of production data. Three relative permeability curves (one per zone) are considered to describe the domain. Parameters corresponding to these water and oil relative permeability curves are resumed in Figure 5.1. The sequential Gaussian simulation code GCOSIM3D (Gómez-Hernández and Journel, 1993) was run in order to generate heterogenous absolute permeability field. The resulting real logarithm absolute permeability field is shown in Figure 5.2. The absolute permeability

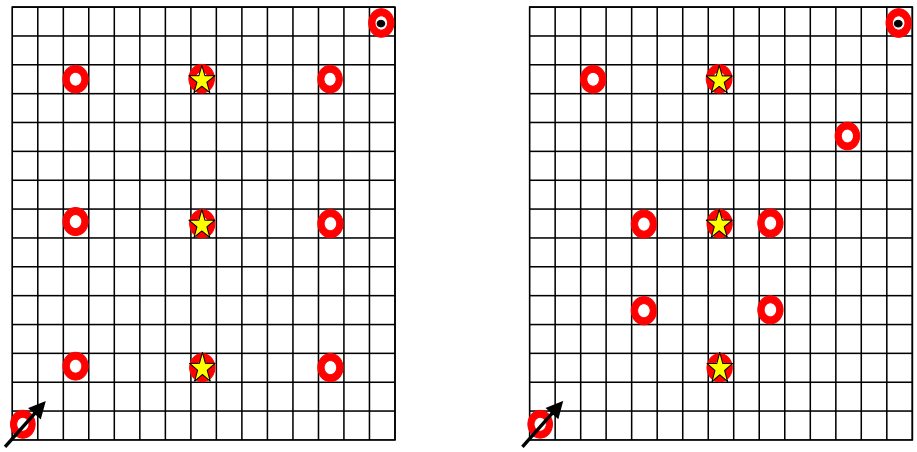

(a) Configuration 1 (b) Configuration 2

Figure 5.4: Master point positions for inversion modeling. Red circles correspond to absolute permeability master points and yellow starts to relative permeability master points.

distribution is assumed to be log-normal with log-mean equal to -13.0 and variance equal to 0.3. It is also assumed that absolute permeability field is isotropic and spatial continuity can be described with a spherical variogram model of range equal to 60 m. Another relevant reservoir property is the porosity, being $\phi = 0.2$. The parameter set given by Figures 5.1 and 5.2 are assigned to be the real values for this example and the next two sections.

Initially, the saturation conditions are considered homogeneous. The reservoir is almost full with oil (90%), and the rest (10%) is filled with water. Water is injected through a well situated in the lower left corner of the computational domain (Figure

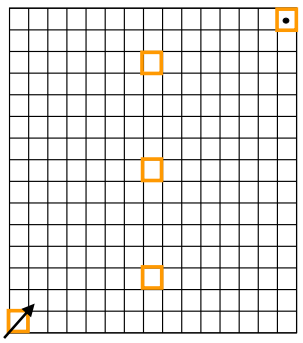

Figure 5.5: Grid blocks positions at which absolute permeability and production data are available. They are indicated with orange squares.

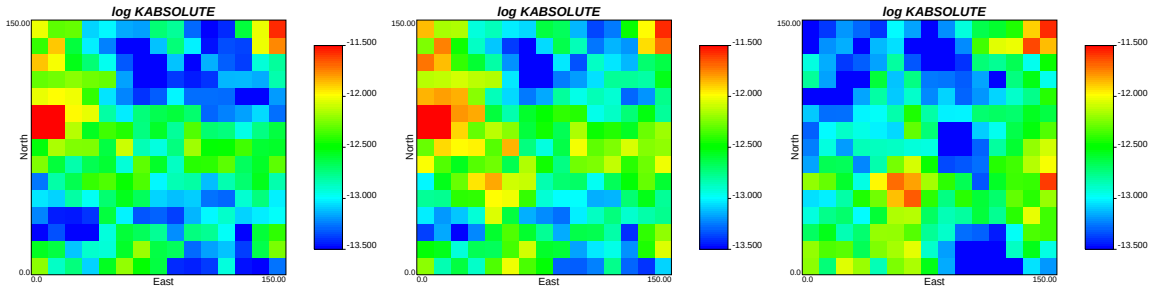

(a) Initial logk (b) Calibrated logk (c) Real logk

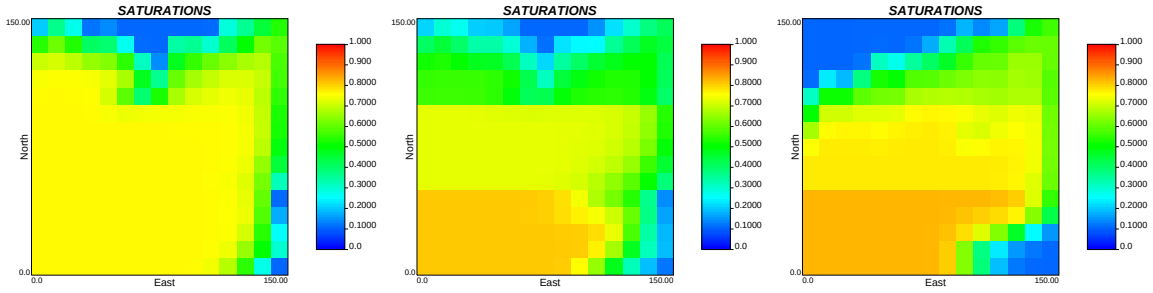

(d) Initial S_w (e) Calibrated S_w (f) Real S_w

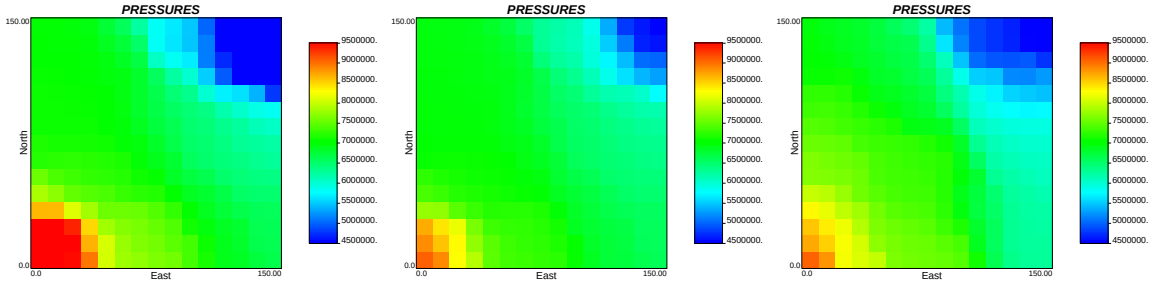

(g) Initial P (h) Calibrated P (i) Real P

Figure 5.6: In this figure initial (first column), calibrated (second column) and real (third column) realizations are presented for comparison. First row corresponds to logarithm of absolute permeability, second row to water saturations after 120 days and third column to pressures after 120 days. Well layout has the form of a quarter five spot problem. Inversion with 5 production data points and 4 absolute permeability measurements was run.

5.1). Water and oil are produced through a well in the upper right corner (Figure 5.1). The absolute and relative permeability realizations, considered as real representations of the reservoir, are introduced in the forward two-phase solver. The initial conditions are $S_w = 0.1$ and $P = 6.895 \times 10^6$ Pa. Water is injected into the porous medium filled

with oil and water at constant rate of 2.5kg/s. Production rate is also constant and equal to 2.5kg/s. For the following examples mobility ratio is taken to be equal to one, $k^0_{rw}\mu_o/k^0_{ro}\mu_w = 1$, and exponents $n_w = n_o = 1$. Constant 4.8 hours time steps are prescribed, an the simulation is run to 120 days. Saturation and pressure fields after the 120 days are given in Figures 5.3(a) and 5.3(b). They represent the behavior of the reservoir assumed to be real.

The hypothetical data production measurements are located in 5 selected grid blocks, indicated in Figure 5.5 with orange squares. Data values are supposed to be measured for 10 times of the 600 time steps during which the forward simulator was run. These are the data introduced in the objective function, S_w^{MEAS} and p^{MEAS}, and the values that are going to be reproducted with the inversion.

Iterations start from an initial set of absolute and relative permeabilities. Initial absolute field is given in Figure 5.6(a). The initial relative permeability field is taken to be homogeneous all over the domain. The parameters that define this relative permeability curve are resumed in Tables 5.1 and 5.2. For the last time step of the simulation the saturation and pressure fields with these initial parameters are shown in Figures 5.6(d) and 5.6(g), respectively.

In the inversion, the parameter space is reduced by the definition of a set of points for the perturbation, called master points. For the calibration the number and locations of the master points must be selected. Capilla et al. (1997) found that 3 master blocks per correlation range was optimal. Here, 3 master points are taken for relative permeabilities (yellow starts in Figure 5.4) and 11 master points for absolute permeability (red circles in Figure 5.4). Hendricks-Franssen (2001) suggests that if the master blocks configuration changes as the iterations proceed the procedure yields a faster convergence. Two different master point configurations where selected in this test problem, which are shown in Figures 5.4(a) and 5.4(b). During the calibration the configuration of master blocks switches between both of them. In 5 grid blocks (orange squares in Figure 5.6) absolute permeability measurements are supposed to be available. The 5 corresponding master points will have a perturbation equal to zero during all the calibration.

With this configuration, the total parameter space to be calibrated is: (5 parameters k, k^0_{rw}, S_{rw}, k^0_{ro}, S_{ro}) x (11 + 3 master points - 5 k data points). This means that the forward simulator must be run in each iteration 45 times, for the computation of the gradient components, plus the runs required in the linear optimization for the calculation of α (perturbation size, equation (4.2)). In order to slow down the simulation time in each iteration it has been decided to avoid the linear optimization. Instead, the size of the perturbation is fixed, and gradually decreased while the objective func-

Zone	k^0_{rw}			k^0_{ro}		
	Initial	Calibrated	Real	Initial	Calibrated	Real
1	0.911	0.991	0.700	0.911	0.896	0.750
2	0.911	0.924	0.800	0.911	0.954	0.850
3	0.911	0.988	0.870	0.911	0.978	0.900

Table 5.1: Initial, calibrated and real values for water and oil end-points of relative permeability curves. The calibration test case is a quarter five spot problem with 5 production data points in 10 times and 5 absolute permeability measurements.

tion diminishes. This is a compromise solution that results in a quite high number of iterations necessary to arrive to the minimum objective function. For this example the calibration process was stopped after 3000 iterations, when the objective function seemed to be low enough.

Zone	S_{rw}			S_{ro}		
	Initial	Calibrated	Real	Initial	Calibrated	Real
1	0.245	0.034	0.100	0.245	0.196	0.180
2	0.245	0.270	0.200	0.245	0.272	0.230
3	0.245	0.165	0.260	0.245	0.433	0.290

Table 5.2: Initial, calibrated and real values for water and oil residual saturations. The calibration test case is a quarter five spot problem with 5 production data points in 10 times and 5 absolute permeability measurements.

In general the output given by the calibration reveals that the inverse technique can perform the calibration in two dimensions. Some of the results after the calibration are resumed in Figure 5.6. Absolute permeability fields are represented in Figures 5.6(a) to 5.6(c) (for initial, calibrated and real cases), and saturation and pressure responses after 120 days, shown in Figures 5.6(d) to 5.6(f) and Figures 5.6(g) to 5.6(i), also for initial, calibrated and real cases. A preliminary qualitative evaluation of the calibration method follows.

Calibrated absolute permeability (Figure 5.6(b)) smooths some of the high and low initial values (Figure 5.6(a)) which do not match with the true field (Figure 5.6(c)). Anyway, the areas where no production data is located, neither absolute permeabilities are available, are not well calibrated. Look for example, the high values (red spot)

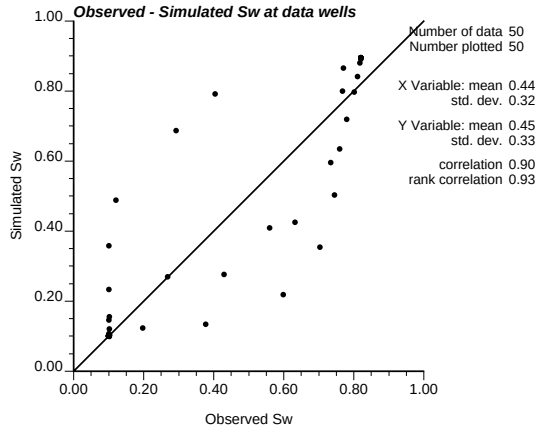

(a) Before inversion

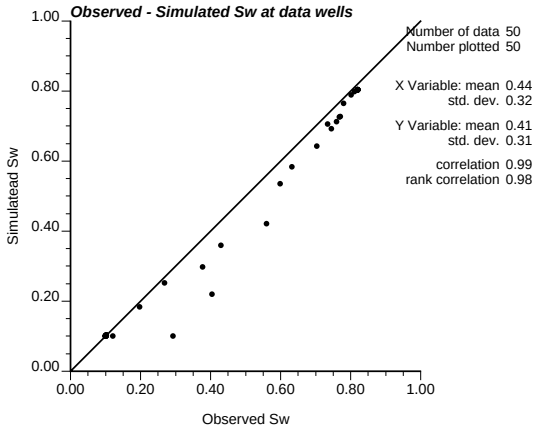

(b) After inversion

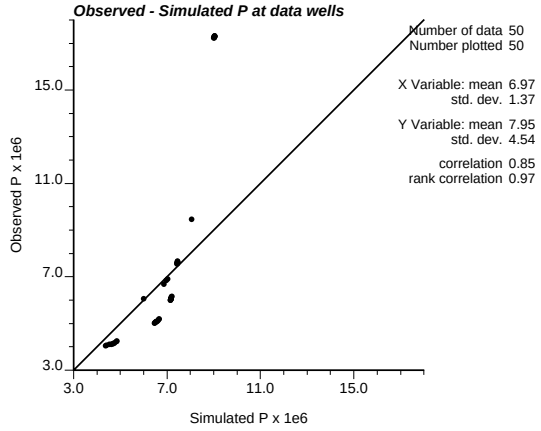

(c) Before inversion

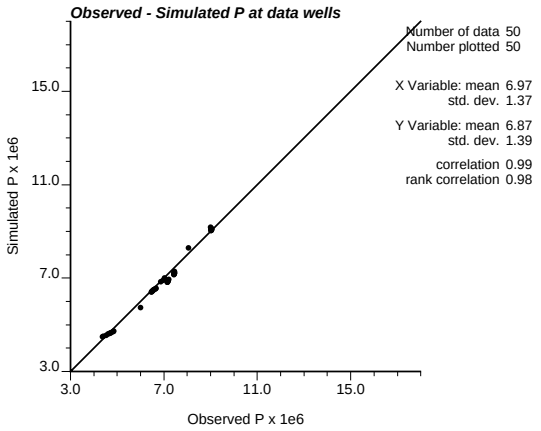

(d) After inversion

Figure 5.7: Simulated versus observed values are plotted for the results before and after the inversion is performed. The graphs presented here correspond to the quarter five spot configuration with 5 data wells and 10 times of measurements. Figures (a) and (b) are the scatter plots for water saturations and (c) and (d) for pressures.

situated in middle left zone. However, the pressure front (Figure 5.6(h)) matches quite well the true values (Figure 5.6(i)). The same happens with the saturation field, in which the different values related with the relative permeability curves are reflected after the calibration (Figure 5.6(e)). Initial values for relative permeability curves where taken to be homogenous (Tables 5.1 and 5.2) and this is reflected in the shape of the initial saturation front (Figure 5.6(d)). After calibration, though the relative permeability parameter values are not matched, with them a better reproduction of the saturation front is achieved (compare Figures 5.6(e) and 5.6(f)). It can be said that the

inversion is well performed and the saturation and pressure data are well reproduced. When no data are available it is normal to find some disagreements between real and simulatead fields. This is what it is reflected in the results found in this test case. The inverse method works and can perform an inversion as the data values are matched.

The calibrated permeability fields shown in Figure 5.6(c) and Tables 5.1 and 5.2 are one possible representation of the reservoir. Indeed, if other input parameters are considered for the initial values the calibrated permeabilities would be different. These examples are shown in order to check that the inverse technique works, however the method must be complemented with an uncertainty study, which is going to be presented in next chapter.

For a quantitative evaluation of the results two different kind of plots have been performed. First, scatter plots for saturation and pressure at well data are graphed. Figure 5.7 compares the production data misfit before (Figures 5.7(a) and (c)) and after the calibration (Figures 5.7(b) and (d)). Though the results still do not match exactly the observed saturation and pressures, the calibration reduces the spread of the scatter plot.

Because this is a synthetic case, true values for saturation and pressure are available all over the domain for every time step. Another way to measure the misfit between the true and simulated values is with the definition of the residuals R:

$$\begin{aligned} R^t_{s,i} &= (S^{SIM}_{i,t} - S^{MEAS}_{i,t}) \\ R^t_{p,i} &= (p^{SIM}_{i,t} - p^{MEAS}_{i,t}) \end{aligned} \tag{5.1}$$

for saturations, R_s, and pressures, R_p, at grid block i and time step t. The histograms of the residuals for 6 time steps are plotted in Figures 5.8 and 5.9. All the histograms are fairly symmetric and do not have long tails. Saturation residuals for first time steps reflect a tendency towards underestimation (negative mean), while overestimation appears for last times. Saturation estimations are quite unbiased as both mean and median error are close to zero. In general pressure values seem to be underestimated. Mean values are very close to zero while the median expresses some asymmetry in the errors. Saturation and pressure error distributions present a small spread. These results show that for the data grid blocks the observed values are well reproduced (Figure 5.7), while when looking at the whole field some disagreements must exist and consecuently the histograms indicate residuals different from zero.

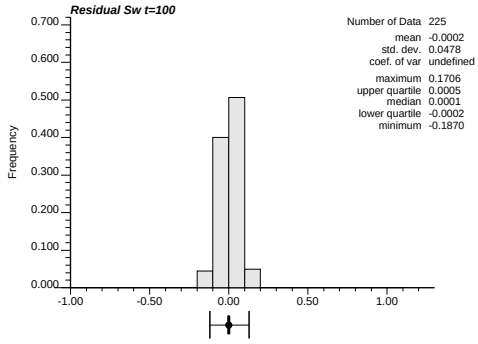

(a) t=100

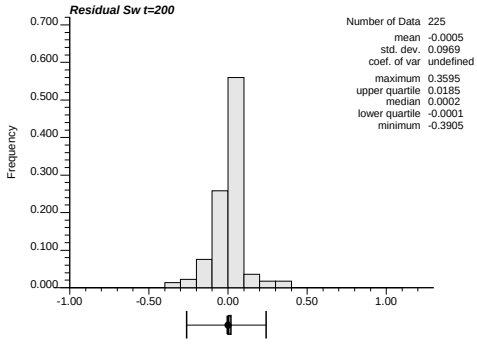

(b) t=200

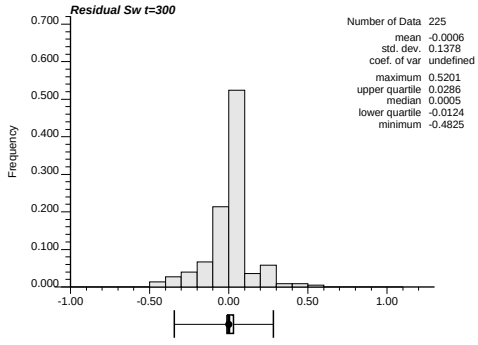

(c) t=300

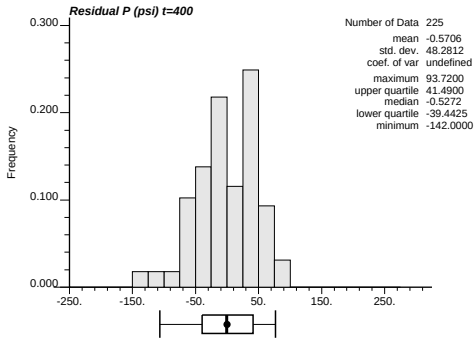

(d) t=400

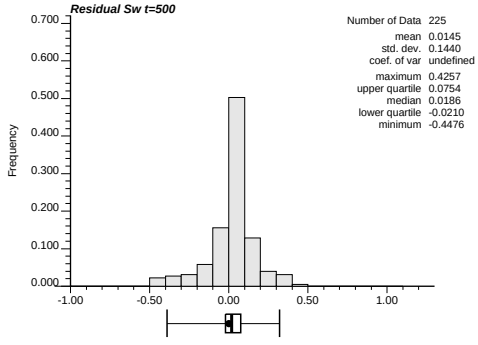

(e) t=500

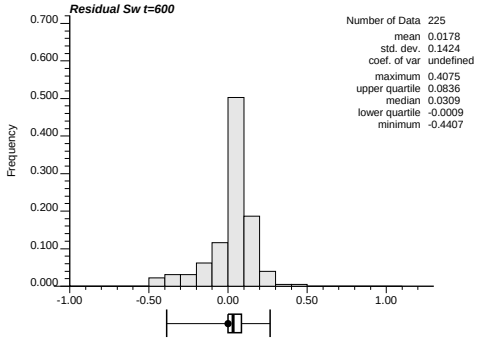

(f) t=600

Figure 5.8: Histograms for the saturation residuals defined in equation (5.1). 6 time steps are chosen: $t = 100$, $t = 200$, $t = 300$, $t = 400$, $t = 500$ and $t = 600$ (graphs (a) to (f)). The graphs presented here correspond to the quarter five spot configuration with 5 production data grid blocks, absolute permeability data in 5 grid blocks, and production data available for 10 times.

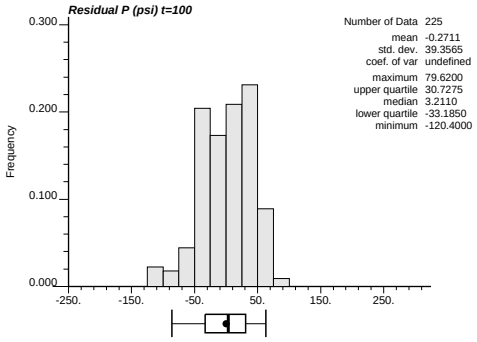

(a) t=100

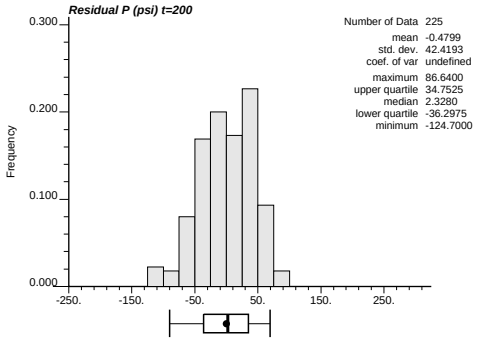

(b) t=200

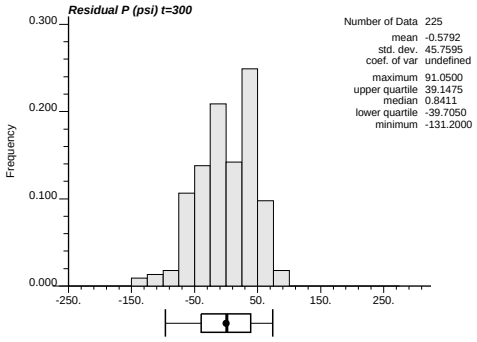

(c) t=300

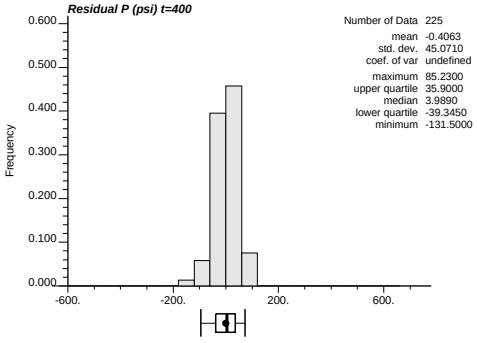

(d) t=400

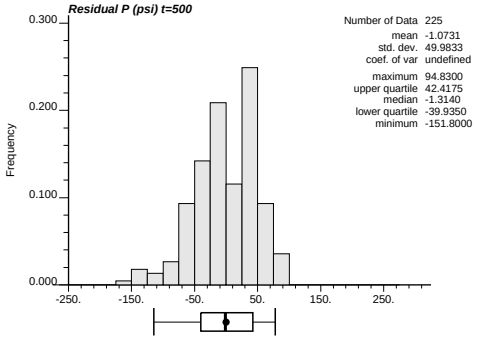

(e) t=500

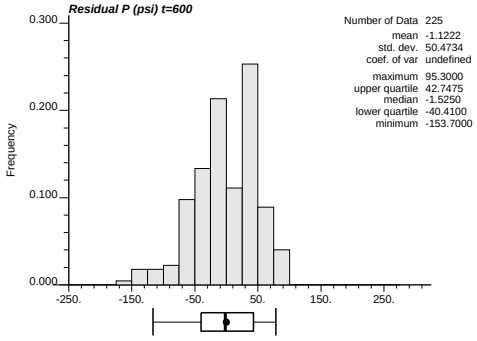

(f) t=600

Figure 5.9: Histograms for the pressure residuals defined in equation (5.1). 6 time steps are chosen: $t = 100$, $t = 200$, $t = 300$, $t = 400$, $t = 500$ and $t = 600$ (graphs (a) to (f)). The graphs presented here correspond to the quarter five spot configuration with 5 production data grid blocks, absolute permeability data in 5 grid blocks, and production data available for 10 times.

5.2 Relative permeability field given in zones: seismic data case

Important decisions in the petroleum industry are based on information from seismic data. Seismic data are originated from acoustic pulses generated on the earth's surface. They are the record of the reflection from the earth's interior. During the last years the geophysics field has developed and refined the 3D and 4D seismic technology. The 3D seismic data comes from a high resolution seismic survey that allows a more detailed three dimensional characterization of the subsurface. When two or more successive 3D surveys are shot over the same area the process is referred to as 4D seismic, to denote the addition of the time dimension.

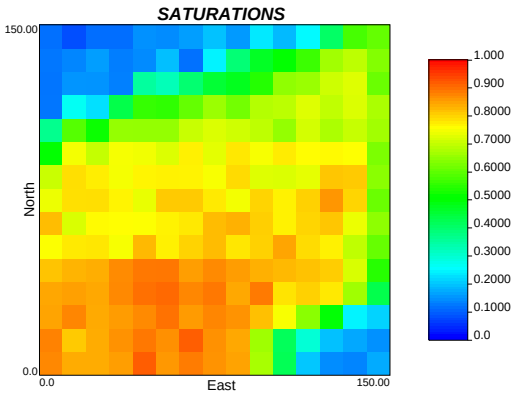

Figure 5.10: Simulated seismic data corresponding to the real water saturation field. The procedure followed was to add a random noise to the water saturation field given in 5.3(a), which corresponds to the last simulation time step. The same procedure has been applied to 10 different time steps.

In general, seismic images are sensitive to the spatial variation of two distinct types of reservoir properties: static geologic properties, as lithology, porosity, cementation or shale content, and dynamic fluid flow properties as saturation and pore pressures. By comparing the data from 3D surveys acquired at different times at the same location, it is possible to eliminate the effects of unknown static properties to focus on the dynamic changes in production related properties. So, the sensitivity to saturation changes allows tracking of the movement of fronts in the reservoir. The outstanding characteristic of the 4D seismic data is that it provides areally distributed information, which can therefore provide a higher areal resolution than well data. With this process, it is possible to estimate the areal distribution of saturation changes in the reservoir due to the production or injection of fluids.

For inverse modeling in reservoir simulation, it is possible to take advantage of this

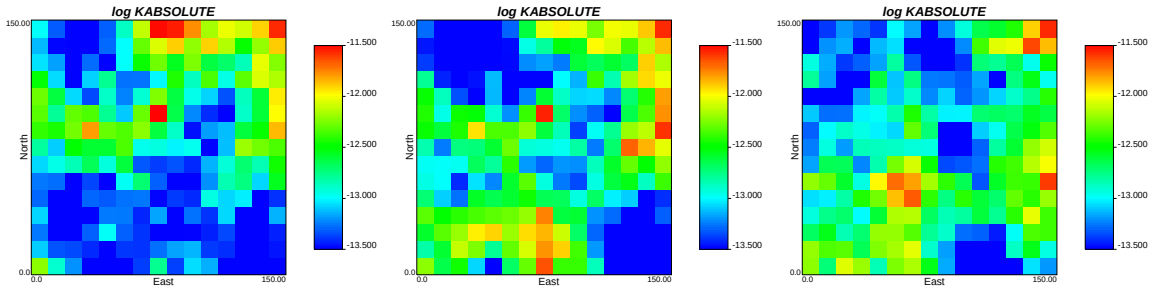

(a) Initial logk (b) Calibrated logk (c) Real logk

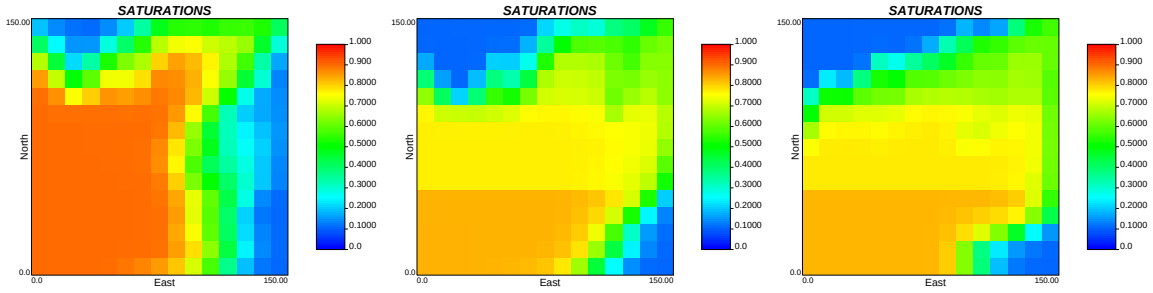

(d) Initial S_w (e) Calibrated S_w (f) Real S_w

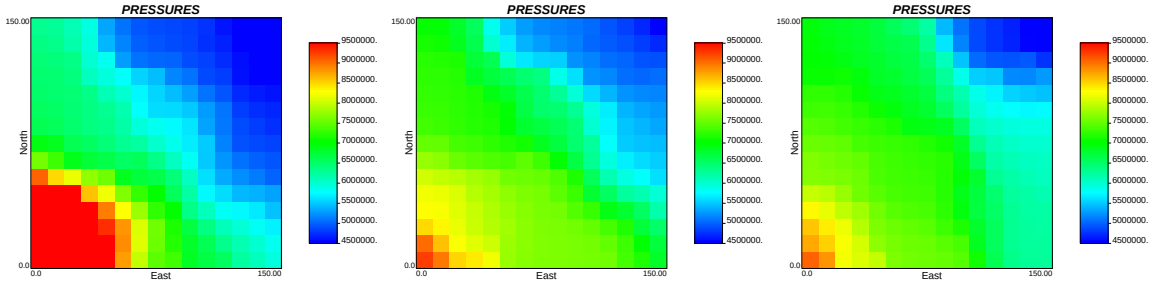

(g) Initial P (h) Calibrated P (i) Real P

Figure 5.11: In this figure initial (first column), calibrated (second column) and real (third column) realizations are presented for comparison. First row corresponds to logarithm of absolute permeability, second row to water saturations after 120 days and third column to pressures after 120 days. Well layout has the form of a quarter five spot problem. Inversion with 3 absolute permeability data, 3 pressure well data and seismic information was run.

properties of 4D seismic to improve the resolution of the calibrations. This has been carried out by Landa (1997), Idrobo et al. (1999) or Wen et al. (2002). Following the same process, here it is presented a synthetic case in which 4D seismic are supposed to be available. The inversion is performed by using 4D seismic data and absolute

permeability data. Let's see how the inversion technique performs.

Zone	k^0_{rw}			k^0_{ro}		
	Initial	Calibrated	Real	Initial	Calibrated	Real
1	0.629	0.764	0.700	0.629	0.740	0.750
2	0.629	0.499	0.800	0.629	0.741	0.850
3	0.629	0.519	0.870	0.629	0.641	0.900

Table 5.3: Initial, calibrated and real values for water and oil end-points of relative permeability curves. Calibration was performed for a quarter five spot problem with seismic data, 3 absolute permeability grid block data nd 3 pressure well measurements.

The true permeability fields are the ones taken in the former section (Figures 5.1 and 5.2), with relative permeabilities taken to be homogeneous within 3 different areas in which the domain can be divided and absolute permeability heterogenous all over the domain. The quarter five spot configuration described before is considered. The same initial conditions ($S_w = 0.1$, $P = 6.895 \times 10^6$ Pa) and other parameters like $\phi = 0.2$, production/injection rate = 2.5kg/s, unit mobility ratio and $n_w = n_o = 1$. Instead of having saturation production data, seismic data are assumed to be available. True water saturation and pressure fields after the 120 days of production are given in Figures 5.3(a) and 5.3(b). To simulate seismic data water saturation plus a percentage random noise is taken. Let's suppose that seismic campaign has been done for 10 times. 10 simulated seismic field images are obtained by adding random noise to the water saturation realizations corresponding to these 10 times. The seismic image corresponding to water saturation in Figure 5.3(a) ($t = 120$ days) is drawn in Figure 5.10.

The objective function can take into account the error that water saturations have when they are deduced from seismic 4D data. Pressure data are assign to be taken at 3 grid blocks (injector, productor and an additional situated in the central grid block) for the same 10 times that seismic data are available. In these 3 wells absolute permeability measurements are availabe (instead of the 5 assumed in the former test problem). After 2014 iterations the calibration is good enough. In the inversion process 3 master points were taken for the relative permeabilities (one per zone), while for the absolute permeability 11 master points were selected, 3 of them corresponding to the absolute permeability measurements (hence, no perturbation is applied to this 3 master points). Absolute permeability master point positions are plotted with red circles in Figure 5.4(a). Yellow starts in Figure 5.4(a) represent relative permeability master

Zone	S_{rw}			S_{ro}		
	Initial	Calibrated	Real	Initial	Calibrated	Real
1	0.105	0.112	0.100	0.105	0.177	0.180
2	0.105	0.170	0.200	0.105	0.235	0.230
3	0.105	0.152	0.260	0.105	0.264	0.290

Table 5.4: Initial, calibrated and real values for water and oil residual saturations. Calibration was performed for a quarter five spot problem seismic data, 3 absolute permeability grid block data nd 3 pressure well measurements.

points. As in the former section, initial, calibrated and real fields are going to be qualitatively analyzed.

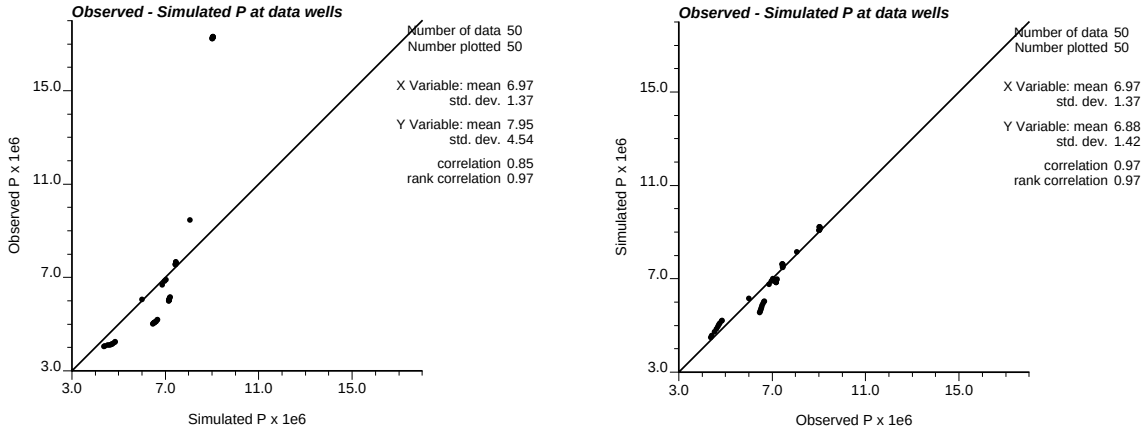

(a) Before inversion

(b) After inversion

Figure 5.12: Simulated versus observed values are plotted for pressures before (a) and after (b) the calibration. The graphs presented here correspond to the quarter five spot configuration with 3 pressure data grid blocks, 3 absolute permeability measurements and seismic data. The data are available for 10 time steps.

Initial, calibrated an real absolute permeability fields are shown in Figures 5.11(a) to 5.11(c). The initial logarithmic absolute permeability was generated again with conditional sequential simulation (GCOSIM3D code). The absolute permeability data in the 3 grid blocks mentioned before where used to generate the conditional simulation. As it was explained in chapter 4 the absolute permeability at these points does not change during the inversion. The iterative process was stopped when water saturation and pressures were well reproduced. Comparing Figures 5.11(b) and 5.11(c) the high

absolute permeability region (near injector and productor well) and low absolute permeability region (the upper left area and the blue spot close to the lower right area) are well captured in the calibrated realization. However, still some differences appear in the location and boundaries of these areas. The differences between the calibrated and true fields are in the normal range, and with the calibration the observed saturation and pressures have been fitted very well. It can be stated that the method also works when using seisimic information.

Results for relative permeability curves in the 3 zones are summarized in Tables 5.3 and 5.4, one for the end-points and the other for the residual saturations. The results obtained in last section have shown that end-points for both water and oil relative permeability curves seem to be quite unsensible to the changes of water saturation and pressure. However, in this example, for the first two zones residual saturations after the calibration turn out to be quite similar to the real values. In comparison with the first test case, much improvement is obtained in the calibrated results by using extra seismic information.

Calibration has been performed taking seismic data values all over the domain for 10 times, which obviously gives a better reproduction of the water saturations response (compare Figures 5.11(e) and 5.11(f)). Just few differences in the shape of the water saturation front exist between calibrated and real values. In the case of pressures, it has been shown that after calibration with few data it is possible to match real values quite well. With seismic data this effect is even improved (compare figure 5.11(h) and 5.11(i)). The method succeeded in applying the inverse two-phase flow technique with seismic data.

Figure 5.12 shows the differences between observed and simulated pressures at well data before and after the calibration. It can be seen that the performance of the calibration is as good as in the former section. A different behavior, when taking into account seismic data, appears more clear looking at the residual histograms. Saturation residuals in Figure 5.13 are less spread than the ones in Figure 5.8, when the exact saturation was measured in 5 points. The same happens with the media and median, which are much closer to zero. Moreover, even for the pressure histograms the results are slightly better with less spread, media and median (Figure 5.14).

The very recent availability of new sensors to measure pressure and temperature downhole in a permanent way has been taken into account for reservoir characterization by Alpak et al. (2001). These prototypes of permanent sensors have been constructed to be used behind casing and hence to be in direct contact with the formation. Even in-situ sensors are not commercially available for the moment, the pressure data acquired with permanent sensors is an important potential application of the inverse method

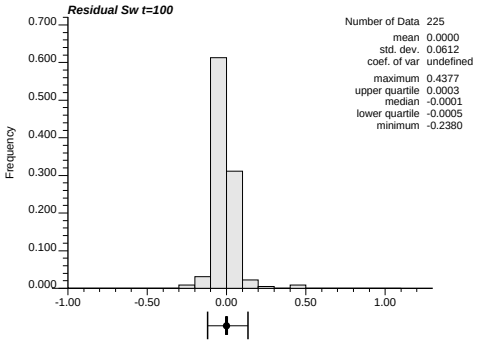

(a) t=100

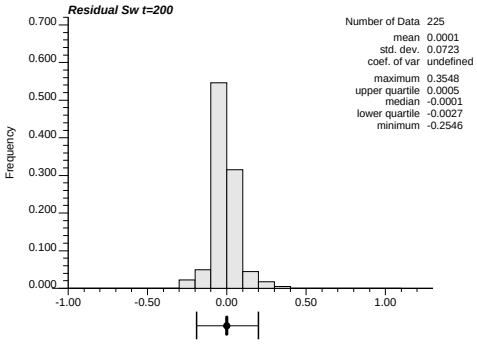

(b) t=200

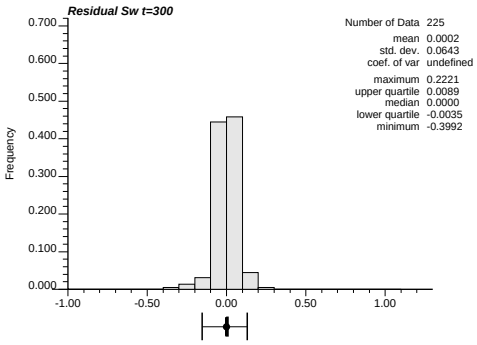

(c) t=300

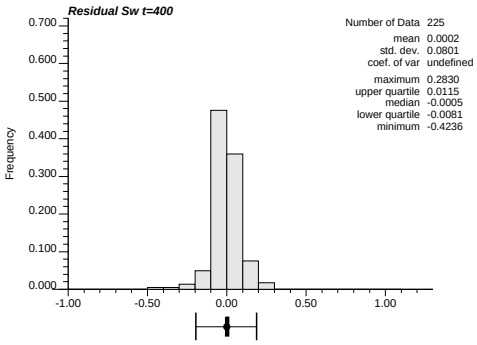

(d) t=400

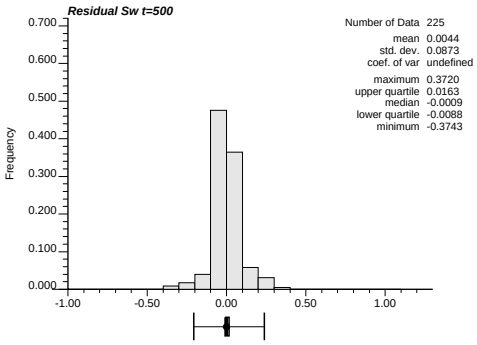

(e) t=500

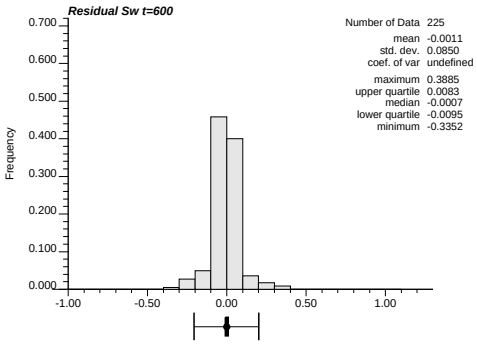

(f) t=600

Figure 5.13: Histograms for the saturation residuals (equation (5.1)). 6 time steps are plotted: $t = 100$, $t = 200$, $t = 300$, $t = 400$, $t = 500$ and $t = 600$ (corresponding to graphs (a) to (f)). The test problem corresponds to the quarter five spot configuration with 3 production data grid blocks for 10 times, absolute permeability data in 3 grid blocks, plus seismic images for 10 time steps.

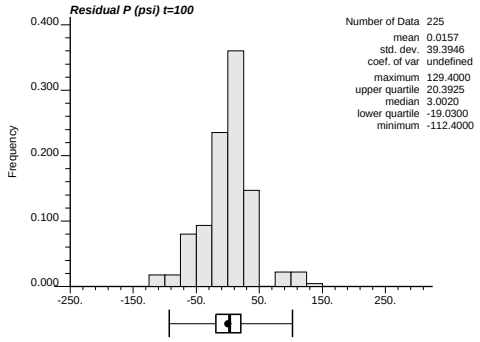

(a) t=100

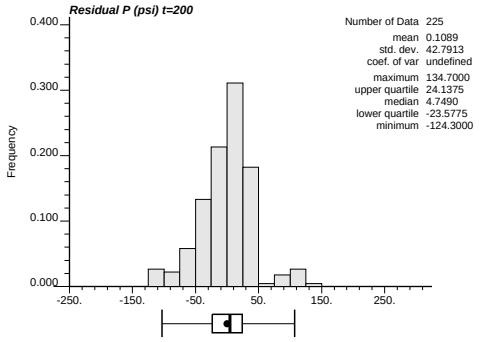

(b) t=200

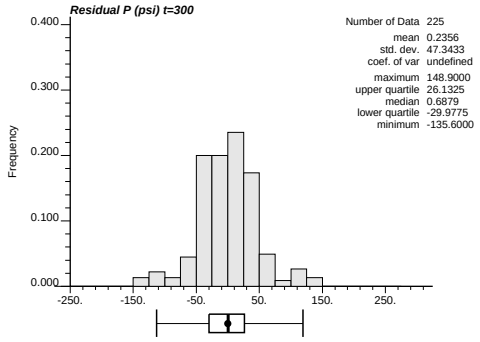

(c) t=300

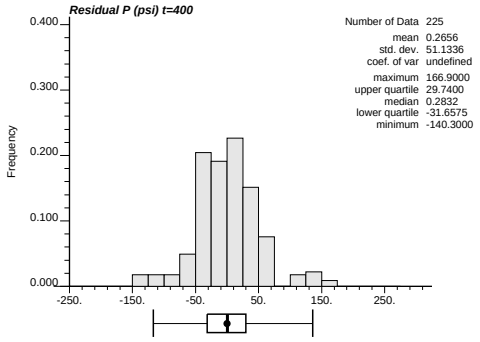

(d) t=400

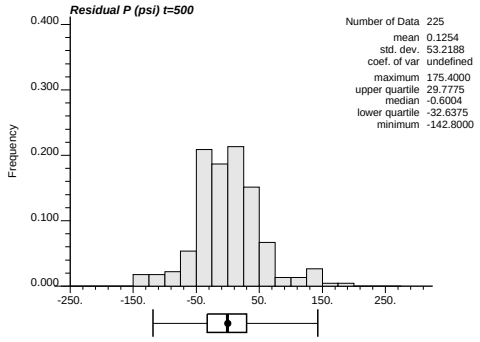

(e) t=500

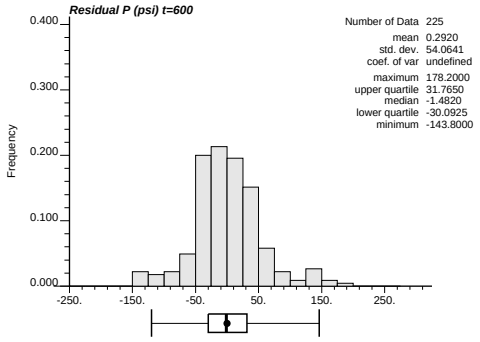

(f) t=600

Figure 5.14: Histograms for the pressure residuals (equation (5.1)). 6 time steps are plotted: $t = 100$, $t = 200$, $t = 300$, $t = 400$, $t = 500$ and $t = 600$ (corresponding to graphs (a) to (f)). The test problem corresponds to the five quarter spot configuration with 3 production data grid blocks for 10 times, absolute permeability data in 3 grid blocks, plus seismic images for 10 time steps.

presented here, very similar to this seismic 4D data example.

5.3 Relative permeability field given in zones: vertical section case.

Another common configuration in 2D reservoir modeling is a vertical section. It is assumed that the reservoir is produced by two fully penetrated wells. At one side of the reservoir water is injected. At the other side a production well is situated. A simple grid discretization is chosen, as in the quarter five spot problem, of 15 by 15 grid blocks with size 10mx10m. The absolute and relative permeability realizations for the real synthetic case are the same as the ones drawn in Figures 5.1 and 5.2.

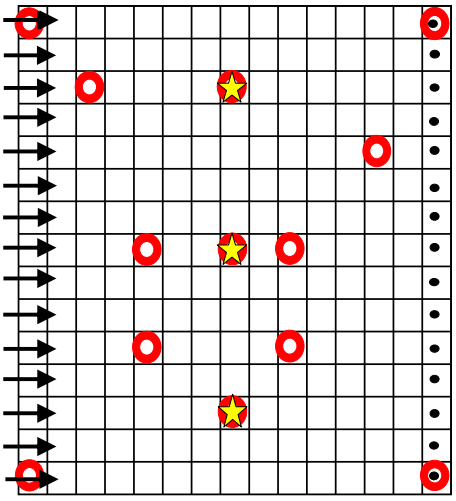

Figure 5.15: Master point positions for inverse modeling. Red circles correspond to absolute permeability master points and yellow starts to the relative permeability master points. This configuration is used in the vertical section test case.

In the same manner that it was done for the former problem, the reservoir is assumed to be saturated with oil and water. The reservoir is almost full with oil (90%). Water is injected through a well that occupies all the left border, with constant injection rate. The production well is situated at the right border with also constant production rate. The absolute and relative permeability realizations, considered as real representations of the reservoir, are introduced in the forward two-phase solver. The initial conditions are $S_w = 0.1$ and $P = 6.895 \times 10^6$ Pa. The water is injected into the porous medium filled with oil and water. Water is injected at constant rate in each of the boundary grid blocks with a rate at each grid block equal to 0.25kg/s. The same configuration is assumed for the production boundary with a constant production

rate at each production grid block equal to 0.25kg/s. Unity mobility ratio is taken, $k^0_{rw}\mu_o/k^0_{ro}\mu_w = 1$, porosity $\phi = 0.2$ and $n_w = n_o = 1$. Similar time discretization as before is chosen (constant 4.8 hours time step and 120 days for the total time). Saturation and pressure fields after 60 days are given in Figures 5.17(f) and 5.17(i). They represent the behavior of the reservoir assumed to be real.

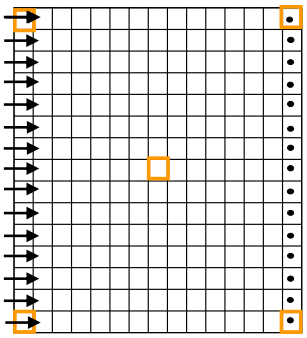

Figure 5.16: Absolute permeability and produciton data positions for inversion modeling in the vertical section example. Orange squares correspond to the grid block measuremets.

Zone	k^0_{rw}			k^0_{ro}		
	Initial	Calibrated	Real	Initial	Calibrated	Real
1	0.629	0.998	0.700	0.629	0.946	0.750
2	0.629	0.662	0.800	0.629	0.619	0.850
3	0.629	0.500	0.870	0.629	0.526	0.900

Table 5.5: Initial, calibrated and real values for water and oil end-points of relative permeability curves. Calibration was performed for the vertical section problem set out with 5 production measurement grid blocks in 10 times and 5 absolute permeability data.

The master points taken are shown in Figure 5.15. Absolute data points are assumed to be measured in the top and bottom of both production wells and in the center grid block (orange squares in Figure 5.16). The calibration process was stopped after 2400 iterations, objective function seemed to be good enough. The results before and after calibration, in comparison with the real and initial fields, can be found in Figures 5.17(a) to 5.17(c) for absolute permeabilities, in Figures 5.17(d) to 5.17(f) for saturations and Figures 5.17(g) to 5.17(i) for pressures. These images correspond to half of the total simulated time, as it is easier to see the situation of the water front.

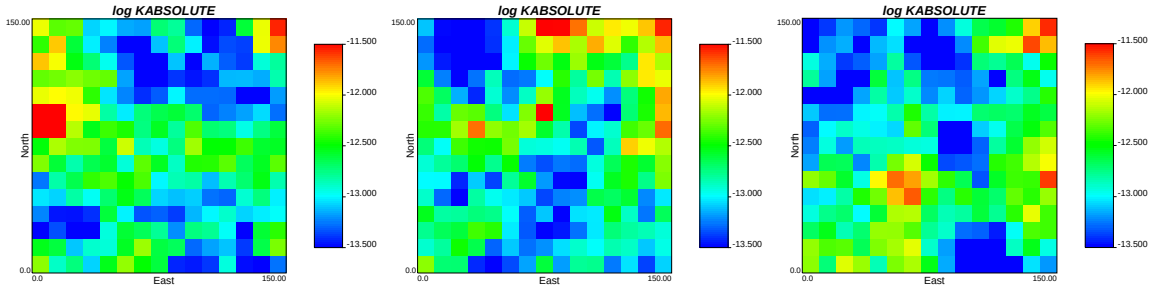

(a) Initial logk (b) Calibrated logk (c) Real logk

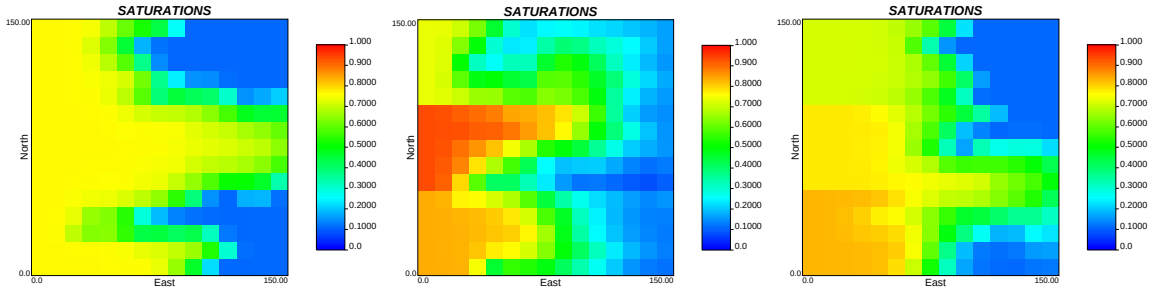

(d) Initial S_w (e) Calibrated S_w (f) Real S_w

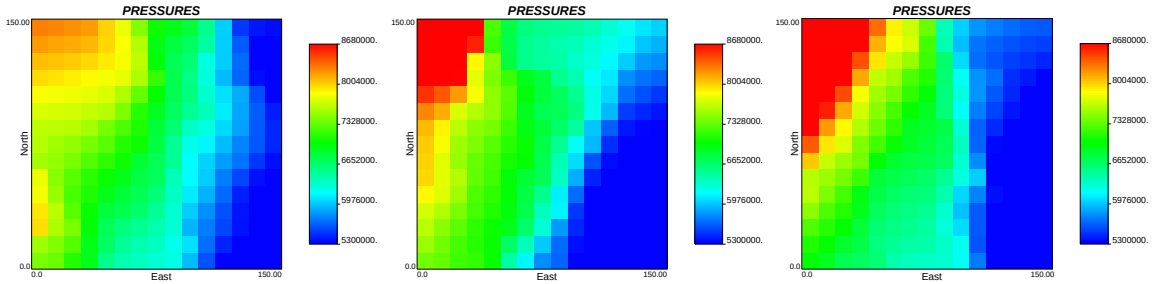

(g) Initial P (h) Calibrated P (i) Real P

Figure 5.17: In this figure initial (first column), calibrated (second column) and real (third column) realizations are presented for comparison. First row corresponds to logarithm of absolute permeability, second row to water saturations after 60 days and third row to pressures after 60 days. The well layout consists in one fully penetrated injection well at left boundary and one fully penetrated production well at the right boundary. The figure represents a vertical section of the reservoir. Inversion with 5 absolute permeability and production data grid blocks was run.

As it has been commented in the quarter five spot case the relative permeability parameter values calibrated are not well reproduced after calibration (look at Tables

Zone	S_{rw}			S_{ro}		
	Initial	Calibrated	Real	Initial	Calibrated	Real
1	0.105	0.124	0.100	0.105	0.174	0.180
2	0.105	0.000	0.200	0.105	0.076	0.230
3	0.105	0.000	0.260	0.105	0.260	0.290

Table 5.6: Initial, calibrated and real values for water and oil residual saturations. Calibration was performed for the vertical section problem set out with 5 production measurement grid blocks in 10 times and 5 absolute permeability data.

5.5 and 5.6). This is probably caused by a lack of sensitivity of saturations and pressures to the parameter values that have being calibrated. Comparing the saturation realization of Figure 5.17(e) with the truth case Figure 5.17(f), it can be seen that the realization captures most of the major features of the truth case. The calibrated saturation response seems to be worse for zone 2 (where the front have just arrived to the data point, which is situated at the central grid block). In zones 1 and 3 the resulted saturations are quite well reproduced by the calibration. The same conclusion taken in the former cases can be stated for this one, the inversion method calibrates saturation and pressure responses. In order to better estimate relative permeability parameters one solution could be to limit the calibrated values with some relative permeability measures.

The misfit in the grid blocks where production data are available is plotted in Figure 5.18. These results are quite similar to the ones obtained in the quarter five spot test case, section 5.1. After the calibration the production values reproduce the observations.

The three examples shown to this point indicate that it is important to take into account the relative permeability curves in order to characterize the behavior of the reservoir. However, these examples suggest that the values of the relative permeability parameters are quite uncertain. This will be further study in next chapter. The use of seismic data gives better estimation for the relative permeability parameters. The integration of seismic data is a good possibility to reduce uncertainty, and to better characterize the relative permeability parameters.

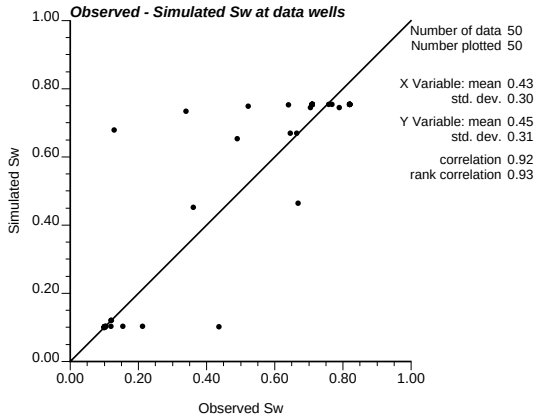

(a) Before inversion

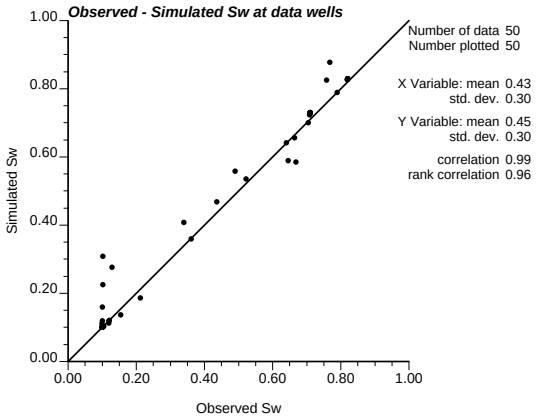

(b) After inversion

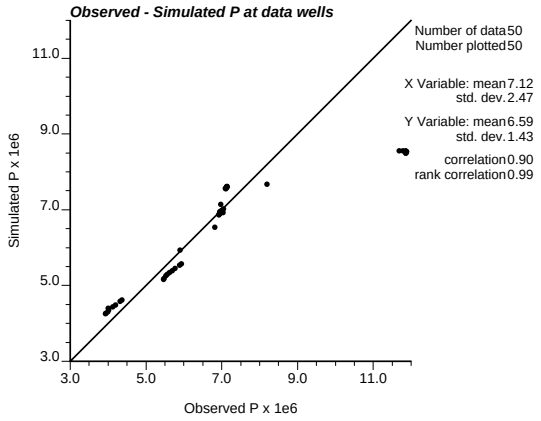

(c) Before inversion

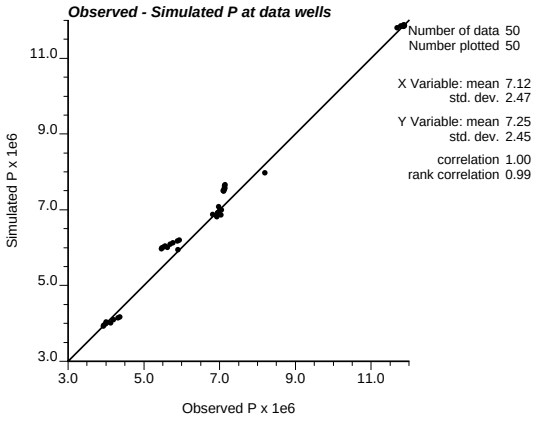

(d) After inversion

Figure 5.18: Simulated versus observed pressure and saturation values are plotted before ((a) and (c)) and after ((b) and (d)) the calibration. The graphs presented here correspond to the vertical section case with 5 production data grid blocks and 10 times of measurements.

5.4 Heterogeneous permeability field

The last test case was run in order to check other possibilities of the inversion method developed. It was supposed that relative permeability curves can vary within the whole domain, having a different value in each grid block. The absolute permeability field taken as real is the equal to the real absolute permeability field used in last sections. The real relative permeability parameters are graphed in the third column of Figure 5.20. The well configuration, initial conditions, porosity and production/injection rates are equivalent to the quarter five spot case in section 5.1. 5 production data grid blocks are assumed to be available for the calibration and 5 absolute permeability

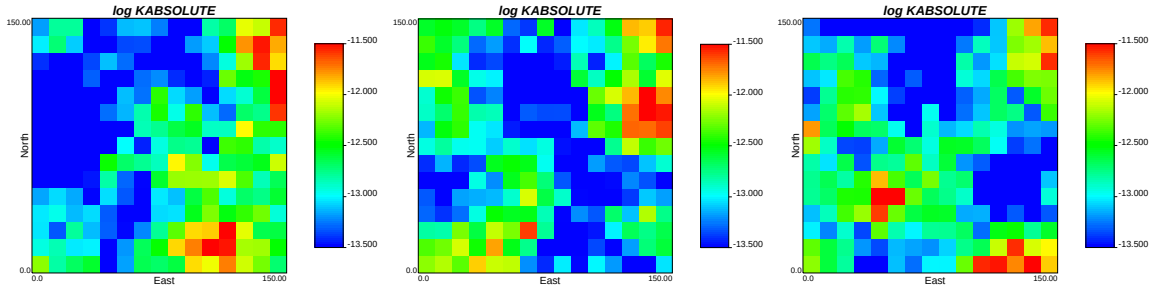

(a) Initial logk (b) Calibrated logk (c) Real logk

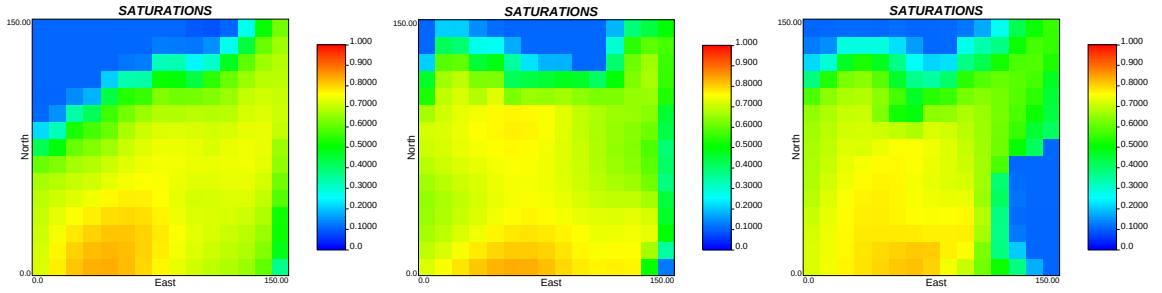

(d) Initial S_w (e) Calibrated S_w (f) Real S_w

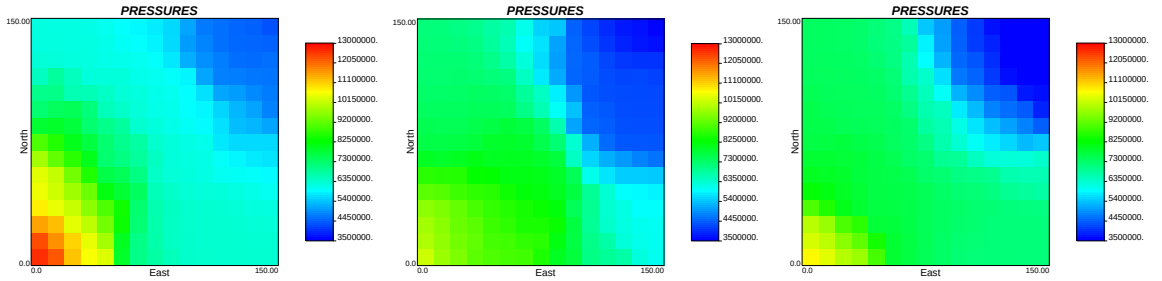

(g) Initial P (h) Calibrated P (i) Real P

Figure 5.19: In this figure initial (first column), calibrated (second column) and real (third column) realizations are presented for comparison. First row corresponds to logarithm of absolute permeability, second row to water saturations after 120 days and third row to pressures after 120 days. The well layout is a quarter five spot problem. Inversion with 5 data grid blocks was run. Relative permeability parameters are taken to vary all over the domain.

measurements. 11 master points are taken to calibrate heterogeneous fields for k, k^0_{rw}, S_{rw}, k^0_{ro} and S_{ro}. Results are given in Figures 5.19 and 5.20.

The shape of the saturation front at the end of the calibration (Figure 5.19(e)) is more similar to the real saturation front (Figure 5.19(f)) than the one given by

the initial parameters (Figure 5.19(d)). The same happens with the pressure values (compare Figures 5.19(h) and (i)), though the saturation lower right zone still does not match the real values. The calibrated heterogeneous logarithm absolute permeability field (Figure 5.19(b)) reproduces the left part of the domain but the right area is not so well fitted (Figure 5.19(c)).

The relative permeability parameters taken as heterogeneous are also calibrated. The fields resulted from the calibration are resumed in Figure 5.20. It looks like the end-points of relative permeability curves are better reproduced than the residual saturations. In general the end-point of oil relative permeability is better calibrated than the end-point of water relative permeability. The shape of the high and low values after calibration are quite similar for the fields of calibrated end-points. This does not happens in the case of water residual saturation. Calibrated oil residual saturation is the parameters that fits worst the real field.

This example with such a complex heterogeneity for relative permeability curves shows that even for very complicate heterogeneities it is possible to inverse model the parameters of relative permeability curves. This case and the rest of the examples presented in this chapter show the possibilities of the inverse method in 2D fields. It can be concluded that it is possible to generate a conditional realization in 2D with different conditions and parameter set. The results obtained after the calibration represent one possible realization to characterize the reservoir, but the results shown are just one of the representations of the reservoir. It is necessary to perform an uncertainty analysis to see if the prediction given by this realization can be close to reality or not. The uncertainty analysis are going to be computed in next chapter.

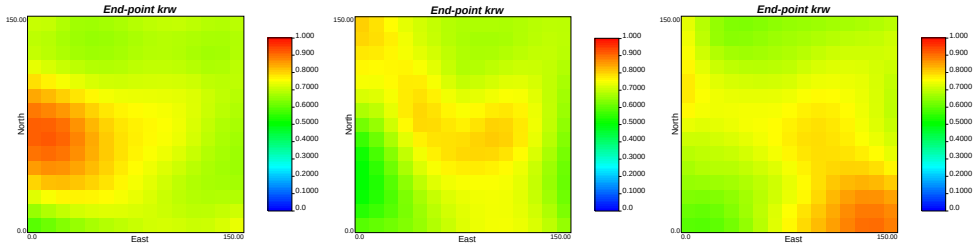

(a) Initial k^0_{rw} (b) Calibrated k^0_{rw} (c) Real k^0_{rw}

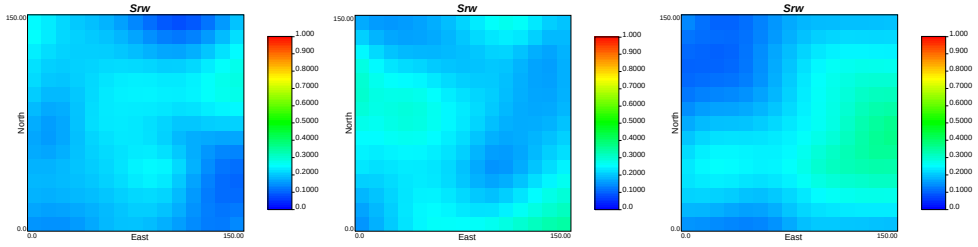

(d) Initial S_{rw} (e) Calibrated S_{rw} (f) Real S_{rw}

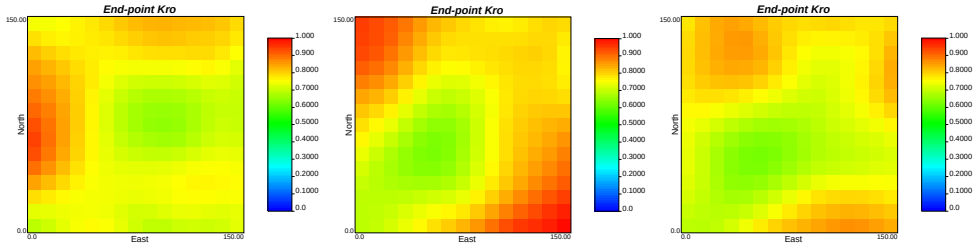

(g) Initial k^0_{ro} (h) Calibrated k^0_{ro} (i) Real k^0_{ro}

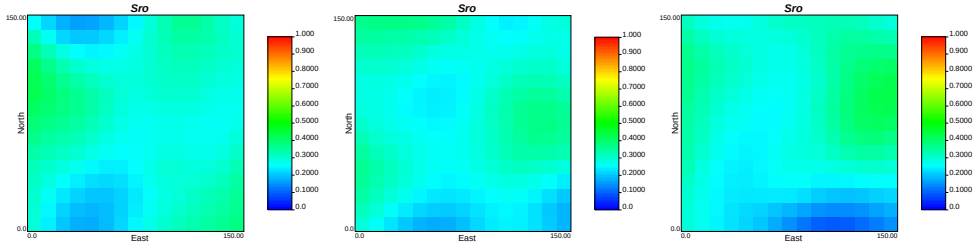

(j) Initial S_{ro} (k) Calibrated S_{ro} (l) Real S_{ro}

Figure 5.20: In this figure initial (first column), calibrated (second column) and real (third column) realizations are presented for comparison. First row corresponds to k^0_{rw}, second row to S_{rw}, third row to k^0_{ro} and fourth column to S_{ro}. The well layout is a quarter five spot problem. Inversion with 5 data grid blocks was run. Relative permeability parameters are taken to vary all over the domain.

Chapter 6

Uncertainty study

The examples described in last chapter have shown that it is possible to generate a conditional realization of effective permeability field to production data. If the spatial distribution of relative permeability curves is considered, there is an important change in the production rate and the sweep efficiency within the reservoir. However, the realizations obtained after the calibrations have pointed out that relative permeability parameters seem to be quite insensitive to saturation and pressure data, at least for some of the 2D examples. In addition, it is commonly known that is not possible to avoid the uncertainties associated with the simple models used in the inverse two-phase modeling. There are different kind of sources of uncertainty (Smith and Schwartz, 1981): unknown spatial variation, the model chosen or boundary conditions. In chapter 2, section 2.3, the importance of uncertainty studies was emphasized. In general, the goal of the uncertainty studies is to quantify the reliability of the predictions given by the numerical simulator. The common approach in this dissertation is to use multiple equally likely realizations of permeabilities in a Monte Carlo study for two-phase flow.

The Monte Carlo approach is used to construct estimates of the multivariate probability distribution function of the output model parameters. This technique consists in the repetitive generation of many different realizations of the reservoir from the stochastic process describing the heterogeneity. An ensemble of permeability fields, and the corresponding ensembles of saturation and pressure solutions (in time and space) are the results of many calibrations. The statistical analysis of these ensembles of realizations produces models of uncertainty for both permeabilities and production data that serve to assess the degree of confidence on the predictions made using these models. A Monte Carlo analysis essentially repeats the entire modeling (in Figure 1.1: process-sampling, input, estimation, and prediction) many times. Each of these hypothetical modeling studies (or replicates) is based on a different synthetically generated parameter description. It might be argued that Monte Carlo methods are too

complex and time-consuming to be practical in reservoir applications. However, for the objectives of the present research, the Monte Carlo method is the best approach.

This chapter explains different uncertainty studies performed. The first two sections are uncertainty studies for relative permeability parameters in 1D, the second one with simultaneous calibration of absolute permeability. Last section shows 2D uncertainty results.

6.1 1D uncertainty study of relative permeability parameters.

The inverse method procedure was described in detail in chapter 4. At the end of that chapter the approach was apply to a 1D calibration case, in which relative and absolute permeabilities were estimated. This test case investigated the little influence of pressure data to relative permeability estimations and the changes that the saturation shock front suffers if the relative permeability curve is considered to be heterogeneous within the domain. The parameters fitted with the calibration gave a very good agreement for the true pressure and saturation fields. Nevertheless, still remains to study the sensibility of these parameters to historical data and to perform the uncertainty analysis of the predictions.

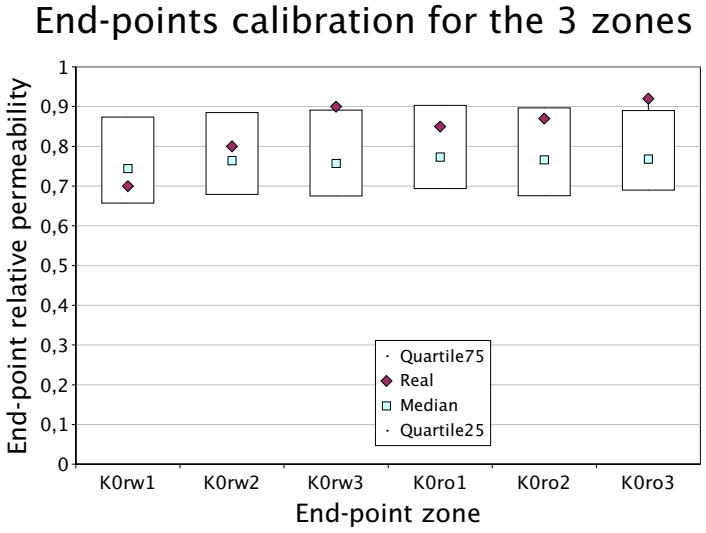

Figure 6.1: Uncertainty related with the end-points of water and oil relative permeability curves for the 3 areas in which the domain is divided. The objective function is defined in terms of water saturation. Real values are represented with a red diamond and median with a light blue square. Probability variables are calculated from 100 different realizations.

In this section, and also in the following one, the uncertainty study has been performed for a 1D hypothetical water injection displacement, equivalent to the inversion example in chapter 4, section 4.4. The uncertainty analysis is done for the four relative permeability parameters chosen for calibration (k^0_{rw}, S_{rw}, k^0_{ro} and S_{ro}), while in this case absolute permeabilities are supposed to be known. The real 1D reservoir is taken from the 1D synthetic case described in chapter 4. The entire domain is divided in three zones within each of them absolute and relative permeabilities are homogeneous. The three zones were depicted in Figure 4.2. The domain is discretized with 50 grid blocks, and the simulation time with 500 time steps. The parameter values corresponding to the real case were resumed in Table 4.1. The same procedure described for the exercise in chapter 4 has been adopted to sample the data. Measurements are assumed to be water saturations taken for 10 different times at 3 different points from the synthetic forward results. 100 different initial values for each of the four parameters subjected to calibration were introduced as initial values in 100 different calibration processes. The result of the 100 different calibrations are 100 representations of the medium that are going to be used to perform the uncertainty analysis related with the four parameters, following the Monte Carlo methodology. The 100 realizations are 100 equally likely representations of the reservoir because they reproduce the measured data. Reflexions expounded in the chapters 3 and 4 turned out that pressure field is not importantly affected by spatial variations in relative permeability curves. Absolute permeability is assumed to be known, hence only water saturation data are included in the objective function ($w_{p,i} = 0$ and $w_{s,i} = 1$ in equation (4.1)).

Figure 6.1 represents with red diamonds the real end-points of water and oil relative permeability curves, k^0_{rw} and k^0_{ro}, for each of the zones in which the domain is divided. Light blue squares are the median of the 100 k^0_{rw} and k^0_{ro} realizations, and the upper and lower part of the rectangles drawn for each of the zones are respectively the Q25 and Q75 probability quartiles. These statistics are obtained from the ensemble of 100 calibrations. The x axis in Figure 6.1 corresponds to the parameter that is calibrated and the zone that characterizes. Figure 6.2 shows similar results but for water and oil residual saturations in each of the zones. Upper and lower quantiles form and interval that can be seen as a measure of uncertainty of the relative permeability parameters when the saturation shock front is predicted.

These results given in Figures 6.1 and 6.2 show that, in 1D, the inter-quantile interval is quite wide for the end-points. For the given information and method used, the inter-quantile interval includes the real data in most of the cases (see Figure 6.1). In the water and oil residual saturation calibrations the inter-quantile interval is very narrow, also including in most of the cases the real value, which at the same time is

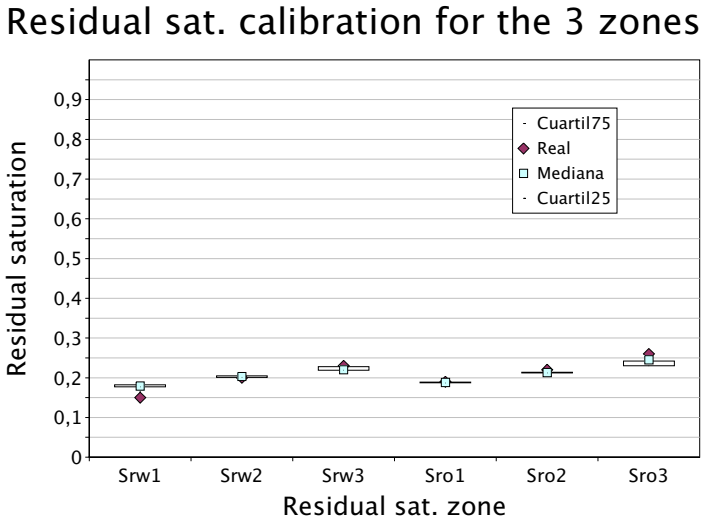

Figure 6.2: Uncertainty related with the water and oil residual saturations for the 3 areas in which the domain is divided. The objective function is defined in terms of water saturation. Real values are represented with a red diamond and median with a light blue square. Probability variables are calculated from 100 different calibrations.

reproduced quite well by the median (see Figure 6.2).

These are the main results when only relative permeability parameters are calibrated, and absolute permeability is known. Let's see in next section what are the differences when absolute and relative permeabilities are calibrated simultaneously.

6.2 1D uncertainty study of absolute permeability and relative permeability parameters.

Another set of 100 calibrations were carried out, but this time simultaneously to relative permeability parameters, absolute permeability was also calibrated. Absolute permeability, likewise the examples shown in chapter 4, is homogeneous within the 3 zones in which the 1D reservoir is divided. 100 different sets of the four relative permeability parameters and absolute permeability are introduced in 100 different calibrations. The results are 100 relative permeability curves and 100 absolute permeabilities for each of the 3 zones. The real parameters are the same as in the section before, taken from chapter 4. In this case absolute permeability is also calibrated and pressure and water saturation data are introduced in the objective function definition ($w_{s,i} \neq 0$ and $w_{p,i} \neq 0$ in equation (4.1)).

The results of the uncertainty analysis when both absolute and relative permeabi-

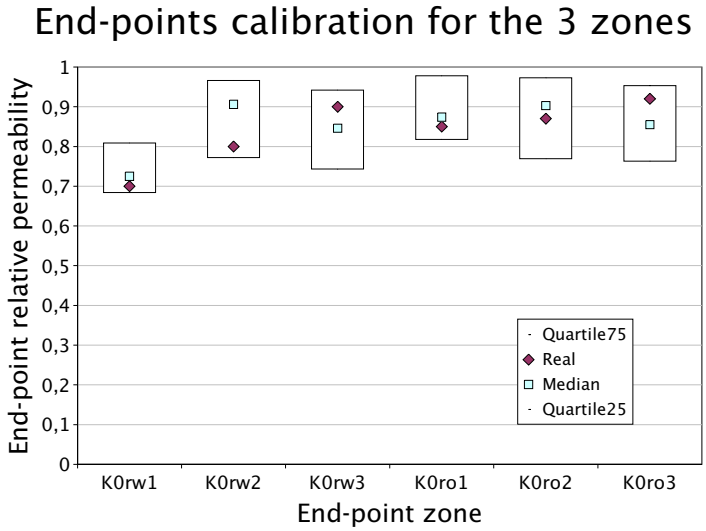

Figure 6.3: Uncertainty related with the end-points of water and oil relative permeability curves for the 3 areas in which the domain is divided. The objective function is defined in terms of water saturation and pressure data. The calibration is performed simultaneously with absolute permeabilities. Real values are represented with a red diamond and median with a light blue square. Probability variables are calculated from 100 different calibrations.

lities are calibrated are resumed in a set of graphics similar to the ones used in the former section. For the end-points of water and oil relative permeability curves, the median and quantiles Q25 and Q75 are drawn in Figure 6.3. In the Figure 6.4 the statiscal analysis for the 100 calibrations of residual saturations can be seen. Lastly, the uncertainty study for absolute permeability can be found in Figure 6.5.

Inter-quantile intervals, seen as a measure of the uncertainty in the prediction of the parameter values, do not change significantly for any of the four relative permeability parameters (k^0_{rw}, k^0_{ro}, S_{rw} and S_{ro}), in comparison with the results in former section. Anyhow, the inter-quantile interval corresponding to the end-points (Figure 6.3) seems to narrow when the pressures are included in the objective function. The inter-quantile intervals for residual saturations (Figure 6.4) and for absolute permeability (Figure 6.5) are very constrict. Figure 6.3 shows that the prediction of the end-points, given by the median, is slightly improved when pressure data are included in the objective function (in all the zones k^0_{rw} and k^0_{ro} median and true values are included in the interquantile interval). The predictions given by the median of absolute permeability values in the 3 zones are quite satisfactory (Figure 6.5).

In the 2D examples shown in chapter 5 calibrated relative permeability parameters appear to indicate an important uncertainty as they were quite insensitive to production data. The 1D uncertainty analysis reflects these results for the end-points, but not for

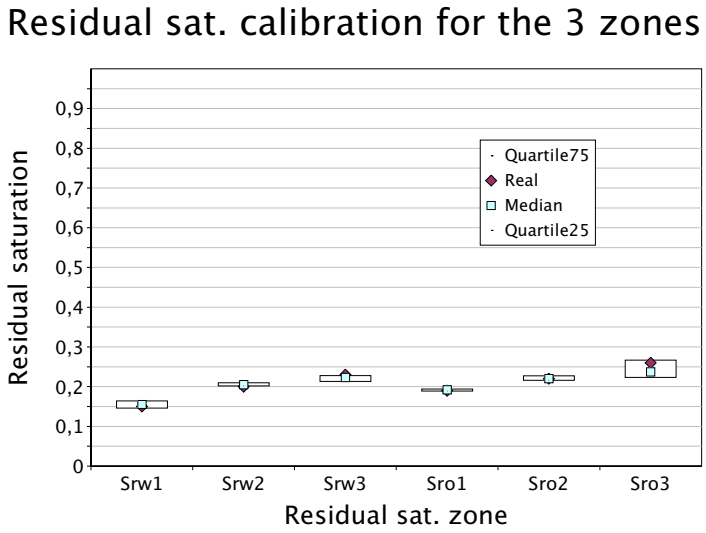

Figure 6.4: Uncertainty related with the water and oil residual saturations for the 3 areas in which the domain is divided. The objective function is defined in terms of water saturation and pressure data. The calibration is performed simultaneously with absolute permeabilities. Real values are represented with a red diamond and median with a light blue square. Probability variables are calculated from 100 different calibrations.

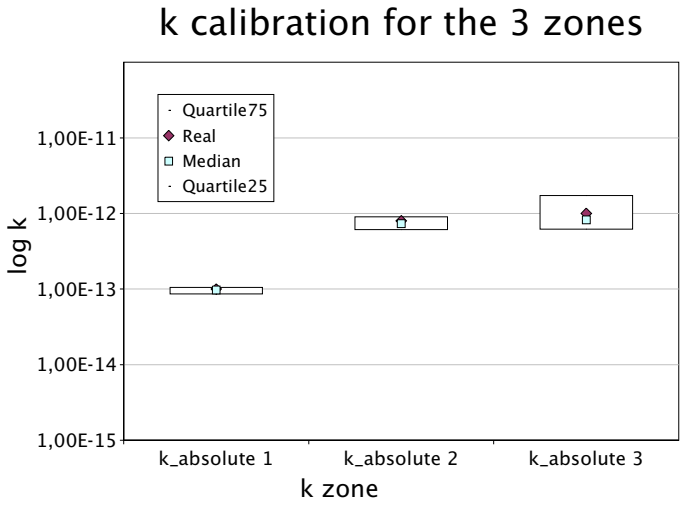

Figure 6.5: Uncertainty related with the absolute permeability for the 3 areas in which the domain is divided. The objective function is defined in terms of water saturation and pressure data. The calibration is performed simultaneously with relative permeability parameters. Real values are represented with a red diamond and median with light blue square. Probability variables are calculated from 100 different calibrations.

the residual saturations. It could have happened that the initial fields taken for residual saturations in the 1D uncertainty analysis were much closer to the real values than the initial residual saturations taken in the 2D examples. Next section explains a 2D uncertainty analysis and further analyze these results.

6.3 2D uncertainty study of absolute permeability and relative permeability parameters.

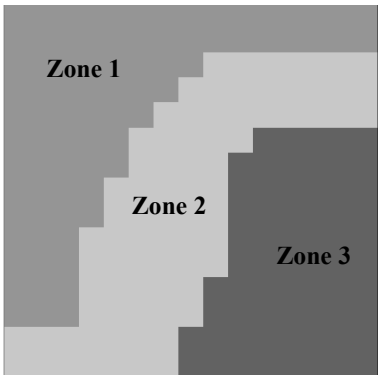

Figure 6.6: Configuration of zones 1, 2 and 3 for relative permeability parameters. Within each zone the relative permeability parameters are considered homogeneous. This configuration is taken for the 2D uncertainty analysis.

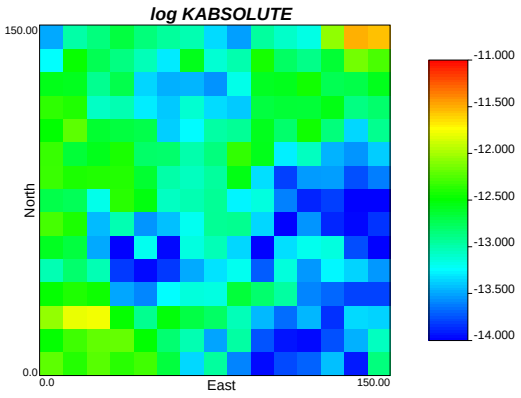

Figure 6.7: 2D heterogeneous absolute permeability field that is taken as the real absolute permeability field for the uncertainty study.

In the calibrations performed in last chapter the production data were reproduced after perturbating absolute and relative permeabilities. Some examples have shown that calibrated values of relative permeability parameters resulted to be insensitive to

saturations and pressures. On the other hand, the uncertainty analysis performed in 1D (last two sections) concludes that the uncertainty related with the end-points is quite wide, while for residual saturations the inter-quantile range is very narrow. The 2D calibrations performed in chapter 5 suggest that also for residual saturations the uncertainty range should be rather wide. In this section a 2D uncertainty analysis is performed. The high computational cost required for each 2D calibration has limited the number of realizations for the uncertainty analysis to 10 runs.

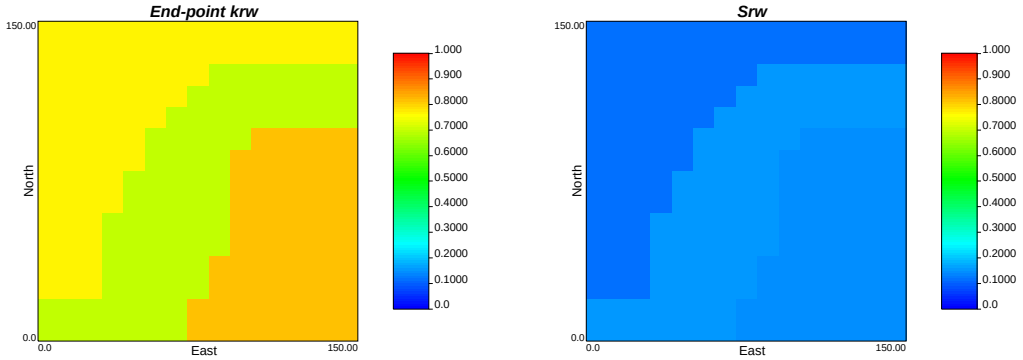

(a) k^0_{rw} (b) S_{rw}

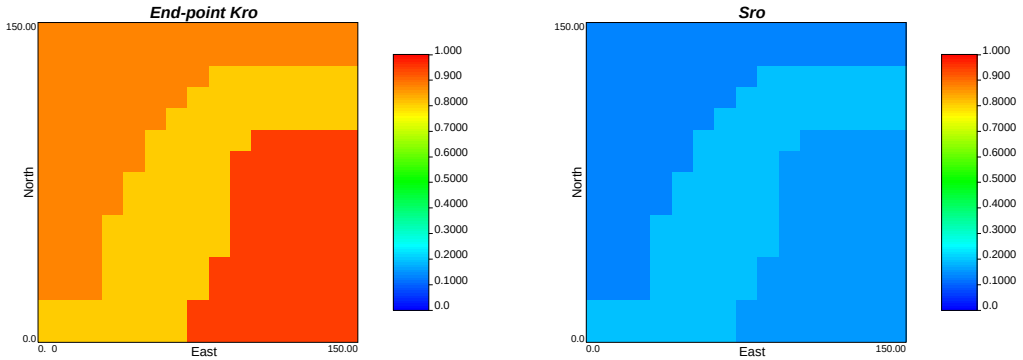

(c) k^0_{ro} (d) S_{ro}

Figure 6.8: 2D values for k^0_{rw}, S_{rw}, k^0_{ro} and S_{ro} given in three zones. They are the true values for the 2D uncertainty study.

The problem configuration is similar to the examples shown in chapter 5. Different geometry has been chosen for the zones that define the heterogeneity of relative permeability in order to reproduce a geology that would be closer to a real realization. As in other cases, 3 zones of the domain are considered to have homogeneous relative permeability parameters. These zones are numbered from 1 to 3 and their contour limits are plotted in Figure 6.6. The true case is represented with absolute and relative

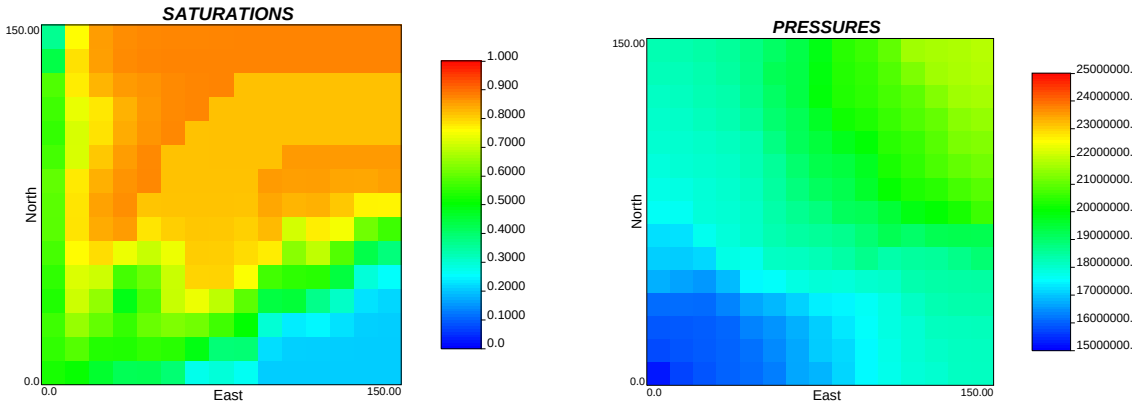

(b) P

Figure 6.9: When introducing real parameters in the forward two-phase flow simulator this is the saturation (a) and pressure (b) field obtained at the end of the simulation. These are saturation and pressure fields corresponding to the true fields for the 2D uncertainty study.

permeability fields, graphed in Figures 6.7 and 6.8. The absolute permeability field, as explained in former chapters, is constructed with GCOSIM3D simulation code. The log-mean is equal to -13.0 and the variance is equal to 0.3. The field is isotropic and spatial continuity can be described with a spherical variogram model of range equal to 60m. The porosity is equal to $\phi = 0.2$. True absolute permeability values are assumed to be known, and only relative permeability parameters are subjected to calibration.

The well configuration is the already used quarter five spot case. The same spatial discretization used in former 2D simulations of 15x15 grid blocks (of 10x10m) is taken. 600 time steps of 4.8 hours are used for the time discretization. In this example the injection well is situated in the upper right grid block of the domain and the production well in the lower left grid block. The injection and production rates are equal to 2.5kg/s. At the end of the forward simulation, for the last time step, the saturation and pressure fields are given in Figure 6.9.

After 10 calibrations, statistical analysis has been applied to the ensemble of end-points and residual saturations estimated. Likewise in the 1D uncertainty analysis, these statistics were median, Q25 and Q75 interquantiles. The results, in comparison with the real values, are graphed in Figures 6.10 and 6.11.

These graphs show a very narrow uncertainty range for the four parameters, which do not envelope the real corresponding values. This result suggest that more calibrations should be performed in order to get a wider range of different possible values, 10 calibrations is not enough to infer the probabilities corresponding to the output ensemble. The results obtained in 1D, and the calibrated values given by the 2D examples

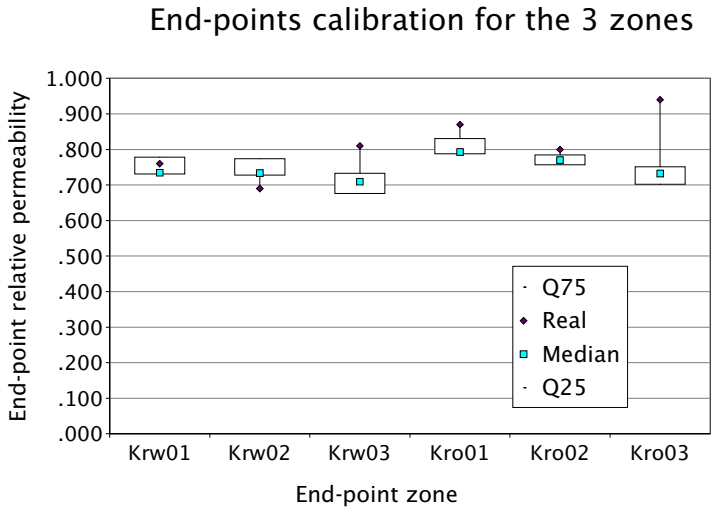

Figure 6.10: Uncertainty related with the end-points of water and oil relative permeability curves for the 3 areas in which the domain is divided. Real values are represented with a red diamond and median with a light blue square. Probability values are calculated from 10 different calibrations in 2D.

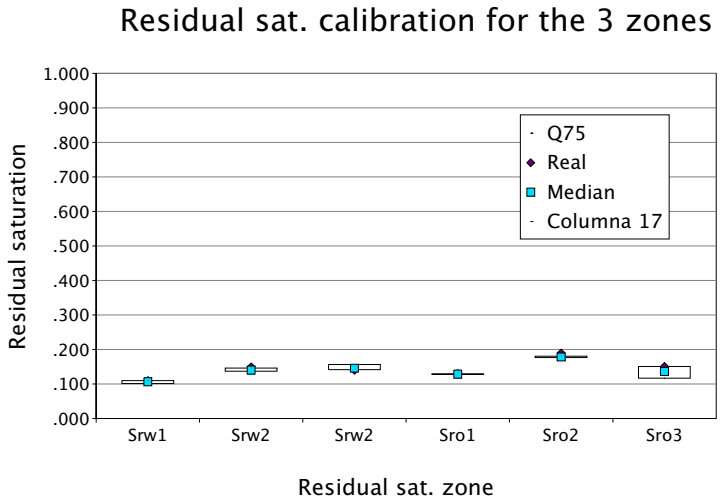

Figure 6.11: Uncertainty related with the water and oil residual saturations for the 3 areas in which the domain is divided. Real values are represented with a red diamond and median with a light blue square. Probability values are calculated from 10 different 2D calibrations.

have point out the large uncertainty related with the end-point of relative permeabilities. Even this uncertainty analysis performed in 2D gives smaller inter-quantile range for the end-points, it is probably due to the few number of calibrations performed. To solve this necessity the method should be improved in order to perform a higher number

of calibrations much faster than in the computations run during this dissertation.

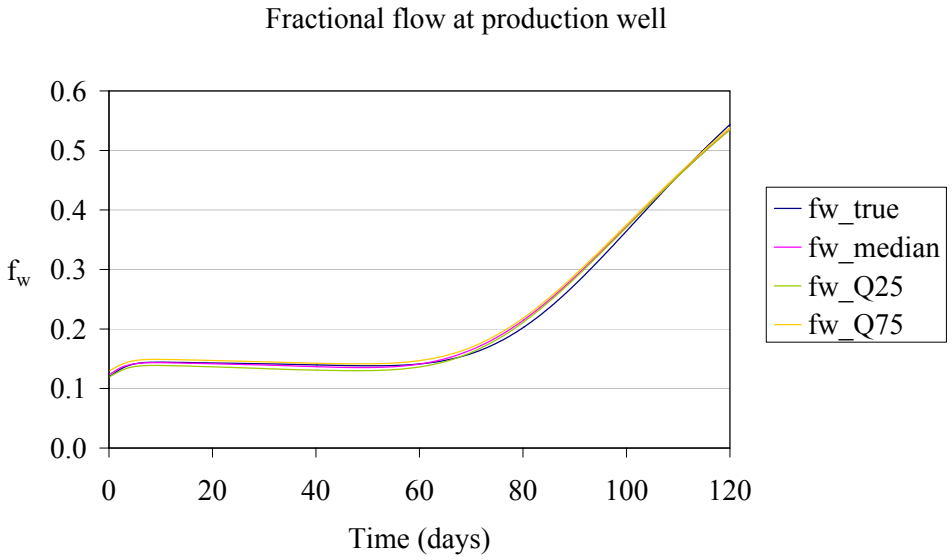

Figure 6.12: Evolution of fractional flow with time. The f_w values are plotted for the true parameters and the statics calculated from 10 different 2D calibrations.

The set of relative permeability values would correspond to 10 different water breakthrough responses. This set of water saturations can also be used to study the uncertainty in the production forecasts. Statistics can also be computed on the set of 10 saturation fields. The results, given in fractional flow terms, are plotted in Figure 6.12. The true curve (plotted in dark blue) in the production well (lower left corner) corresponds to the fractional flow values in function of time. Statistical values are computed from the 10 equivalent curves of the 10 calibrations, plotted in the same Figure 6.12. It has been pointed out that more realizations should be run to obtain a better uncertainty study, but these values give an idea of the behavior of the production forecast. At the initial stages of the production upper and lower quantiles envelope both median an real values. However, when the water production increases its rate, the uncertainty range gives worse prediction. In any case, all the curves are very close to each other indicating the good predictions that could be obtained by using the inversion method described here.

All these results indicate that uncertainties related with the end-points of relative permeability curves are higher than the uncertainties related with residual saturations. However, the calibrated values for the 2D examples presented an important lack of sensitivity of these parameters to saturation and pressure production data. Further research is needed in order to improve the computational time to be able to perform more simulations and more uncertainty analysis in different situations. The importance of the heterogeneity in relative permeability functions has been marked during the

tests shown in former chapters. The values and spatial distribution of these parameters influence so much on the saturation shock front distribution that more attention should be paid to the role of these parameters in multiphase flow simulations.

Chapter 7

Conclusions and further research

7.1 Conclusions

The main objective of this dissertation is to take into account relative permeability heterogeneities in inverse two-phase flow modeling for reservoir characterization purposes. After performing a literature review (chapter 2) it was found out that, to the best of our knowledge, there is an important gap in inverse two-phase flow techniques in what refers to the role of relative permeabilities. Then, the different possibilities to implement the heterogeneities of relative permeability curves in forward two-phase flow simulators were analyzed (chapter 3). A new tool to carry out inverse modeling of relative permeability parameters was developed (chapter 4). Once the tool was ready to use, different examples in 2D have shown the applicability of the method (chapter 5) and uncertainty analysis were performed (chapter 6). It is the aim of this dissertation to investigate the influence of relative permeabilities on the behavior of dynamic variables in the reservoir. From the research done, the principal conclusions that can be extracted are:

1. A literature research showed that it is very common to perform stochastic inverse modeling in order to characterize the heterogeneity of absolute permeability. The majority of the references checked assume homogeneous relative permeability curves when multiphase flow is subjected to inverse modeling. However, some approaches consider heterogeneous relative permeability. The few works that estimate relative permeability parameters with inverse modeling, considering these functions to be heterogeneous, are applied to core sample scale cases and not to reservoir scale. In these studies some of the parameters that define the relative permeability functions are chosen to be estimated by history matching processes. Furthermore, the conclusions given by these research works reveal the impor-

tance of the estimation of relative permeability functions. In general, there is not a technique to inverse model relative permeability functions considering their heterogeneity within the reservoir, at reservoir scale.

2. It has been possible to develop and implement a code that calibrates simultaneously relative and absolute permeability functions to historical data. In this code relative permeabilities are assumed to be function of saturation, and are expressed as power functions. Four parameters were chosen to characterize the relative permeability curves: the two end-points of the curves and the residual saturations. These parameters are subjected to calibration to dynamic variables such as saturations and pressures. The method not only allows to estimate relative permeability functions, another important contribution is that the calibration of relative permeability parameters is performed simultaneously with the calibration of absolute permeability when absolute and relative permeabilities are considered to be spatially variable.

3. Inverse calibration has been computed following the ideas given by the Sequential Self-Calibrated method. This methodology allows to reduce the parameter space for the calculation of perturbations, making the process faster. The concept of master point perturbations has been successfully implement in the two-phase flow simulation showing the advantages of this method not only in single phase flow simulations, but also when the concept of relative permeability is necessary to define the flow equations.

4. It has been shown that the code can be successfully applied to different kind of 1D and 2D cases. Different type of data are integrated with the inversion method developed. Static variable measurements such as absolute permeabilities are considered in the examples shown. Dynamic variables as saturations and pressures are integrated through the iterative inversion method, keeping the static variable measurements. The possibilities given by the integration of soft data, as the seismic information, are shown in one of the examples run. 4D seismic information can enormously improve the estimation of the absolute and relative permeabilities at the same time that the uncertainty related with calibrated relative permeability parameters seems to be reduced.

5. All the inverse modeling examples, and even the forward simulations, reveal that the heterogeneity of the relative permeability functions can dramatically change the dynamic behavior of the reservoir. When oil is displaced by injected water, this influence of relative permeabilities spatial variation is very important for

the saturation shock front. This means that if the relative permeabilities (or fractional flow, which is a variable dependent on relative permeabilities) are going to be estimated it is not sufficient to calibrate them to pressure data, saturations must also be considered to get a real estimation.

6. The uncertainty analysis studied in 1D has shown that uncertainties related with the end-points of water and oil relative permeability curves are quite wide. These uncertainties are reduced if instead of just consider saturation measurements, pressures are also included in the objective function. The uncertainties related with residual saturations in this 1D analysis resulted very narrow, as well as for the estimated absolute permeabilities.

7. In 2D, the uncertainty analysis gives results similar with the 1D uncertainty analysis. The number of realizations performed in 2D was limited by the computational cost, and more runs would be necessary to perform a complete analysis as it has been done in 1D. The ensemble of water breakthrough values allows to perform an uncertainty study in the production predictions. Better production forecasts are obtained in the first stages of the exploitation.

All these points resume the principal conclusions of the research done in this dissertation, and give an answer to the objectives that were proposed at the beginning of the research work (explained in chapter 1). However, there were parts of the work that did not result as it was expected, and new options have appeared during the research. Thus, further research must be continued to investigate in this direction and to facilitate the creation of a more practical tool to inverse estimate relative permeabilities at reservoir scale.

7.2 Suggestions for further research

The following issues deserving further research have been identified:

- The difficulty of the method is the high computational cost that the method requires at each iteration. The forward 2D problem requires a considerable time to be run, and this is one of the main reasons why at each iteration so much time was needed. Thus more research has to be conducted in what refers to forward modeling, especially in the area of numerical solvers for non linear differential system of equations. One of the possible solutions would be to apply streamline simulators and fractional flow formulation. Making the forward method computationally faster, each iteration could be speed up, and the inverse method could be applied to higher domains and discretizations.

- Altough the use of the concept of master points reduces the number of parameters in which the perturbations must be computed, there is still another area which needs further research to obtain less computational time: the optimization algorithm used in the iterative inversion. Presently, the inverse method uses a numerical approach of the gradient of the objective function. It also uses gradient approaches to solve the optimization process. These approximations are valid, but it would be desirable to implement other approximations in order to make the process faster. One possible solution for further research it would be the implementation of the sensitivity equations to use a second order method to perform the optimization during the inversion. As the forward two-phase flow simulator, the optimization algorithm needs an improvement in order to make possible the study of higher dimensional fields with more discretization.

- Other possibility to increase the performance of the method it would be the study of parallel computing advantages to speed up the CPU cost. These new techniques offer the possibility to get good computational times in complex non linear problems as the one study here.

- The information used in the examples shown in this dissertation has consisted in absolute permeability data, saturations and pressures. The use of relative permeability measurements was not explored in this work, and further research to include relative permeability available data should be considered.

- The use of seismic information has shown the improvements that can be obtained in the model. The very recent availability of new sensors to measure pressure and temperature downhole in a permanent way is still on research and develop in order to build a new pressure sensor. The pressure data acquired with this kind of new techniques is an important potential application of the inverse method presented here, very similar to the seismic 4D data application.

- As it is available an inverse code for the numerical solver used during this dissertation (TOUGH code) called ITOUGH, it would be very interesting to compare the proceduce presented here with the inverse code ITOUGH. A modification of the code to take into account heterogeneities of the relative permeabilities parameters for the inversion would have to be done.

- If the improvement in the computational cost of the process is reached, the next step that should be considered is the application of the method to a real case. The examples and studies shown in this dissertation are created synthetically and still remains to show how the estimation of relative permeability curves by

inverse two-phase flow can improve the characterization of the reservoir in a real case.

Appendix A

Buckley-Leverett solution

The formulation of the 1D two-phase immiscible flow with the fractional flow is described in chapters 2 and 3. The equation that must be solved is (equation (3.12)):

$$\phi\frac{\partial S_w}{\partial t} + u_T\frac{\partial f_w}{\partial S_w}\nabla S_w = f_w q_T - q_w$$

To solve this equation Bukley y Leverett assumed the following initial and boundary conditions:

$$\begin{aligned} S_w(x,0) &= S_{wI},\ x \geq 0 \\ S_w(0,t) &= S_{wJ},\ t \geq 0 \end{aligned} \tag{A.1}$$

Initially the medium has a saturation equal to S_{wI}. At the origin position $x = 0$ water is injected with constant rate q_w, keeping constant the saturation at the injection well, equal to S_{wJ}. At origin and initial time, $t = x = 0$, all the values for S_w are possible ranging between S_{wI} and S_{wJ}.

Assuming that there are not injection nor production terms, the equation (3.12) and (A.1) can be rewritten in a simpler way (adimensional):

$$\left(\frac{\partial S_w}{\partial t_D}\right) + \left(\frac{\partial f_w}{\partial S_w}\right)\left(\frac{\partial S_w}{\partial x_D}\right) = 0 \tag{A.2}$$

$$S_w(x_D,0) = S_{wJ},\ x_D \geq 0 \tag{A.3}$$

$$S_w(0,t_D) = S_{wJ},\ t_D \geq 0 \tag{A.4}$$

where x_D and t_D are adimensional variables equal to:

$$x_D = \frac{x}{L}$$

$$t_D = \int_0^t \frac{u_T dt}{\phi L}$$

x_D is the adimensional space variable and t_D is the adimensional time variable. L is the total length of the porous medium in the direction of x. In these equations u_T can be function of time but it cannot be function of position because incompressibility has been assumed. Moreover, $\frac{df_w}{dS_w}$ is the total derivative because f_w is function of S_w (unique dependent variable).

Equation (A.2) is a differential equation of first order partial derivatives, the unique dependent variable is $S_w = S_w(x,t)$ because $\frac{\partial f_w}{\partial S_w}$ is function of S_w. This equation can be solved with numerical methods or with the method of characteristics (Marle, 1981).

Multiplying and dividing by the transversal section A, the adimensional time can also be expressed as:

$$t_D = \int_0^t \frac{Audt}{A\phi L} = \int_0^t \frac{Q_T dt}{V_p} \tag{A.5}$$

where Q_T is the volumetric flux rate and V_p is the porous volume. t_D is the total volume injected until time t divided by the total porous volume.

Starting from equation (A.2), saturation S_w can be written in a differential form:

$$dS_w = \left(\frac{\partial S_w}{\partial x_D}\right)_{t_D} dx_D + \left(\frac{\partial S_w}{\partial t_D}\right)_{x_D} dt_D \tag{A.6}$$

The velocity v_{s_w} can be deduced from this equation (A.6). For a point at constant saturation S_w in the space $x_D - t_D$ the velocity is equal to:

$$\left(\frac{dx_D}{dt_D}\right)_{S_w} = -\frac{(\partial S_w/\partial t_d)_{x_D}}{(\partial S_w/\partial x_D)_{t_D}} \equiv v_{S_w} \tag{A.7}$$

This is the specific velocity of saturation S_w because it has been normalized with u/ϕ.

Applying the equation (A.7) to equation (A.2) the result is:

$$v_{S_w} = \frac{df_w}{dS_w} \tag{A.8}$$

The meaning of the equation (A.8) is that the specific velocity of constant saturation S_w is equal to the derivative of the fractional flow curve at this point S_w of the curve $f_w - S_w$. This equation is the solution of the one dimensional problem of displacement of petroleum with water, and can be used to predict the rate of displacement of the shock front. Selecting different S_w between S_{wI} and S_{wJ}, the curve $S_w(x_D, t_D)$ can be built. Fractional flow, f_w, is a function of relative permeabilities, thus a function of

saturation. Once f_w in known in function of S_w it is possible to compute the derivative $\frac{df_w}{dS_w}$. With this derivative, with the equation (A.8) and with initial and boundary conditions, it is possible to calculate the spatial distribution of saturation in function of the space and time variables. For the initial time $t = 0$ the resistance to the flux is exclusively motivated by the presence of oil, as at this point no water has been injected yet.

The Buckley and Leverett equation can be readily solved graphically. Relative permeability functions, $k_{rl} = k_{rl}(S)$, and fractional flow $f_w = f_w(S_w)$ are normally given in form of curves, in which $\frac{df_w}{dS_w}$ is calculated graphically (Morel-Seytoux, 1973; Lake, 1989; Dake, 1978; Marle, 1981). The steps in the graphical solution are:

1. Evaluate $k_{rw}(S_w)$ and $k_{ro}(S_w)$ for values of S_w.
2. Find $f_w(S_w)$.
3. Plot f_w versus S_w.
4. Measure df_w/dS_w from the curve.

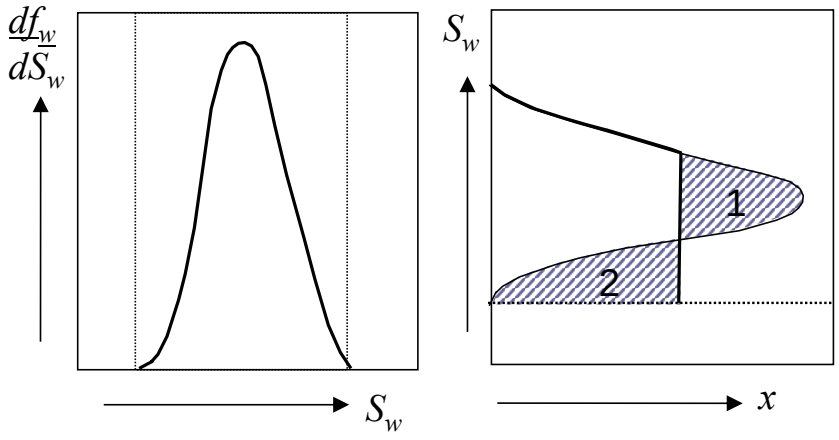

Figure A.1: Left graph: saturation derivative of a typical fractional flow curve. Right graph: resulting water saturation distribution in the displacement graph.

From the form Buckley and Leverett equation it is expected the position of the front to be continuosuly increasing function of time, as well as a single value for S_w at each time for every position. In practice, the curves $f_w = f_w(S_w)$ present in some cases a maximum. This means that for a single position, x, the Buckley and Leverett equation predicts two values of saturation S_w. These values do not have any physical meaning, though they are mathematically correct. This problem is solved with the concept of shock front. A graphical correction to the empirical df_w/S_w leads to an acceptable

solution. A value of df_w/dS_w is chosen such that the areas 1 y 2 (look Figure A.1) are equal. The derivative curve is truncated so the value of x is the same for all S_w below the threshold. This implies an abrupt jump in S_w at a specific x-position. This is observed in practice and is called the shock front. This implies that there are discontinuous changes of saturation. Strictly speaking the discontinuities do not exist in nature because there is always a diffusive effect that spreads the discontinuity effect. Although this phenomenon exists, the role that discontinuity has in the displacement is fundamental for the theory of the fractional flow, where the diffusive mechanisms are ignored. The solution given by Buckley and Leverett is a good approximation when capillary effects are neglected and the flow rates are high (Bear, 1972).

Appendix B

Sensitivity equations for the fractional flow formulation

In chapter 4 it was described how the perturbation of the master points can be calculated numerically. The gradient vector containing the partial derivatives of the objective function with respect to perturbations at the master point locations must be calculated. In this appendix the fractional flow formulation given in chapter 3 is taken to describe another way to compute the perturbations, with adjoint states. The following steps are similar to the explanation given in Hendricks-Frassen (2001).

B.1 Adjoint states

The fracional flow formulation has the water saturations S_w as the state variables. There are $N \times T$ state variables, where N is the total number of discretization nodes and T is the number of times in which the simulation time is discretized. Let's define the vector $\{p\}$, with dimension M containing all the parameters to be calibrated. The water saturations and the parameters are related through $N \times T$ state equations:

$$\Psi(\{S_w\}, \{p\}) = 0 \tag{B.1}$$

State equations can be expressed with the fractional flow formulation, or with other approaches mentioned in the literative review as the two pressures method. Let's take for this case the fractional flow approach. The matix form of the two-phase flow equation is (equation (**??**)):

$$[A]\left(\{S^{t+1}\} - \{S^t\}\right) = \{Q^{t+1}\} \tag{B.2}$$

where $[A]$ is $N \times N$ matrix and $\{Q\}$ and $\{S\}$ are vectors of dimension N. A_i elements are equal to:

$$A_i = \frac{V_i}{\Delta t} \tag{B.3}$$

and Q_i^t:

$$Q_i^t = Q_T f_{w,i-1}^{t+1} - Q_{w,i}^{t+1} \tag{B.4}$$

The state equations for two sucessive time steps can be written as:

$$\{\Psi_t\} = [A]\left(\{S^t\} - \{S^{t-1}\}\right) - \{Q^t\} = 0 \tag{B.5}$$

$$\{\Psi_{t+1}\} = [A]\left(\{S^{t+1}\} - \{S^t\}\right) - \{Q^{t+1}\} = 0 \tag{B.6}$$

The Lagrangian of the objetive function to be minimized buject to the constrains B.5 and B.6 is:

$$\Im = J + \{\lambda\}'\{\Psi\} \tag{B.7}$$

where λ is a vector of length $N \times T$, which elements are the Lagrange multipliers, also called adjoint states. $\{\lambda\}'$ represents the transpose of the vector $\{\lambda\}'$. For each of the times in shcih teh adjoint state equation is solved a vector $\{\lambda\}$ of dimensions N is estimated. The Lagrange multipliers obtained for the state $\{\Psi_t\}$ are $\{\lambda^t\}$, the Lagrange multiplier for state $\{\Psi_{t+1}\}$ are $\{\lambda^{t+1}\}$, and similarlty for the following time steps.

The derivatives of the Lagrangian with respect the perturbation parameters, $\{p\}$, are given by the equation:

$$\frac{d\Im}{d\{p\}} = \frac{dJ}{d\{p\}} = \frac{\partial J}{\partial\{p\}} + \frac{\partial J}{\partial\{S_w\}}\frac{\partial\{S_w\}}{\partial\{p\}} + \{\lambda\}'\left(\frac{\partial\{\Psi\}}{\partial\{p\}} + \frac{\partial\{\Psi\}}{\partial\{S_w\}}\frac{\partial\{S_w\}}{\partial\{p\}}\right) \tag{B.8}$$

This derivatives are similar to the derivatives of the objective function with respect the perturbation parameters. Equation (B.8) can be rearrange as:

$$\frac{dJ}{d\{p\}} = \frac{\partial J}{\partial\{p\}} + \left(\frac{\partial J}{\partial\{S_w\}} + \{\lambda\}^T\frac{\partial\{\Psi\}}{\partial\{S_w\}}\right)\frac{\partial\{S_w\}}{\partial\{p\}} + \{\lambda\}^T\frac{\partial\{\Psi\}}{\partial\{p\}} \tag{B.9}$$

The adjoing state is taken as the solution of the expression:

$$\frac{\partial J}{\partial\{S_w\}} + \{\lambda\}^T\frac{\partial\{\Psi\}}{\partial\{S_w\}} = 0 \tag{B.10}$$

which makes that equation (B.9) can be simplified resulting:

$$\frac{dJ}{d\{p\}} = \frac{\partial J}{\partial\{p\}} + \{\lambda\}^T \frac{\partial\{\Psi\}}{\partial\{p\}} \tag{B.11}$$

The adjoint states vector is estimated by solving equation (B.8). The result can be used to compute the gradient of the objective function given by equation (B.11).

B.2 Calculation of the adjoint states for the fractional flow formulation

The objective function has been defined in chapter 4. For the fractional flow formulation let's consider that only water saturation measurements are available, and that the weighting terms are equal to 1. Then, the objective function is:

$$J = \sum_{t=1}^{T_s} \sum_{i=1}^{N_s} \left(S_{w,i}^{t,SIM} - S_{w,i}^{t,MEAS} \right)^2 \tag{B.12}$$

N_s is the number of water saturation measurements and T_s the number of times in which the water saturation data are taken. Exponents SIM and $MEAS$ refer to simulated and measured values.

With this definition of the objective function, the derivatives with respect the state variables, that appear in equation (B.10), can be expressed as:

$$\frac{\partial J}{\partial\{S_w^t\}} = 2 \sum_{t=1}^{T_s} \sum_{i=1}^{N_s} \left(S_{wi}^{t,SIM} - S_{wi}^{t,MEAS} \right) \tag{B.13}$$

The derivatives of the state equation with respect the water saturation in the time step t (second term in equation (B.10)) are not equal to zero only for the times t and $t+1$:

$$\frac{\partial\{\Psi_t\}}{\partial\{S_w^t\}} = \left([A] - \frac{\partial\{Q^t\}}{\partial\{S_w^t\}} \right) \tag{B.14}$$

$$\frac{\partial\{\Psi_{t+1}\}}{\partial\{S_w^t\}} = \left(-[A] - \frac{\partial\{Q^{t+1}\}}{\partial\{S_w^t\}} \right) \tag{B.15}$$

Combining the equations (B.13) and (B.15) with equation (B.10) the adjoint state equation is:

$$\begin{aligned} 2 \sum_{t=1}^{T_s} \sum_{i=1}^{N_s} \left(S_{wi}^{t,SIM} - S_{wi}^{t,MEAS} \right) + \{\lambda^t\}' \left([A] - \frac{\partial\{Q^t\}}{\partial\{S_w^t\}} \right) \\ + \{\lambda^{t+1}\}' \left(-[A] - \frac{\partial\{Q^{t+1}\}}{\partial\{S_w^t\}} \right) = 0 \end{aligned} \tag{B.16}$$

Remember that $Q_i^t = Q_T f_{w,i-1}^{t+1} - Q_{w,i}^{t+1}$, hence the partial derivatives $\frac{\partial\{Q^t\}}{\partial\{S_w^t\}}$ and $\frac{\partial\{Q^{t+1}\}}{\partial\{S_w^t\}}$ are equal to zero. The adjoint state equation simplies to the following form:

$$2\sum_{t=1}^{T_s}\sum_{i=1}^{N_s}\left(S_{wi}^{t,SIM} - S_{wi}^{t,MEAS}\right) + \{\lambda^t\}'([A]) + \{\lambda^{t+1}\}'(-[A]) = 0 \tag{B.17}$$

which rearranging terms is:

$$[A]\left(\{\lambda^{t+1}\}' - \{\lambda^t\}'\right) = 2\sum_{t=1}^{T_s}\sum_{i=1}^{N_s}\left(S_{wi}^{t,SIM} - S_{wi}^{t,MEAS}\right) \tag{B.18}$$

This is the adjoing state equation, which has a similar form to the flow equation expressed with the fractional flow formulation. In this equation (B.18) the unknowns are the adjoint states and the independent term is not function of fractional flow. This similarity is normally used in order to reduce the time of calcuation for the coefficients of the system of equations.

B.3 Calculation of the gradient of J using the adjoint states

Once the adjoint states are computed following the steps given in former sectioin, it is possible to used them to calculate the gradient of the objective function with equation (B.11). The derivatives that appear in that equation can be expressed as follows:

$$\frac{\partial J}{\partial\{p\}} = 0 \tag{B.19}$$

$$\frac{\partial\{\Psi_t\}}{\partial\{p\}} = \frac{\partial[A]}{\partial\{p\}}\left(\{S_w^t\} - \{S_w^{t-1}\}\right) - \frac{\partial\{Q^t\}}{\partial\{p\}} \tag{B.20}$$

As all the element of $[A]$ are constants, its derivative with respect the parameters is zero. Then, it is possible to solve the equation (B.11) calculating:

$$\frac{\partial\{\Psi_t\}}{\partial\{p\}} = -\frac{\partial\{Q^t\}}{\partial\{p\}} \tag{B.21}$$

With the definition of Q_i^t:

$$\frac{\partial Q_i^t}{\partial p_k} = Q_T\frac{\partial f_{w,i-1}^{t+1}}{\partial p_k} \tag{B.22}$$

where $f_{w,i}^{t+1}$ is function of p_i. Those p_i are the paremeter values in all the nodes, that are expressed as a linear combination of the parameters in a few points (master points) p_k:

$$p_i = \sum_k e_i^k p_k \tag{B.23}$$

e_i^k could be, for exmple, the ordinary kriging coefficients when p_i is estimated with the values at the master points, p_k. If the parameters are expressed in this way, the derivatives of the fractional flow with respect the parameters are:

$$\frac{\partial Q_i^t}{\partial p_k} = Q_T \frac{\partial f_{w,i-1}^{t+1}}{\partial p_i} \frac{\partial p_i}{\partial p_k} = Q_T \frac{\partial f_{w,i-1}^{t+1}}{\partial p_i} \frac{\partial p_i}{\partial p_k} \tag{B.24}$$

where:

$$\frac{\partial p_i}{\partial p_k} = e_i^k \tag{B.25}$$

$\frac{\partial f_{w,i-1}^{t+1}}{\partial p_i}$ can be deduced from the expression of f_w in potential form:

$$f_w = \frac{1}{1 + \frac{\mu_w k_{ro}^0}{\mu_o k_{rw}^0} \frac{(1-S)^{n_o}}{S^{n_w}}}$$

where S is the water reduced saturation:

$$S = \frac{S_w - S_{rw}}{1 - S_{rw} - S_{ro}}$$

If the perturbation parameter is k_{rw}^0 the derivative is:

$$\frac{\partial f_w}{\partial k_{rw}^0} = \frac{1}{k_{rw}^0} \frac{\frac{\mu_w k_{ro}^0}{\mu_o k_{rw}^0} \frac{(1-S)^{n_o}}{S^{n_w}}}{\left(1 + \frac{\mu_w k_{ro}^0}{\mu_o k_{rw}^0} \frac{(1-S)^{n_o}}{S^{n_w}}\right)^2} = \frac{\mu_w k_{ro}^0}{\mu_o k_{rw}^{02}} \frac{(1-S)^{n_o}}{S^{n_w}} f_w^2$$

This derivatives for all the perturbation parameters have to be introduced in equation (B.24), in order to get the derivatives of the state equation (B.21). This derivatives are sustituted in equation (B.11) to finally get the derivatives of the objective function with respect the perturbation parameters.

Bibliography

[1] R.C. Abbaspour, M.T. van Genuchten, R. Schulin, and E. Schlappi. A sequential uncertainty domain inverse procedure for estimating subsurface flow and transport parameters. *Water Resources Research*, 33(8):1879–1892, 1997.

[2] L. M. Abriola and G. F. Pinder. A multiphase approach to the modelling of porous media contamination by organic compounds 1. Equation development. *Water Resources Research*, 21(1):11–18, 1985.

[3] L. M. Abriola and G. F. Pinder. A multiphase approach to the modelling of porous media contamination by organic compounds 2. Numerical simulation. *Water Resources Research*, 21(1):19–26, 1985.

[4] L. M. Abriola and K. Rathfelder. Mass balance errors in modelling two-phase inmiscible flows: causes and remedies. *Advances in Water Resources Research*, 16:223–239, 1993.

[5] B. Agarwal and J. Blunt. A full-physics, streamline-based method for history matching performance data of a north sea field. *SPE 66388*, 2001.

[6] S. Akin. Estimation of fracture relative permeabilities from unsteady state corefloods. *Petroleum Science and Engineering*, 30:1–14, 2001.

[7] F. O. Alpak, C. Torres-Verdín, and K. Sepehrnoori. Numerical simulation and inversion of pressure data acquired with permanent sensor. *SPE 71612*, 2001.

[8] M. Armstrong and P.A. Dowd, editors. *Geostatistical simulations*. Proceedings of the Geostatistical Simulation Workshop, Fontainebleau, France, 27-28 May, 1993, Kluwer Academic Publishers, Dordrecht, Holland, 1994.

[9] H. Ates and M. Kelkar. Incorporation of two-phase production data into reservoir characterization. *SPE Annual Technical Conference and Exhibition hel in New Orleans, Loisiana, 27-30 September*, 1998.

[10] H. Ates and M. Kelkar. History matching with dual-loop techniques. *SPE/DOE Imporved Oil Recovery Symposium held in Tulsa, Oklahoma, 3-5 April*, 2000.

[11] K. Aziz and A. Settari. *Petroleum Reservoir Simulation*. Applied Science Publishers, 1979.

[12] A. A. Bakr, L. W. Gelhar, A. L. Gutjahr, and J. R. MacMillan. Stochastic analysis of spatial variability in subsurface flow, 1, Comparison of one- and three-dimensional flows. *Water Resources Research*, 14(2):263–271, 1978.

[13] R. P. Batycky. *A Three-Dimensional Two-Phase Field Scale Streamline Simulator*. PhD thesis, Stanford University. Dept. of Petroleum Engineering, Stanford, CA, 1997.

[14] R. P. Batycky, M. J. Blunt, and M. R. Thiele. A 3D multi-phase streamline simulator with gravity and changing well conditions. In *Proceedings of the 17th International Energy Agency Collaborative Project on Enhanced Oil Recovery, Sydney, Australia*, September 1996.

[15] R. P. Batycky, M. R. Thiele, and M. J. Blunt. A streamline simulator to model field sacle three-dimensional flow. In *Proceedings of the 5th Euopean Conference on Mathematics of Oil Recovery, Leoben, Austria*, September 1996.

[16] R. P. Batycky, M. R. Thiele, and M. J. Blunt. A streamline-based reservoir simulator to the house mountain waterflood. In *Stanford Center for Reservoir Forecasting (SCRF) Annual Report, Stanford U.*, 1997.

[17] J. Bear. *Dynamics of Fluids In Porous Media*. Dover, 1972.

[18] J. Bear. *Hydraulics of Groundwater*. Mc Graw-Hill, New York, 1979.

[19] F. Bennett and T. Graf. Use of geostatistical modeling and automatic history matching to estimate production forecast uncertainty. *SPE 74389*, 2002.

[20] P. Binning and M. A. Celia. Practical implementation of the fractional flow approach to multi-phase flow simulation. *Advances in Water Resources*, 22(5):461–478, 1999.

[21] R. H. Brooks and A. T. Corey. Properties of porous media affecting fluid flow. In *J. Irrigation and Drainage Division*, IR2, pages 61–88. Proceedings of the American Society of Civil Engineers, 1966.

[22] S.E. Buckely and M.C. Leverett. Mechanism of fluid displacement in sands. *Transactions AIME*, 146:107–116, 1942.

[23] J.E. Capilla, J.J. Gómez-Hernández, and A. Sahuquillo. Stochastic simulation of transmissivity fields conditional to both transmissivity and piezometric data, 2, Demonstration on a synthetic aquifer. *Journal of Hydrology*, 203(1–4):175–188, 1997.

[24] J.E. Capilla, J.J. Gómez-Hernández, and A. Sahuquillo. Stochastic simulation of transmissivity fields conditional to both transmissivity and piezometric data, 3, Application to the WIPP site. *Journal of Hydrology*, 207(3–4):254–269, 1998.

[25] J. Carrera and S. P. Neuman. Estimation of aquifer parameters under transient and steady state conditions, 1, Maximum likelihood method incorporating prior information. *Water Resources Research*, 22(2):199–210, 1986.

[26] J. Carrera and S. P. Neuman. Estimation of aquifer parameters under transient and steady state conditions, 2, Uniqueness, stability, and solution algorithms. *Water Resources Research*, 22(2):211–227, 1986.

[27] J. Carrera and S. P. Neuman. Estimation of aquifer parameters under transient and steady state conditions, 3, Application to synthetic and field data. *Water Resources Research*, 22(2):228–2427, 1986.

[28] R. D. Carter, L. F. Kemp, A. C. Pierce, and D. L. Williams. Permformance matching with constrains. *Society of Petroleum Engineers Journal*, 14(4):187–196, 1974.

[29] M. A. Celia, H. Rajaram, and L. A. Ferrand. A multi-scale computational model for multiphase flow in porous media. *Adv. Water Resources*, 16:81–92, 1993.

[30] M. A. Cella, E. T. Bouloutas, and R. L. Zarba. A general mass-conservative numerical solution for the unsaturated flow equations. *Water Resources Research*, 26(7):1483–1496, 1990.

[31] Z. Chen, M. Espedal, and R. E. Ewing. Continuous-time finite element analysis of multiphase flow in groundwater hydrology. *Applications of Mathematics*, 40:203–226, 1995.

[32] J.-P. Chiles and P. Delfiner. *Geostatistics. Modeling spatial uncertainty.* John Wiley and Sons Inc., New York, 1999.

[33] L. Chu, A. C. Reynolds, and D. S. Oliver. Computation of sensitivity coefficients for conditioning the permeability field to well-test pressure data. *In Situ*, 19(2):179–223, 1995.

[34] K. H. Coats, R. L. Nielsen, M. H. Terhune, and A. G. Weber. Simulation of three-dimensional, two-phase flow in oil and gas reservoirs. *Transactions AIME*, 240:377–388, 1967.

[35] G. Dagan. Stochastic modeling of groundwater flow by unconditional and conditional probabilities, 2, The inverse problem. *Water Resources Research*, 21(4):573–578, 1985.

[36] G. Dagan. Statistical theory of groundwater flow and transport: Pore to laboratory, laboratory to formation, and formation to regional scale. *Water Resources Research*, 22(9):120S–134S, 1986.

[37] G. Dagan and Y. Rubin. Stochastic identification of recharge, transmissivity and storativity in aquifer unsteady flow: a quasi-steady approach. *Water Resources Research*, 24(10):1698–1710, 1988.

[38] H.K. Dahle, M.S. Espedal, R.E. Ewing, and O. Saevareid. Characteristic adaptive subdomain methods for reservoir flow problems. *Numerical Methods for Partial Differential Equations*, 6:279–309, 1990.

[39] L. P. Dake. *Fundamentals of Reservoir Engineering.* Elsevier, New York, 1978.

[40] A. Datta-Gupta, L. W. Lake, and G. A. Pope. Characterizing heterogeneous permeable media with spatial statistics and tracer data using sequential simulated annealing. *Math Geol*, 27(6):763–787, 1995.

[41] G. de Marsily. *Quantitative Hydrogeology.* Academic Press, 1986.

[42] G. de Marsily, G. Lavedau, M. Boucher, and G. Fasanino. Interpretation of interference test in a well field using geostatistical techniques to fit the permeability distribution in a reservoir model. In G. W. Verly, M. David, A. G. Journel, and A. Marechal, editors, *Geostatistics for Natural Resources Characterization*, pages 831–849. Proceedings of the NATO Advanced Study Institute, South Lake Tahoe, California, September 6-17, D. Reidel, Dordrecht, Holland, 1984.

[43] C.V. Deutsch. *Geostatistical Reservoir Modeling.* Oxford University Press, New York, first edition, 2002.

[44] J. Jr. Douglas. Finite difference method for two-phase incompressible flow in porous media. *SIAM Journal of Numerical Analysis*, 20:681–696, 1983.

[45] J. Jr. Douglas, D. W. Peaceman, and H. H. Jr. Tachford. A method for calculating multi-dimensional immiscible displacement. *Transactions AIME*, 216:297–306, 1956.

[46] F. A. L. Dullien. *Porous Media Fluid Transport and Pore Structure*. Academic Press, New York, 1979.

[47] R.E. Ewing. Simulation of multiphase flows in porous media. *Transport in Porous Media*, 6:479–499, 1991.

[48] R. W. Falta, K. Pruess, S. Finsterle, and A. Battistelli. T2voc user's guide. Technical Report LBL-36400, Enerst Orlando Lawrence Berkeley National Laboratory, Berkeley, 1995.

[49] C. R. Faust. Transport of immiscible fluids within and below the unsaturated zone: a numerical model. *Water Resources Research*, 21(4):587–596, 1985.

[50] S. Finsterle and K. Pruess. Optimizing multiphase aquifer remediation using itough2. Report LBL-36088, Lawrence Berkeley Laboratory, Berkeley, CA., 1994.

[51] S. Finsterle and K. Pruess. Solving the estimation-identification problme in two-phase flow modeling. *Water Resources Research*, 31(4):913–924, 1995.

[52] F. J. T. Floris, M. D. Bush, M. Cuypers, F. Roggero, and A.-R. Syversveen. Comparison of production forecast uncertainty quantification methods: An integratd study. *Petroleum Geoscience*, 7:S87–S96, 2001.

[53] F.J.T. Floris and C.F.M.Bos. Quantification of uncertainty reduction by conditioning to dynamic production data. In *Proceedings of European Conference on the Mathematics of Oil Recovery, Peebles, Scotland, 8-11 September*, 1998.

[54] P. A. Forsyth, A. J. A. Unger, and E. A. Sudicky. Nonlinear iteration methods for nonequilibrium multiphase subsurfase flow. *Advances in Water Resources*, 18:25–38, 1995.

[55] P. A. Forsyth, Y. S. Wu, and K. Pruess. Robust numerical methods for saturated-unsaturated flow with dry intial conditions in heterogeneous media. *Advances in Water Resources*, 18:25–38, 1995.

[56] R.A. Freeze. A stochastic-conceptual analysis of one-dimensional groundwater flow in nonuniform heterogeneous media. *Water Resources Research*, 11(5):725, 741 1975.

[57] P. Frykman and H.F. Lindgaard. Dynamic upscaling of relative permeability in chalk. Technical Report 1997/145, Geological survey of Denmark and Greenland, 1997.

[58] L.W. Gelhar. Stochastic subsurface hydrology from theory to application. *Water Resources Research*, 22(9):135S–145S, 1986.

[59] J. Gomez-Hernandez, A. Sahuquillo, and J.E. Capilla. Stochastic simulation of transmissivity fields conditional to both transmissivity and piezometric data. 1. Theory. *Journal of Hydrology*, 203(1-4):162–174, 1997.

[60] J.J. Gómez-Hernández and A.G. Journel. Joint simulation of multiGaussian random variables. In Amilcar Soares, editor, *Geostatistics Tróia '92, volume 1*, pages 85–94. Kluwer, 1993.

[61] P. Goovaerts. *Geostatistics for Natural Resources Evaluation*. Oxford University Press, New York, 1997.

[62] A. A. Grimstad, K. Kolltveit, J. E. Nordtvedt, A. T. Watson, T. Mannseth, and A. Sylte. The uniqueness and accuracy of porous media multiphase properties estimated from displacement experiments. In *Proceedings of the International Symposium of the Society of Core Analysis*, September 1997.

[63] P. Grindrod and M. D. Impey. Channeling and fickian dispersion in fractal simulated porous media. *Water Resources Research*, 29(12):4077–4089, 1993.

[64] D. Guerillot and F. Roggero. Matching the future for the evaluation of extreme reservoir development scenarios. In *8th European Symposium on Improved Oil Recovery, Vienna, Austria, 15-17 May*, 1995.

[65] A. Gutjahr, S. Hatch, and B. Bullard. Conditional simulation and contaminant flow modeling: effects of linearization. Technical Completion Report Project Number: WER-91-08, New Mexico Institute of Mining and Technology, 1993.

[66] A. Gutjahr, S. Hatch, and B. Bullard. Conditional simulation and contaminant flow modeling: effects of linearization. Technical Completion Report Project Number: WER-91-08, New Mexico Institute of Mining and Technology, 1994.

[67] A. L. Gutjahr, L. W. Gelhar, A. A. Bakr, and J. R. MacMillan. Stochastic analysis of spatial variability in subsurface flows. 2. Evaluation and application. *Water Resources Research*, 14(5):953–959, 1978.

[68] A.L. Gutjahr. Fast fourier transforms for random field generator. Technical Completion Report A-R58-2690R, New Mexico Institute of Mining and Technology, 1989.

[69] S. Hanna and T.C. Jim Yeh. Estimation of co-coditional moments of transmissivity, hydraulic head, and velocity fields. *Advances in Water Resources*, 22(1):87–95, 1998.

[70] C. F. Harvey and S. M. Gorelick. Mapping hydraulic conductivity: Sequential conditioning with measurements of solute arrival time, hydraulic head, and local conductivity. *Water Resources Research*, 31(7):1615–1626, 1995.

[71] J.J. Hastings, A.H. Muggeridge, and M.J. Blunt. A new streamline method for evaluating uncertainty in small-scale, two-phase flow properties. *SPE 66349*, 2001.

[72] B. K. Hegstad and H. Omre. Uncertainty assessment in history matching and forecasting. In Baafi and Schofield, editors, *Fifth International Geostatistics Congress, Wollongong*. Kluwer, 1997.

[73] B. K. Hegstad and H. Omre. Reservoir characterization integrating well obervations, seismic data and producting history. *Prepints Statistics no. 11/1998, Deparment of mathmatical sciences, NTNU, Trondheim, Norway*, 1998.

[74] B. K. Hegstad, H. Omre, H. Tjelmeland, and K. Tyler. Stochastic simulation and conditioning by annealing reservoir description. In M. Armstrong and P. Dowd, editors, *Geostatistical Simulation*, pages 43–55. Kluwer, 1994.

[75] H. J. Hendricks-Franssen. *Inverse Stochastic Modelling of Groundwater Flow and Mass Transport*. PhD thesis, Universidad Politécnica de Valencia, Spain, 2001.

[76] D. Higdon, H. Lee, and Z. Bi. A bayesian approach to characterizing uncertainty in inverse problems using coarse and fine-scale information. *IEEE Transactions on signal proceesing*, 50(2):389–399, 2002.

[77] R. J. Hoeksema and P. K. Kitanidis. An application of the geostatistical approach to the inverse problem in two-dimensional groundwater modeling. *Water Resources Research*, 20(7):1003–1020, 1984.

[78] R. J. Hoeksema and P. K. Kitanidis. Analysis of the spatial structure of properties of selected aquifers. *Water Resources Research*, 21(4):563–572, 1985.

[79] R. J. Hoeksema and P. K. Kitanidis. Comparison of Gaussian conditional mean and kriging estimation in the geostatistical solution of the inverse problem. *Water Resources Research*, 21(6):825–836, 1985.

[80] L. W. Holm, A. K. Csaszar, and G. G. Bernard. Field test shows stp advantage in waterflood. *Oil Gas Journal*, 63:72–76, 1965.

[81] L.Y. Hu. Gradual deformation and iterative calibration of gaussian-related stochastic models. *Mathematical Geology*, 32(1):87–108, 2000.

[82] L.Y. Hu. Gradual deformation of non-gaussian stochastic simulations. In W.J. Kleingeld and D.G. Krige, editors, *Geostats 2000 Cape Town*. Document Transformation Technologies, 2000.

[83] L.Y. Hu. Combination of dependent realizations with the gradual deformation method. *Mathematical Geology*, 34(8):953–963, 2002.

[84] X. Huang, A. Gajraj, and M. Kelkar. The impact of integrating static and dynamic data in quatifying uncertatinties in the future prediction of multi-phase systems. *SPE Annual Technial Conference and Exhibition held in Denver, Colorado, USA, 6-9 Oct.*, 1996.

[85] E. A. Idrobo, A. H. Malallah, A. Datta-Gupta, and J. O. Parra. Characterizing fluid saturation distribution using cross-well seismic and well data: A geostatistical study. *SPE 56515*, 1999.

[86] P. Jacquard and C. Jain. Permeability distribution from field pressure data. *Society of Petroleum Engineers Journal*, 5(4):281:294, 1965.

[87] M. Jang and J. Choe. Stochastic optimization for global minimization and geostatistical calibration. *Journal of Hydrology*, 266:40–52, 2002.

[88] J. J. Kaluarachchi and J. C. Parker. An efficient finite elements method for modeling multiphase flow. *Water Resources Research*, 25(1):43–54, 1989.

[89] C. E. Kees and C. T. Miller. Higher order time integration methods for two-phase flow. *Advances in Water Resources*, 25:159–177, 2002.

[90] J. H. Kim, M. K. Stenstrom, and T. C. Harmon. A study on fluid flow and mass transformations in immiscible liquids. In *Proceedings of the 69th Annual Water*

Environment Federation Conference and Exposition, Dallas, TX, USA, October 5-9, 9605001, pages 1–15, 1996.

[91] W. Kinzelbach. *Groundwater modelling: An introduction with sample programs in BASIC.* Elsevier, 1986.

[92] B. H. Kueper and E. O. Frind. Two-phase flow in heterogeneous porous media. 1. model development. *Water Resources Research*, 27(6):1049–1057, 1991.

[93] B. H. Kueper and E. O. Frind. Two-phase flow in heterogeneous porous media. 2. model application. *Water Resources Research*, 27(6):1059–1070, 1991.

[94] K.N. Kulkarni and A. Datta-Gupta. Estimating relative permeability from production data: a streamline approach. *SPE Annual Technical Conference and Exhibition held in Houston, Texas, 3-6 Oct.*, 1999.

[95] L. W. Lake. *Enhaced Oil Recovery.* Prentice-Hall, 1 edition, 1989.

[96] J.L. Landa. *Reservoir Parameter Estimation Constrained to Pressure Transients, Performance History and Distributed Saturation Data.* PhD thesis, Standord University, Stanford, CA, 1997.

[97] J.L. Landa. Technique to integrate production and static data in a self-consisten way. *SPE Annual Technical Conference and Exhibition held in New Orleans, Lousiana, 30 September - 3 October*, 2001.

[98] P. Langlo and M. S. Espedal. Macrodispersion for two phase, inmiscible flow in porous media. *Advances in Water Resources Research*, 17:297–316, 1994.

[99] J. Larsen and N. Bech. Parallel simulation of petroelum reservoirs. In D. Guerillot and O.Guillon, editors, *2nd European Conference on the Mathematics of Oil Recovery*, pages 1–15, Paris, 1990. EDITIONS TECHNIP.

[100] A. M. LaVenue and J. F. Pickens. Application of a coupled adjoint sensitivity and kriging approach to calibrate a groundwater flow model. *Water Resources Research*, 28(6):1543–1569, 1992.

[101] M. LeRavlec-Dupin, L. Y. Hu, and B. Noetinger. Sampling the conditional realization space using the gradual deformation method. In W.J. Kleingeld and D.G. Krige, editors, *Geostats 2000 Cape Town.* Document Transformation Technologies, 2000.

[102] B. Li, Z. Chen, and G. Hun. Control volume function approximation methods and their applications to modeling porous media flow. *Advances in Water Resources*, 26:435–444, 2003.

[103] X. Li, O. C. Zienkiewicz, and M. Xie. A numerical model for immiscible two-phase fluid flow in porous medium and its time domain solution. *International Journal for Numerical Methods in Engineering*, 30:1195–1212, 1990.

[104] C. M. Marle. *Multiphase Flow in Porous Media*. Gulf Publishing, Houston, 1981.

[105] G. F. Matheron. The intrinsic random functions and their applications. *Adv. Appl. Probabilities*, 5:439–458, 1973.

[106] C. T. Miller, G. Christakos, P. T. Imhoff, J. F. McBride, J. A. Pedit, and J. A. Trangenstein. Multiphase flow and transport modeling in heterogeneous porous media: challenges and approaches. *Adv. in Water Resources*, 21:77–120, 1998.

[107] V. Mitlin, B. Lawton, and L. Owen. A semi-analytical procedure for estimating relative permeability from displacement experiments: account for pre-breakthrough data. *International Journal of Engineering Science*, 37:1051–1067, 1999.

[108] E. M. Mkhlouf, W. H. Chen, M. L. Wasserman, and J. H. Seifeld. A general history matching algorithm for three-phase, three-dimensional petroleum reservoirs. *SPE Advanced Technology Series*, 1(2):83–92, 1993.

[109] H. J. Morel-Seytoux. Two-phase flow in porous media. *Advances in Hydroscience*, 9:119–202, 1973.

[110] H. J. Morel-Seytoux and J. A. Billica. A two-phase numerical model for prediction of infiltration: Applications to a semi-infinite column. *Water Resources Research*, 21:607–615, 1985.

[111] H. J. Morel-Seytoux and J. A. Billica. A two-phase numerical model for prediction of infiltration: Case of impervious bottom. *Water Resources Research*, 21:1389–1396, 1985.

[112] D. S. Oliver, L. B. Cunha, and A. C. Reynolds. Markov chain monte carlo methods for conditioning field to pressure data. *Mathematical Geology*, 29(1):61–91, 1997.

[113] D. S. Oliver, N. He, and A. C. Reynolds. Conditioning permeability fields to pressure data. In *5th European Conference of the Mathematics of Oil Recovery, Leoben, Austria, 3-6 September*, 1996.

[114] D. S. Oliver, A. C. Reynolds, Z. Bi, and Y. Abacioglu. Integration of production data into reservoir models. *Petroleum Geoscience*, 7:S65–S73, 2001.

[115] H. Omre. Stochstic reservoir models conditioned to non-linear production history observations. In Kleingeld and Krige, editors, *Geostatistics 2000 Cape Town, volume 1*, pages 166–175. Kluwer, 2002.

[116] H. Omre and H. Tjelmand. Petroleum geostatistics. In Baafi and Schofield, editors, *Geostatistics Wollongong 1996*, pages 41–52. Kluwer, 1997.

[117] D. W. Peaceman and H. H. Jr. Rachford. Numerical calculation of multidimensional miscible displacement. *Transactions AIME*, 225:327–339, 1962.

[118] G. F. Pinder and L. M. Abriola. On the simulation of non-aqueous phase organic compounds in the subsurface. *Water Resources Research*, 22:109–119, 1986.

[119] K. Pruess and C. Oldenburg. Tough2 user ś guide. Report LBNL-43134, Ernert Orlando Lawrence Berkeley National Laboratory, Berkeley, 1999.

[120] B. S. Ramarao, A. M. LaVenue, G. de Marsily, and M. G. Marietta. Pilot point methodology for automated calibration of an ensemble of conditionally simulated transmissivity fields, 1, Theory and computational experiments. *Water Resources Research*, 31(3):475–493, 1995.

[121] F. Roggero and D. Guerillot. Gradient method and bayesian formalism application to petrophysical parameter characterization. In *5th European Conference on the Mathematics of Oil Recovery, Leoben, Austria, 3-6 September*, 1996.

[122] F. Roggero and L. Y. Hu. Gradual deformation of continuous geostatistical models for history matching. *SPE 49004, presented at the Annual Technical Conference*, 1998.

[123] C. E. Romero and J. N. Carter. Using genetic algorithms for reservoir characterisation. *Journal of Petroleum Science and Engineering*, 31:113–123, 2001.

[124] C. E. Romero, J. N. Carter, A. C. Gringarten, and R. W. Zimmerman. A modified genetic algorithm for reservoir characterization. *SPE Annual Technical Conference and Exhibition held in Beijing, China, 7-10 Nov.*, 2000.

[125] C. E. Romero, J. N. Carter, R. W. Zimmerman, and A. C. Gringarten. Improved reservoir characterization through evolutionary computation. *SPE Annual Technical Conference and Exhibition held in Dallas, Texas, 1-4 Oct.*, 2000.

[126] Y. Rubin and G. Dagan. Stochastic identification of transmissivity and effective recharge in steady groundwater flow, 1, Theory. *Water Resources Research*, 23(7):1185–1191, 1987.

[127] Y. Rubin and G. Dagan. Stochastic identification of transmissivity and effective recharge in steady groundwater flow, 2, Case study. *Water Resources Research*, 23(7):1192–1200, 1987.

[128] Y. Rubin and G. Dagan. Conditional estimation of solute travel time in heterogeneous formations: Impact of transmissivity measurements. *Water Resources Research*, 28(4):1033–1040, 1992.

[129] A. Sahuquillo, J. E. Capilla, J. J. Gómez-Hernández, and J. Andreu. Conditional simulation of transmissivity fields honouring piezometric head data. In W. R. Blair and E. Cabrera, editors, *Hydraulic Engineering Software IV, Fluid Flow Modeling*, volume II, pages 201–214, London, UK, 1992. Elsevier Applied Science.

[130] L. E. Scales. *Introduction to Non-Linear Optimization*. MacMillan Publishers, Hong Kong, 1985.

[131] B. A. Schrefler and Z. Xiayong. A fully coupled model for water flow and airflow in deformable porous media. *Water Resources Research*, 29(1):155–167, 1993.

[132] B. E. Sleep and J. F. Sykes. Modeling the transport of volatile organics in variably saturated media. *Water Resources Research*, 25(1):81–92, 1989.

[133] E. H. Smith. The influence of small-scale heterogeneity on average relative permeability. In L.W. Lake, H.B. Carroll Jr., and T.C. Wesson, editors, *Reservoir Characterization II*, pages 52–76, New York, 1991. Academic Press.

[134] L. Smith. Spatial variability of flow parameters in a stratified sand. *Math. Geology*, 13(1):1–21, 1981.

[135] L. Smith and F. W. Schwartz. Mass transport 2. analysis of uncertainty in prediction. *Water Resources Research*, 17(2), 1981. 351–369.

[136] E. A. Sudicky. A natural gradient experiment on solute transport in a sand aquifer: Spatial variability of hydraulic conductivity and its role in the dispersion process. *Water Resources Research*, 22(13):2069–2082, 1986.

[137] Ne-Zheng Sun. *Inverse Problems in Groundwater Modeling.* Kluwer Academic Publishers, 1994.

[138] M. R. Thiele. Streamline simulation. In *6th International Forum on Reservoir Simulation, 3-7 September, 2001, Schloss Fuschl, Austria*, 2001.

[139] H. Tjelmeland and H. Omre. A complex sand-shale facies model conditioned on observations from wells, seismics, and production. In E. Baafi and N. Schofield, editors, *Fifth International Geostatistics, Wollongong.* Kluwer, 1997.

[140] R. Valestrand, A. A. Grimstad, K. Kollveit, G. Naevdal, and J. E. Nordtvedt. Simultaneous determination of absolute and relative permeabilities. *International Journal of Thermal Sciences*, 41(6):546–556, 2002.

[141] R. Valestrand, A. A. Grimstad, K. Kollveit, J. E. Nordtvedt, and G. Naevdal. Simultaneous determination of absolute and relative permeabilities. *Inverse problems and experimental design and thermal and mech. eng. Seminar no 68, 5-7 March, ENSMA FUTUROSCOPE, France*, 2001.

[142] M. T. van Genuchten. A closed form equation for predicting the hydraulic conductivity of unsaturated soils. *Soil Sic. Soc. Am. J.*, 44:892–898, 1980.

[143] D. W. Vasco, S. Yoon, and A. Datta-Gupta. Integrating dynamic data into high-resolution reservoir models using streamline-based analytic sensitivity coefficients. *SPE Journal*, 4(4):389–399, 1999.

[144] Y. Wang and A. R. Kovscek. A streamline approach for history-matching production data. *SPE/DOE Improved Oil Recovery Symposium held in Tulsa, Oklahoma, 3-5 April*, 2000.

[145] M. Wangen. Vertical migration of hydrocarbons modelled with fractional flow theory. *Geophysical Journal International*, 115:109–131, 1993.

[146] A.T. Watson, J.G.Wade, and R.E. Ewing. Parameter and system identification for fluid flow in underground reservoirs. In H.W. Engl and J. JcLaughlin, editors, *Proceeding of the Conference: Inverse Problmes and Optimal Design in Industry, July 8-10, 1993, Philadelphia, Pa.* B.G.Teubner, Stuttgart, Germany, 1994.

[147] X.-H. Wen. *Stochastic Simulation of Groundwater Flow and Mass Transport in Heterogeneous Aquifers: Conditioning and the problem of scales.* PhD thesis, Universidad Politécnica de Valencia, Dep. de Ing. Hidráulica y Medio Ambiente, Valencia, Spain, 1996.

[148] X.-H. Wen, C. V. Deutsch, and A. S. Cullick. A review of current approaches to integrate flow production data in geological modeling. In *Stanford Center for Reservoir Forecasting (SCRF) Annual Report, Stanford U.*, May 1997.

[149] X. H. Wen, C. V. Deutsch, and S. Cullick. Integrating pressure and fractional flow data in reservoir modeling with fast streamline-based inverse method. *SPE 4897*, 1998.

[150] X.-H. Wen, J. J. Gómez-Hernández, J. E. Capilla, and A. Sahuquillo. Significance of conditioning to piezometric head data for predictions of mass transport in groundwater modeling. *Math. Geology*, 28(7):951–968, 1996.

[151] X. H. Wen, T. T. Tran, R. A. Behrens, and J. J. Gómez-Hernández. Production data integration in sand/shale reservoirs using sequential self-calibration and geomorphing: A comparison. *SPE Reservoir Evaluation and Engineering*, pages 255–265, June 2002.

[152] Yu-Shu Wu and P. A. Forsyth. On the selection of primary variables in numerical formultaion for modeling multiphase flow in porous media. *Journal of Contaminant Hydrology*, 48:277–304, 2001.

[153] Yu-Shu Wu, K. Zhang, C. Ding, K. Pruess, E. Elmroth, and G. S. Bodvarsson. An efficient parallel-computing method for modeling nonisothermal multiphase flow and multicomponent transport in porous and fractured media. *Advances in Water Resources*, 25:243–261, 2002.

[154] Zhan Wu, A. C. Reynolds, and D. S. Oliver. Conditioning geostatistical models to two-phase production data. *SPE Journal*, 4(2):142–155, 1999.

[155] W. W-G. Yeh. Review of parameter identification procedures in groundwater hydrology: The inverse problem. *Water Resources Research*, 22(2):95–108, 1986.

[156] W. W-G. Yeh, M. Jin, and S. Hanna. An iterative stochastic inverse method: Conditional effective transmissivity and hydraulic head fields. *Water Resources Research*, 32(1):85–92, 1996.

[157] Z. Ying and J. J. Gómez-Hernández. An improved deformation algorithm for automatic history matching. In *Stanford Center for Reservoir Forecasting (SCRF) Annual Report, Stanford U.*, 2000.

[158] S. Yoon, A.H. Malallah an dA. Datta-Gupta, D. W. Vasco, and R. A. Behrens. A multiscale approach to production data integration using streamline models. *SPE 56653*, 1999.

[159] L. C. Young. A study of spatial approximation for simultaing fluid displacements in petroleum reservoirs. *Computer Methods in Applied Mechanics and Engineering*, 47:3–46, 1984.

[160] D. Zhang, L. Li, and H. Tchelepi. Stochastic formulation for uncertainty analysis of two-phase flow in heterogeneous reservoirs. *SPE Journal*, 5(1):60–70, 2000.

[161] D. Zhang and H. Tchelepi. Stochastic analysis of immiscible two-phase flow in heterogeneous media. *SPE Journal*, 4(4):380–388, 1999.

[162] C. Zhen and G.D. Bennett. *Applied contaminant transport modelling. Theory and practice.* John Wiley and Sons Inc., 1995.

[163] D. A. Zimmerman and D. P. Gallegos. A comparison of geostatistically-based inverse techniques for use in performance assessment analyses at the WIPP site. Results from test case no 1. In *High Level Radioactive Waste Management, Proceedings of the 4th International Conference*, pages 1426–1436, Las Vegas, Nevada, April 1993.